Cell

Distinct longevity mechanisms across and within species and their association with aging

Graphical abstract

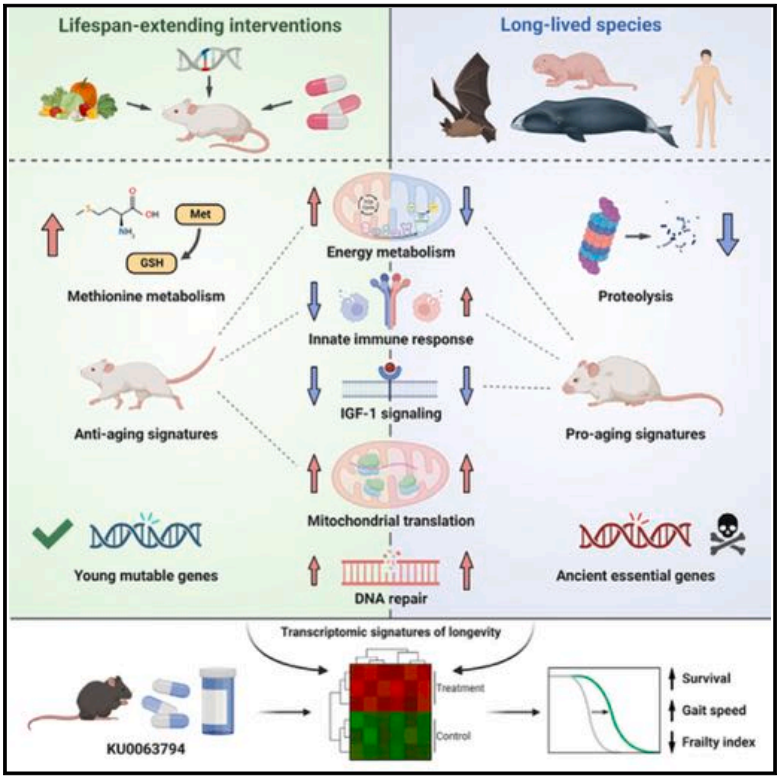

Highlights

- Distinct molecular mechanisms control lifespan within and across species
- Aging effects are reversed by longevity interventions but not by species longevity
- Regulation of *Igf1* and mitochondrial translation are shared signatures of longevity
- Longevity signatures enable the discovery of geroprotectors, such as KU0063794

Authors

Alexander Tyshkovskiy, Siming Ma, Anastasia V. Shindyapina, ..., Sergey E. Dmitriev, Richard A. Miller, Vadim N. Gladyshev

Correspondence

vgladyshev@rics.bwh.harvard.edu

In brief

The analysis of multi-tissue gene expression signatures associated with longevity across mammalian species and their interaction with biomarkers of aging and signatures of lifespan-extending interventions reveals universal and distinct strategies of lifespan regulation within and across species and provides tools for the discovery of longevity interventions in mammals.

Tyshkovskiy et al., 2023, Cell *186*, 1–21
June 22, 2023
https://doi.org/10.1016/j.cell.2023.05.002

CellPress

Please cite this article in press as: Tyshkovskiy et al., Distinct longevity mechanisms across and within species and their association with aging, Cell (2023), https://doi.org/10.1016/j.cell.2023.05.002

Cell

CellPress

Article

Distinct longevity mechanisms across and within species and their association with aging

Alexander Tyshkovskiy,[1,2,10] Siming Ma,[1,10] Anastasia V. Shindyapina,[1,10] Stanislav Tikhonov,[2] Sang-Goo Lee,[1] Perinur Bozaykut,[1,3] José P. Castro,[1,4,5] Andrei Seluanov,[6] Nicholas J. Schork,[7] Vera Gorbunova,[6] Sergey E. Dmitriev,[2] Richard A. Miller,[8] and Vadim N. Gladyshev[1,9,11,*]

[1]Division of Genetics, Department of Medicine, Brigham and Women's Hospital, Harvard Medical School, Boston, MA 02115, USA
[2]Belozersky Institute of Physico-Chemical Biology, Moscow State University, Moscow 119234, Russia
[3]Department of Molecular Biology and Genetics, Faculty of Engineering and Natural Sciences, Acibadem Mehmet Ali Aydinlar University, Istanbul 34752, Turkey
[4]i3S, Instituto de Investigação e Inovação em Saúde, Universidade do Porto, 4200-135 Porto, Portugal
[5]Aging and Aneuploidy Laboratory, IBMC, Instituto de Biologia Molecular e Celular, Universidade do Porto, 4200-135 Porto, Portugal
[6]Departments of Biology and Medicine, University of Rochester, Rochester, NY, USA
[7]Quantitative Medicine and Systems Biology Division, Translational Genomics Research Institute, Phoenix, AZ, USA
[8]Department of Pathology and Geriatrics Center, University of Michigan, Ann Arbor, MI 48109, USA
[9]Broad Institute, Cambridge, MA, USA
[10]These authors contributed equally
[11]Lead contact
*Correspondence: vgladyshev@rics.bwh.harvard.edu
https://doi.org/10.1016/j.cell.2023.05.002

SUMMARY

Lifespan varies within and across species, but the general principles of its control remain unclear. Here, we conducted multi-tissue RNA-seq analyses across 41 mammalian species, identifying longevity signatures and examining their relationship with transcriptomic biomarkers of aging and established lifespan-extending interventions. An integrative analysis uncovered shared longevity mechanisms within and across species, including downregulated *Igf1* and upregulated mitochondrial translation genes, and unique features, such as distinct regulation of the innate immune response and cellular respiration. Signatures of long-lived species were positively correlated with age-related changes and enriched for evolutionarily ancient essential genes, involved in proteolysis and PI3K-Akt signaling. Conversely, lifespan-extending interventions counteracted aging patterns and affected younger, mutable genes enriched for energy metabolism. The identified biomarkers revealed longevity interventions, including KU0063794, which extended mouse lifespan and healthspan. Overall, this study uncovers universal and distinct strategies of lifespan regulation within and across species and provides tools for discovering longevity interventions.

INTRODUCTION

Mammals exhibit substantial variability of lifespan both within and across species. Generally, there is a strong positive association between adult weight (AW) and species longevity,[1] exemplified by Etruscan shrews (*Suncus etruscus*), weighing 1.8 g with lifespan of 3.2 years, and bowhead whales (*Balaena mysticetus*), weighing >100 tons with a maximum lifespan (ML) of >200 years.[2] However, there are also exceptions to this rule, the so-called exceptionally long-lived species, that live significantly longer than expected based on their AW, such as the naked mole rat (*Heterocephalus glaber*),[3] some microbats, e.g., the Brandt's bat (*Myotis brandtii*),[4] and humans. This variability is achieved on the evolutionary timescale, and multiple mechanisms that may contribute to species longevity have been identified.[5–10]

Mammalian lifespan may also be extended within species. Dozens of genetic, pharmacological, and environmental interventions increasing murine lifespan and healthspan are known today. They include mutations such as growth hormone receptor knockout (GHRKO),[11] drugs such as rapamycin,[12] and diets such as calorie restriction (CR).[13–16] In contrast to the inter-species data, body size within species is often negatively associated with longevity. Life expectancy across dog breeds is inversely correlated with body mass,[17] and various murine dwarf models are often characterized by ~30%–60% longer median and ML compared with wild-type mice,[18,19] which appears to be mediated through the decreased activity of growth hormone (GH) and insulin-like growth factor 1 (IGF-1) signaling.[20] Therefore, some features appear to be differently associated with lifespan across and within species. Establishing shared and distinct molecular mechanisms of longevity, as well as their causative relationship with aging, is critically important for our understanding of drivers of lifespan regulation and the development of effective geroprotectors.

High-throughput data, including transcriptomics, metabolomics, and epigenomics, were used to evaluate molecular features of longevity and aging. Aging-related changes in DNA methylation[21,22] and gene expression[23,24] were thoroughly examined in individual mammalian species. Several studies also conducted qualitative meta-analyses of transcriptomic aging signatures for different tissues and species,[25,26] although quantitative meta-analyses of age-related gene expression changes (ECs) have been lacking. Associations between species longevity and molecular patterns of mammalian organs or cells were also assessed at the level of the metabolome,[27] ionome,[28] lipidome,[29] and transcriptome.[30–32] Finally, by carrying out a large-scale meta-analysis, we previously characterized gene expression signatures of lifespan extension induced by various longevity interventions in mouse tissues.[33]

Despite the growing number of established geroprotectors and high-throughput data, a comprehensive analysis of universal and model-specific signatures of longevity has been lacking. Do existing lifespan-extending interventions in mice induce molecular mechanisms shared by long-lived mammals, such as the naked mole rat, human, and bowhead whale? How do these signatures interplay with age-associated features? What are the common and distinct mechanisms of longevity induced by interventions and selected in species during evolution? Can these signatures be utilized to identify lifespan-extending interventions?

To answer these questions, we (1) performed RNA sequencing (RNA-seq) and characterized gene expression signatures of mammalian longevity across 41 species, including the long-lived naked mole rat, Brandt's bat, and bowhead whale; (2) identified species-specific, tissue-specific, and universal transcriptomic biomarkers of mammalian aging through a quantitative meta-analysis of 92 publicly available datasets; (3) investigated common and distinct molecular mechanisms of aging and longevity within and across species; and (4) demonstrated that the identified signatures can be used to discover and characterize lifespan-regulating interventions in mammals.

RESULTS

RNA-seq of tissues across mammalian species

To investigate gene expression signatures of mammalian lifespan, we collected RNA-seq data for 48 young adult animals and aggregated it with publicly available data.[4,31,34–41] This resulted in 371 biological samples covering six tissues (brain, kidney, liver, cerebellum, heart, and testis) of 41 mammalian species from 12 taxonomic orders with a wide range of longevity-associated traits (Figure 1A; Table S1A), including 4 exceptionally long-lived mammals: naked mole rat, Brandt's bat, bowhead whale, and human. Utilizing a previously developed pipeline[30] (see STAR Methods), we identified 13,784 one-to-one orthologs across examined species (Figures S1A and S1B; Table S2).

Principal-component analysis revealed that the samples were segregated predominantly by their organ origin (Figure 1B). The cerebellum and cerebral cortex samples were clustered together, whereas the testis samples were distant from the other organs (Figure S1C). Analysis of variance (ANOVA) confirmed that organs and species were the primary sources of variation in gene expression, capturing, on average, 84% of the total variance across samples. Within tissues, 78%–95% of the variance was explained by species, even after controlling for batch effect (Figure S1D). Correlation analysis among species revealed a high similarity of expression profiles in neural tissues, whereas testis profiles were diverse across species (Figures 1C and S1E), consistent with the notion that this organ rapidly evolves under the impact of reproduction-related selection.[37,42–44]

To characterize organ-specific expression patterns, we identified 6,050 genes that significantly upregulated or downregulated (p value, $p < 0.01$) in one organ relative to the others (Figure 1D). In the kidney, genes involved in ion transport and sodium transport were overexpressed, consistent with their functions in ultrafiltration and selective reabsorption. In the liver, a higher expression was detected for genes involved in steroid metabolism, detoxification, and complement and coagulation cascades. Consistent with its energy demand, the heart exhibited an overexpression of genes related to oxidative phosphorylation and the tricarboxylic acid (TCA) cycle. The brain cortex and cerebellum specifically expressed genes involved in synaptic transmission and neuronal differentiation, whereas the testis was characterized by overexpression of genes encoding cyclins, centrosomal proteins, and spermatogenesis-associated proteins, consistent with their roles in sexual reproduction. Overall, organ-specific expression patterns were congruent with their biological roles, and samples from the same tissues clustered together. The exceptions were chicken and platypus samples, which clustered by species and away from the rest of the samples (Figure 1D, bottom), probably due to their significant evolutionary distance from other examined species.

Transcriptomic signatures of longevity across species

We employed brain, kidney, and liver samples, representing >35 species, to identify gene expression signatures of long-lived mammals. Using phylogenetic regression (see STAR Methods), we identified ~100–500 genes that were significantly associated (p adjusted < 0.05) with animal ML (Figures 2A–2C) and female time to maturity (FTM) (Figure S2A). Expression of ~40%–70% of these genes was significantly associated with species ML and FTM after adjustment for body mass (MLres and FTMres, respectively) (Figures S2B and S2C).

To assess if organ gene expression predicts species ML, we utilized the Elastic Net linear regression model and leave-one-out (LOO) technique, iteratively training the model on all but one species and testing it on the remaining species. When applied to the test set, the model captured 78% of the total variation in lifespan in the log scale (Figure 2D). The addition of mammalian AW did not further improve the model, and body mass alone captured only 39% of lifespan variation (Figure S2D), suggesting that tissue gene expression significantly outperforms AW in predicting mammalian longevity. Several genes, including *Sdc1* and *Dtl*, were consistently selected by Elastic Net models trained on different LOO subsets (Figure 2E). *Sdc1* encodes proteoglycan syndecan-1, whose deficiency induces inflammation in mice,[45,46] whereas an increased expression of *Dtl* is associated with bladder cancer progression, presumably through the regulation of the AKT/mTOR pathway.[47] In agreement, *Sdc1*

Please cite this article in press as: Tyshkovskiy et al., Distinct longevity mechanisms across and within species and their association with aging, Cell (2023), https://doi.org/10.1016/j.cell.2023.05.002

CellPress

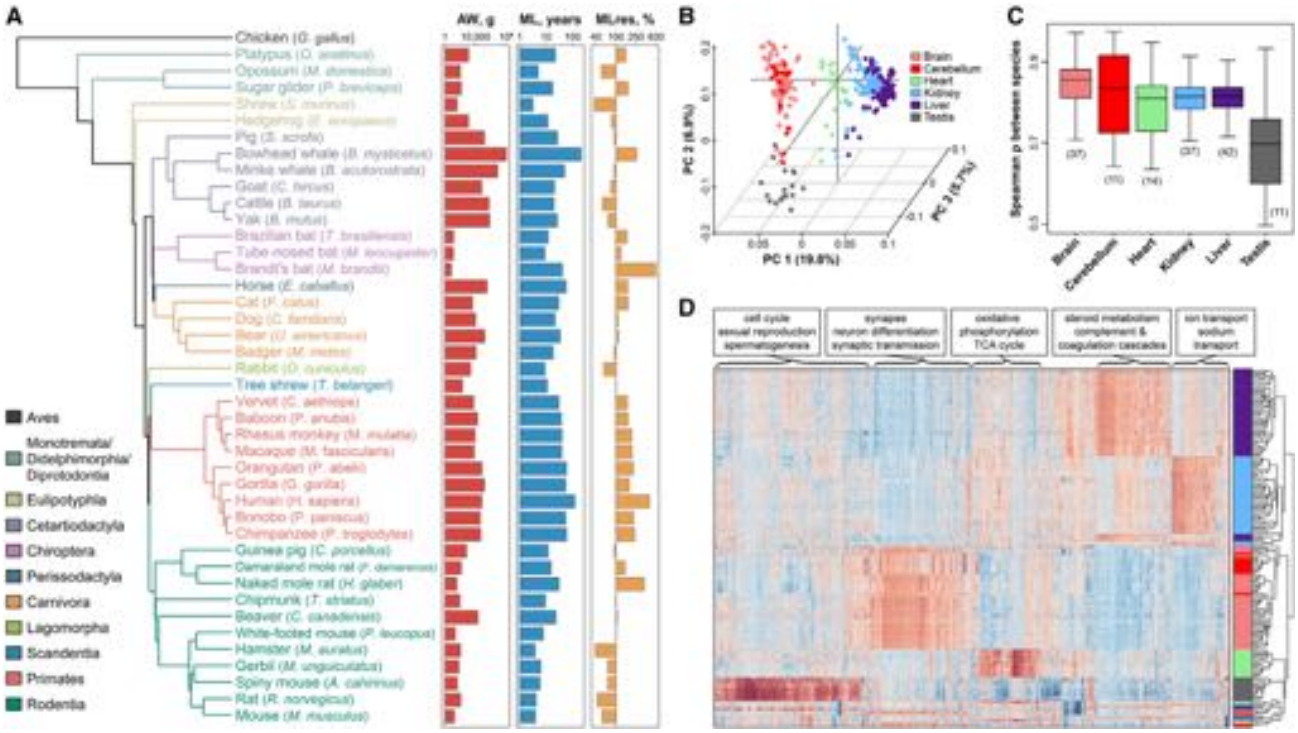

Figure 1. RNA-seq of mammalian tissues

(A) Phylogenetic tree of examined species and their longevity traits. Adult weight (AW), maximum lifespan (ML), and ML residual adjusted for body mass (MLres) are shown on barplots in logarithmic scale.

(B) Principal-component analysis of mammalian samples. First 3 principal components (PCs) are shown. The percentage of total variance explained by each PC is indicated in parentheses.

(C) Within-organ variability across mammalian species. Pairwise Spearman correlation coefficients between species expression profiles were calculated for each organ. The number of available species is indicated in parenthesis.

(D) Expression of genes significantly enriched or depleted in specific organs. Columns represent genes; rows represent biological samples colored by organ, as in (B). Top pathways enriched for corresponding gene sets are indicated in the text. Ch, chicken; Pl, platypus.

See also Figure S1 and Tables S1 and S2.

and *Dtl* were upregulated and downregulated in the tissues of long-lived species, respectively (Figure 2E).

Comparison of signatures across tissues revealed significant pairwise overlaps for both up- and downregulated genes associated with ML (p adjusted $< 2 \times 10^{-5}$) (Figure 2F) and MLres (p adjusted < 0.042) (Figure 2G). Accordingly, longevity-associated ECs were positively correlated across all analyzed organs (Spearman $\rho > 0.21$) (Figure 2H). To examine if common signatures of longevity were driven by universally expressed genes or blood cell-specific biomarkers, we utilized Tabula Muris single-cell atlas.[24] The identified signatures of ML in every organ were, on average, expressed in >49% of cell types (Figure S2E). Shared biomarkers of longevity across tissues, aggregated with the harmonic mean p value (HMP) method,[48] demonstrated even more universal expression, being detected in 66% of the individual cell types, whereas blood cell-specific biomarkers accounted for <1.5% of ML-associated genes.

Cell type deconvolution[49] revealed that liver samples were largely composed of hepatocytes, kidney samples consisted of epithelial and endothelial cells, and brain samples included neurons, oligodendrocytes, astrocytes, and other glial cells (Figure S2F). In contrast, the total proportion of immune cells was, on average, <3% in every organ. Following adjustment for blood cell abundance across samples, we still detected statistically significant associations with ML for >95.9% of signature genes in every examined tissue, suggesting that modest variation in blood cell composition is not a defining factor for the observed effects.

Interestingly, longevity-associated ECs in all organs were also positively correlated with signatures of lifespan in cultured primary skin fibroblasts (Figure S2G) collected from 16 mammalian species.[30] Although a similarity between longevity biomarkers in organs may be partially driven by the systemic effect of signaling and catalytic molecules circulating in the bloodstream, including cytokines,[50–52] extracellular miRNAs,[53] metabolites,[54] and enzymes,[55] these results suggest that numerous conserved molecular mechanisms of lifespan regulation are preserved at the level of cultured cells and are likely to be encoded in the genome.

To identify pathways associated with species longevity, we performed functional gene set enrichment analysis (GSEA) of the lifespan-associated ECs (Figures 2I and S2H; Table S3A). Shared molecular features of long-lived mammals across

Please cite this article in press as: Tyshkovskiy et al., Distinct longevity mechanisms across and within species and their association with aging, Cell (2023), https://doi.org/10.1016/j.cell.2023.05.002

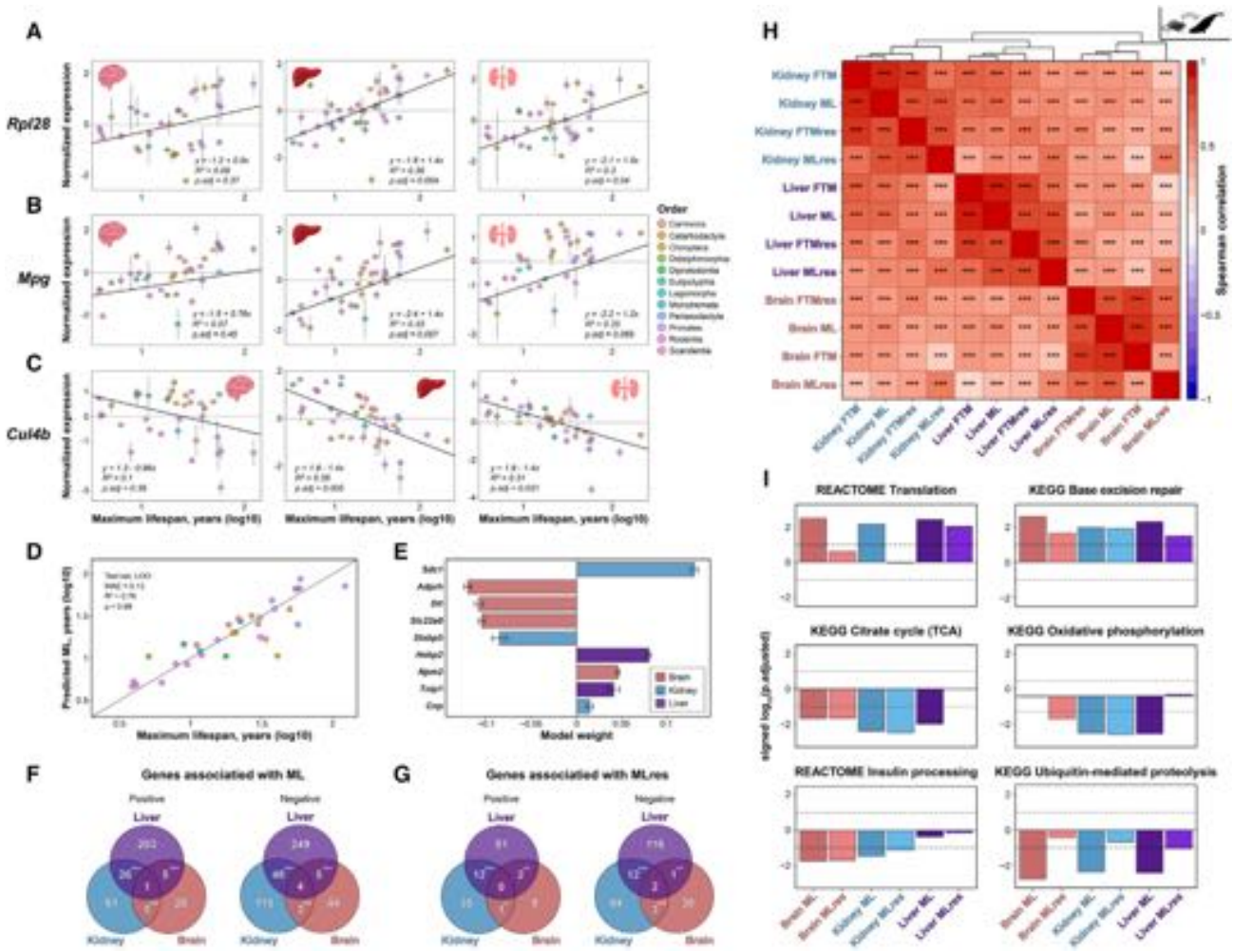

Figure 2. Gene expression signatures of species longevity

(A–C)Representative genes associated with species maximum lifespan. Selected genes include *Rpl30* (A), *Rpl28* (B), and *Cul4b* (C). The association between log10(maximum lifespan) and average normalized log10(expression) is shown for brain (left), liver (middle), and kidney (right). Linear model equation, slope adjusted p value and R^2 estimated with phylogenetic regression are displayed. Data are mean ± SE.

(D) Accuracy of Elastic Net prediction of species maximum lifespan (ML) based on tissue gene expression. Mean absolute error (MAE), R^2, and Pearson's correlation coefficient were estimated on LOO test set. Each dot represents a single species and is colored by taxonomic group, as in (A)–(C).

(E) Gene expression predictors of maximum lifespan. For each gene, data represent mean weight in Elastic Net models trained on different subsets ± SE. Only genes with non-zero average weight are included (p adjusted < 0.05).

(F and G) Overlap of genes associated with maximum lifespan unadjusted (F) and adjusted for body mass (MLres) (G) across mammalian tissues. p value was calculated with Fisher exact tests.

(H) Spearman correlation of longevity-associated gene expression changes. Asterisks reflect statistical significance.

(I) Functional enrichment of lifespan-associated genes. Dotted lines reflect threshold of p adjusted = 0.1. The whole list of enriched functions is in Table S3A.

*p adjusted < 0.05; **p adjusted < 0.01; ***p adjusted < 0.001.

FTM, female time to maturity; FTMres, female time to maturity residual.

See also Figure S2 and Table S3.

multiple organs included the upregulation of genes involved in translation (e.g., *Rpl28* encoding a large ribosomal subunit component [Figures 2A and S2B]) and base excision repair (e.g., *Mpg* encoding N-methylpurine DNA glycosylase [Figure 2B]), and downregulation of genes involved in ubiquitin-mediated proteolysis (e.g., *Cul4b* encoding a cullin protein family member [Figures 2C and S2C]), TCA cycle, and insulin processing (Figures 2I and S2H).

Gene expression biomarkers of mammalian aging

To identify consistent transcriptomic signatures of aging, we aggregated data on the mouse (*Mus musculus*), rat (*Rattus norvegicus*), and human (*Homo sapiens*) age-related gene ECs from 92 publicly available datasets (Table S1B) (see STAR Methods). Aging-associated ECs were positively correlated across datasets, especially after restricting the analyses to the top statistically significant genes for each pair of datasets (Figure S3A).

Please cite this article in press as: Tyshkovskiy et al., Distinct longevity mechanisms across and within species and their association with aging, Cell (2023), https://doi.org/10.1016/j.cell.2023.05.002

CellPress

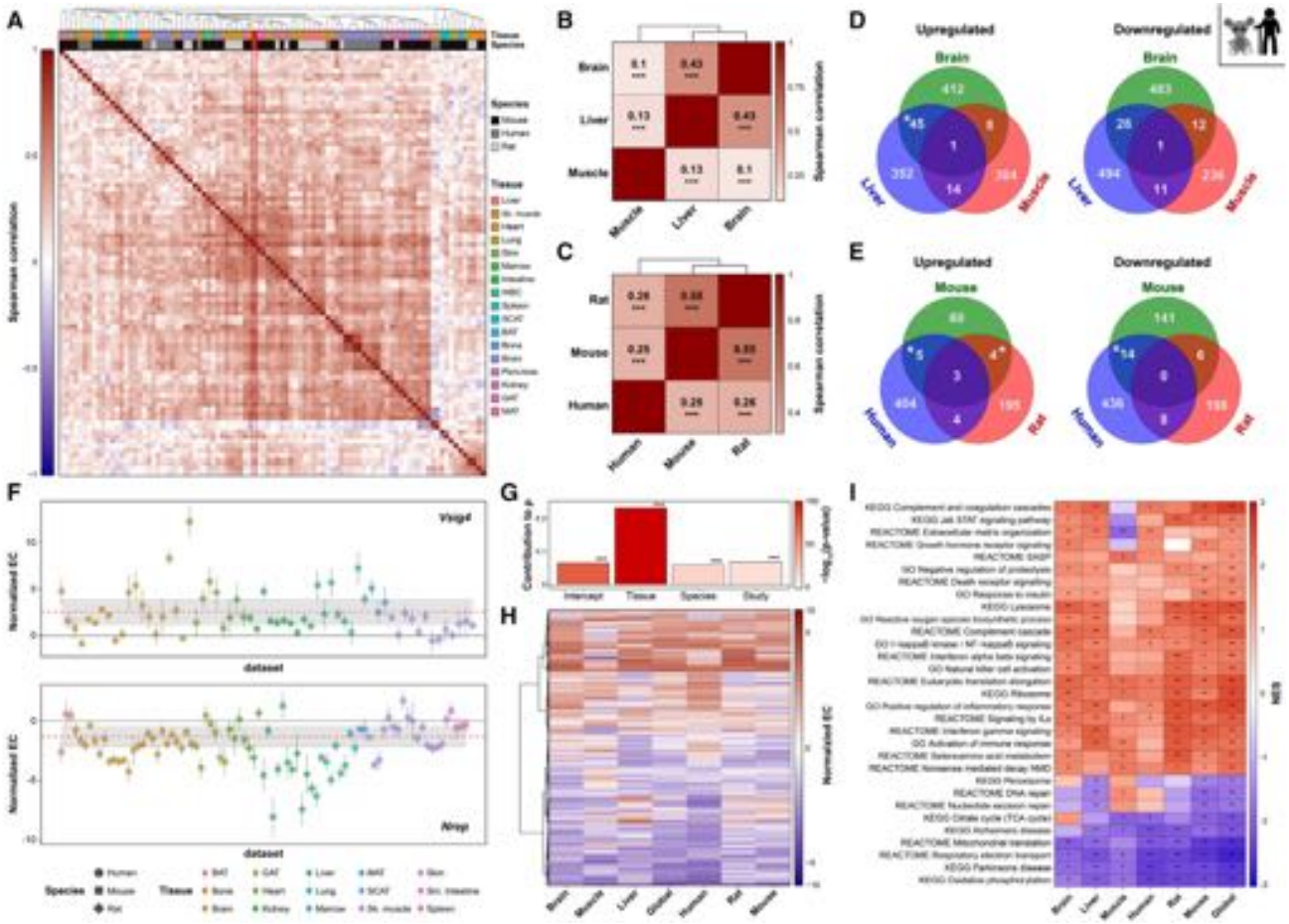

Figure 3. Transcriptomic signatures of mammalian aging

(A) Spearman correlation of age-related expression changes (ECs) across datasets estimated using a global aging signature. Red frame highlights aggregated (global) age-related ECs.

(B and C) Spearman correlation of aging-associated ECs between tissues (B) and species (C). Text and asterisks represent correlation coefficient and adjusted p value, respectively.

(D and E) Overlap of genes with significant age-related ECs across tissues (D) and species (E). p value was calculated with Fisher exact tests.

(F) *Vsig4* (upper) and *Nrep* (lower) age-related ECs. Each dot represents normalized average gene EC calculated from a single dataset ± SE. Red dotted line and shaded area represent weighted mean EC estimated using mixed-effect model and 95% confidence interval, respectively.

(G) Contribution of tissue, species, and source to pairwise Spearman correlation of age-related ECs. Bar color and asterisks reflect the statistical significance of factor contribution, assessed with multiple linear regression.

(H) Normalized age-associated ECs across tissues and species. Only genes significantly associated with aging in at least one signature (p adjusted < 0.05) are shown.

(I) Functional enrichment (GSEA) of aging signatures. Only functions significantly enriched by at least one signature are shown (p adjusted < 0.1). The whole list of enriched functions is in Table S3B.

°p adjusted < 0.1; *p adjusted < 0.05; **p adjusted < 0.01; ***p adjusted < 0.001.

WBC, white blood cells; SCAT, subcutaneous adipose tissue; BAT, brown adipose tissue; MAT, marrow adipose tissue; muscle, skeletal muscle.

See also Figures S3 and S4 and Tables S1 and S3.

We observed a higher similarity for age-related ECs from the same tissue or species (Figures 3G and S3B), although a positive correlation was detected even for ECs from different tissues, species, and sources ($p < 10^{-25}$), suggesting that there are also universal molecular mechanisms of mammalian aging.

Following the normalization of age-related ECs via multiple Deming regression (Figure S4) and quantitative meta-analysis based on a linear mixed-effect model (see STAR Methods), we identified ~200–900 statistically significant gene expression signatures of aging (p adjusted < 0.05) for individual tissues (liver, brain, and skeletal muscle) and species (human, mouse, and rat). We also discovered 13 universal aging-associated genes shared across 3 species and 17 tissues. As expected, age-related ECs exhibited a stronger positive correlation across datasets when estimated using significant signature genes (Figures 3A and S3C). To verify the introduced algorithm, we

conducted 4-fold cross-validation, identifying significant age-associated biomarkers in a training set and applying them to calculate the correlation between ECs from independent test datasets. The utilized normalization and meta-analysis approach resulted in higher correlations across test ECs (p adjusted = 10^{-15}) (Figure S3D), supporting the generalizability of the discovered molecular features of aging.

Aging signatures of all examined tissues and species were positively correlated with each other (Figures 3B and 3C). Some of them also exhibited significant pairwise overlaps between aging-associated genes (Figures 3D and 3E). Similar to biomarkers of species longevity, age-related transcriptomic changes were mainly driven by widely expressed genes, detected, on average, in >48% of the cell types (Figure S3E). Blood cell-specific biomarkers accounted for <5% of the aging-associated genes, and their removal did not affect the significant positive correlation between age-related ECs of individual tissues and species (Spearman $\rho > 0.1$; p adjusted < 10^{-5}), suggesting that molecular mechanisms of aging are generally conserved across various cell types.

Among top genes associated with aging in most tissues and species, we identified *Vsig4* and *Nrep*, up- and downregulated with age, respectively (global signature p adjusted < 0.05) (Figure 3F). *Vsig4* encodes an immune checkpoint protein, whose expression is positively correlated with the physiological frailty index in male mice,[56] and the progression of cancer[57–59] and several inflammatory diseases[60] in humans. Downregulation of *Nrep* was found to produce learning and memory defects,[61] blood pressure abnormalities,[62] and obesity.[63] Based on our meta-analysis, these genes may be considered universal deleterious signatures of aging, shared by multiple species and tissues.

Individual tissues and species demonstrated similar transcriptomic age-related changes both at the level of individual genes (Figure 3H) and enriched functions (Figure 3I). Functional GSEA revealed a number of shared aging mechanisms across organs and species (Table S3B), including the upregulation of pathways associated with established hallmarks of aging, such as biosynthesis of reactive oxygen species, senescence-associated secretory phenotype (SASP), and inflammation.[64,65] In contrast, genes involved in energy metabolism and mitochondrial translation were significantly downregulated with age, according to multiple signatures (Figure 3I).

Global interplay between signatures of longevity and aging

To examine the relationship between molecular mechanisms of longevity and aging, we performed a correlation analysis of the identified signatures along with mouse gene expression patterns of lifespan-extending interventions discovered previously[33] (Figure 4A). The latter included genes differentially expressed in response to individual interventions (CR, rapamycin, and mutations associated with GH deficiency), shared biomarkers of longevity interventions, and ECs associated with their effect on murine maximum and median lifespans. Transcriptomic signatures were generally consistent within each examined model: aging, species longevity, and lifespan-extending interventions (median Spearman $\rho > 0.55$ within each model). Biomarkers of aging were negatively correlated with several signatures of interventions, including CR, rapamycin, and biomarkers of maximum and median lifespan (median Spearman $\rho = -0.11$) (Figures 4A and 4B). This dependence may be partly driven by the decreased biological age of intervention-treated animals, as previously demonstrated at the level of DNA methylation.[66–68] In contrast, features of long-lived species strikingly showed a significant positive association with aging across different tissues (median Spearman $\rho = 0.16$). Since animals used to identify signatures of species longevity had a similar biological age (young adults), this finding can hardly be explained by selection bias. Rather, it seems to indicate that not all age-related changes are harmful and that adaptive (compensatory) molecular mechanisms regulated by gene expression are also involved,[69] being at the same time selected in long-lived species. Interestingly, transcriptomic patterns of longevity across species and lifespan extension within species did not show a strong correlation, exhibiting both shared and distinct features (Figures 4A and 4B).

To establish if the observed global patterns were reproduced in evolutionarily distinct taxons of life, we performed a similar analysis in the budding yeast model, utilizing (1) gene expression biomarkers of replicative lifespan (RLS) across 40 naturally evolved strains of *Saccharomyces cerevisiae*,[70] (2) signatures of RLS in lab yeast strains affected by 1,376 single-gene deletions,[71,72] and (3) transcriptomic biomarkers of yeast replicative aging.[73] Interestingly, the interplay between yeast signatures of aging, lifespan-extending deletions, and longevity across evolved strains was consistent with the patterns observed in mammals (Figure S5A). Gene expression signatures of yeast aging were positively correlated with those of long-lived natural strains and negatively with those of lifespan-extending mutations, suggesting that divergence of molecular mechanisms of longevity in response to simple interventions and selection at great evolutionary distances may be a universal pattern shared across distinct branches of life.

Common and distinct biomarkers of longevity and aging

To reveal shared and distinct molecular features of mammalian longevity and aging, we aggregated individual transcriptomic signatures within every model using HMP,[48] obtaining >450 statistically significant genes in each case. Consistent with the correlation analysis, we observed a significant overlap between co-regulated aggregated signatures of aging and long-lived species ($p = 1.8 \times 10^{-20}$), whereas aggregated biomarkers of lifespan-extending interventions were enriched for genes counteracting aging ($p = 7.5 \times 10^{-6}$) (Figure 4C).

Interestingly, 9 genes were significantly co-regulated with age and in both longevity models (Table S4). They included *Igf1*, a crucial component of insulin and IGF-1 signaling.[20,74] Reduced activity of IGF-1 extends lifespan in various species ranging from yeasts to mice.[74] IGF-1 plasma level in mice is decreased by established lifespan-extending interventions, including GHRKO[75] and CR,[76] and declines with age,[77] providing an example of a healthspan-promoting aging feature. Based on our data, decreased expression of *Igf1* is a universal biomarker of aging and longevity (Figure 4D, upper left), shared by lifespan-extending interventions and long-lived mammals, even after adjustment for AW ($p < 0.012$ for liver signatures).

Please cite this article in press as: Tyshkovskiy et al., Distinct longevity mechanisms across and within species and their association with aging, Cell (2023), https://doi.org/10.1016/j.cell.2023.05.002

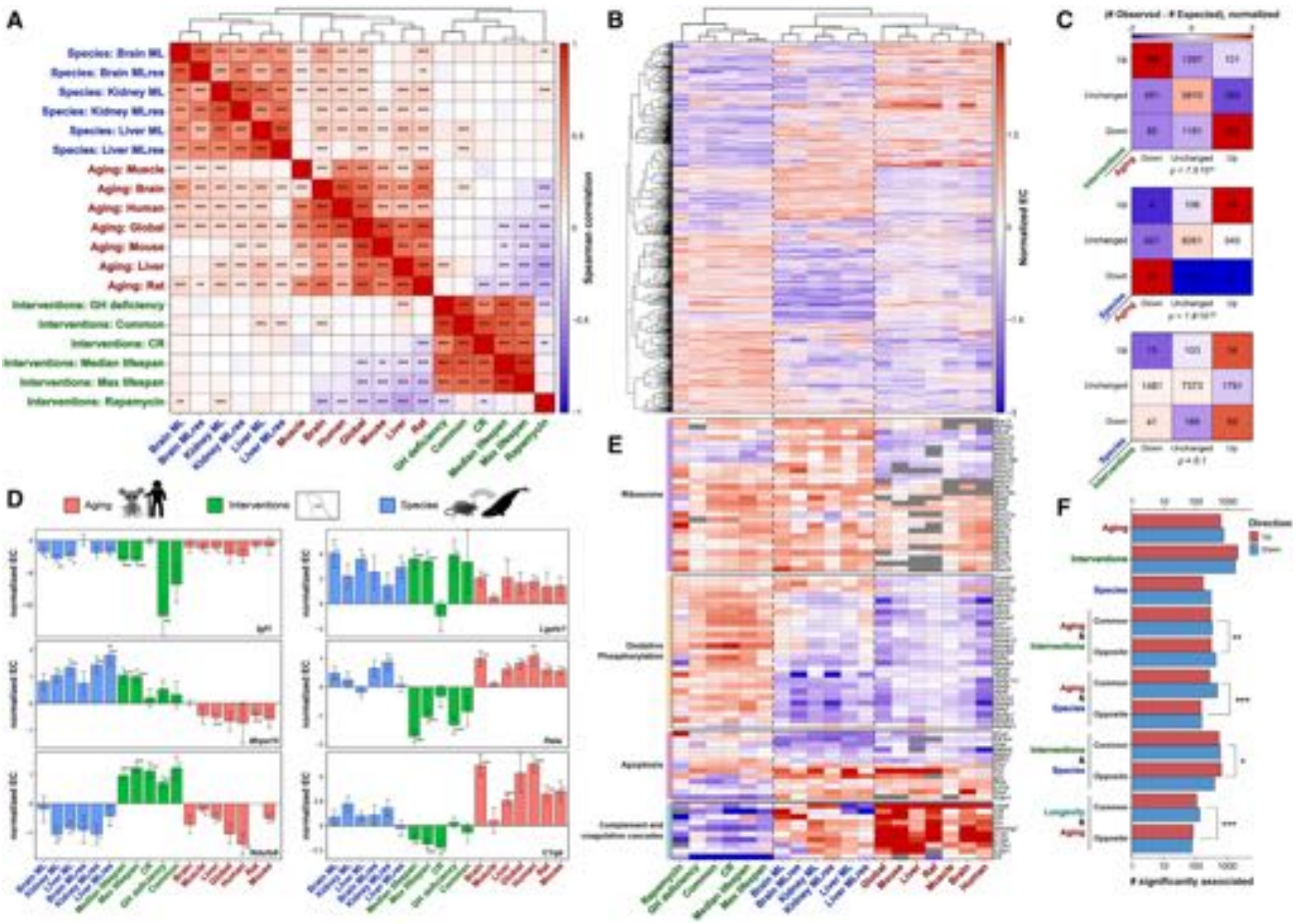

Figure 4. Interplay between transcriptomic signatures of aging and longevity

(A) Denoised Spearman correlation of signatures of aging (red), lifespan-extending interventions (green), and species longevity (blue). Asterisks reflect statistical significance of each pairwise correlation.

(B) Normalized expression changes (ECs) of genes associated with aging and longevity. Only genes significantly associated with at least one trait are shown (p adjusted < 0.05). x axis represents individual signatures.

(C) Overlap of aging- and longevity-associated genes. Number of aggregated signature genes and deviation from the expected random overlap are indicated with text and color, respectively. p value was estimated with Pearson's chi-square tests.

(D) Association of *Igf1*, *Mrps15*, *Ndufa9*, *Lgals1*, *Rela*, and *C1qb* expressions with aging and longevity. Statistical significance of each association denoted with asterisks was estimated with phylogenetic regression (for species longevity signatures) and mixed-effect model (for other signatures). Data are mean normalized ECs ± SE.

(E) Functional enrichment of gene signatures shared by several models. Presented functions were annotated by Kyoto Encyclopedia of Genes and Genomes (KEGG). Missing data are shown in gray.

(F) Number of aggregated, shared, and distinct signature genes associated with aging and longevity. For each pair of models, the difference between the number of co-regulated and distinct genes was assessed using two-sample proportion tests.

'p adjusted < 0.1; *p adjusted < 0.05; **p adjusted < 0.01; ***p adjusted < 0.001.

CR, calorie restriction; GH, growth hormone; Common, shared signatures of longevity interventions; Median/Max lifespan, signatures of intervention effect on median/maximum mouse lifespan; ML, maximum lifespan; MLres, maximum lifespan residual; Longevity, shared biomarkers of lifespan-extending interventions and long-lived species.

See also Figure S5 and Table S4.

In contrast, *Lgals1* demonstrated a positive association with all examined models (Figure 4D, upper right). Its product, Galectin-1 (Gal-1), regulates cell proliferation and has a prominent anti-inflammatory and proangiogenic activity[78,79] that is protective during recovery from cardiovascular diseases.[80] Mice lacking Gal-1 demonstrated cardiac inflammation and increased susceptibility to chronic inflammatory diseases.[81] Gal-1 was also decreased in the cerebrospinal fluid of patients with Parkinson's disease.[82] Therefore, its upregulation with age, especially in the brain (p adjusted = 0.004), and in the longevity models may provide a beneficial effect, protecting against aging-related chronic inflammation.

Utilizing Fisher's combined probability test,[83] we identified a comprehensive list of common and distinct molecular biomarkers

Please cite this article in press as: Tyshkovskiy et al., Distinct longevity mechanisms across and within species and their association with aging, Cell (2023), https://doi.org/10.1016/j.cell.2023.05.002

of longevity and aging (see STAR Methods). Consistent with previous results, we detected more distinct than shared features of aging and lifespan-extending interventions (p adjusted = 0.0045), whereas more co-regulated signatures were observed for aging and long-lived species (p adjusted = 7.4×10^{-48}) and for long-lived species and interventions (p adjusted = 0.012) (Figure 4F). Shared signatures of species longevity and aging included genes involved in oxidative phosphorylation (e.g., *Ndufa9*), apoptosis (e.g., *Rela*), and complement and coagulation cascades (e.g., *C1qb*) (Figures 4D and 4E). Interestingly, the expression of these genes was changed in the opposite direction by lifespan-extending interventions. In contrast, some signatures were shared by both longevity models but not aging, including several mitochondrial ribosomal protein genes (e.g., *Mrps15*) (Figures 4D and 4E). Finally, >200 gene expression biomarkers were shared across aging and both longevity models (Figure 4F), further indicating that age-related changes may include not only harmful but also beneficial compensatory effects.

Longevity-associated metabolic pathways

To uncover specific metabolic mechanisms of longevity (Figures 5A–5C), we expanded gene expression signatures with the data on metabolite profiling.[27,33] Using a phylogenetic regression pipeline, we discovered metabolite biomarkers of ML across 26 mammalian species in various tissues, including brain, liver, kidney, and heart. By comparing metabolite profiles of wild-type mice and mice subjected to longevity interventions (acarbose, rapamycin, GHRKO, and Snell dwarf mice), we also identified metabolite signatures of lifespan extension within species.

Comparison of the identified metabolites revealed shared biomarkers of longevity, including adenosine, xanthosine, and succinic acid, whereas several others (e.g., uric acid) showed a distinct effect (Figure S5B). The metabolite signatures (Figures 5D–5G) were strongly supported by the corresponding transcriptomic signatures (Figures 5H–5J), allowing us to characterize metabolic pathways with consistent multi-omics association.

Uric acid exhibited one of the strongest associations with lifespan (Figure S5B). Its concentration in various tissues was higher in long-lived species but was reduced by lifespan-extending interventions in mice (Figure 5D), whereas its direct metabolite allantoin showed the opposite behavior (Figure 5E). In mammals, urate is converted to allantoin by urate oxidase (uricase).[84] Accordingly, the expression of uricase gene *Uox* in the liver was negatively correlated with ML across species (Figure 5H, upper). In part, this is related to the pseudogenization of the uricase gene in hominoids,[85–87] although its expression was also low in other long-lived mammals, including naked mole rats and Damaraland mole rats. In contrast, *Uox* was upregulated by lifespan-extending interventions in mice (Figure 5H, lower). Therefore, long-lived mammals seem to accumulate uric acid through the reduced activity of *Uox*, whereas the opposite happens in mice subjected to longevity interventions (Figure 5A).

Another metabolite regulated by lifespan-extending interventions is nicotinamide adenine dinucleotide (NAD^+). NAD^+ levels decline with age and affect SIRT1 function, whereas supplementation with nicotinamide mononucleotide (NMN) or nicotinamide riboside (NR) can improve healthspan in mouse models.[88–90] NAD^+ concentration in murine liver was substantially increased following longevity interventions (Figure 5F). Lifespan extension was also accompanied by upregulation of genes involved in NAD^+ biosynthesis, including *Naprt*, *Nampt*, *Nmnat3*, and *Nadsyn1*, encoding NAD^+ synthetase 1 (p adjusted < 0.008 for association with median and maximum mouse lifespan) (Figures 5I and S5C). In contrast, we did not observe a significant association between NAD^+ levels and ML across species. However, there was a slight accumulation of its precursor, quinolinic acid, in long-lived species (p adjusted = 0.09 for multi-tissue ML signature), along with the upregulation of *Nadsyn1* in the brain, even after the adjustment for AW (p < 0.007) (Figures 5I and S5C). Therefore, NAD^+ biosynthesis pathway may be involved in lifespan regulation, although its role appears to be more prominent at the intraspecies level (Figure 5B).

Genes involved in NAD^+ level regulation were also associated with aging and longevity in yeast. The deletion of genes encoding mitochondrial NAD^+ transporters extended the chronological lifespan of *S. cerevisiae*, whereas their overexpression resulted in a shorter lifespan.[91] We observed the downregulation of mitochondrial NAD^+ carrier *NDT1* in response to RLS-extending deletions and across long-lived natural strains, and its upregulation in aged yeast cells (Figure S5D). Besides, *NPT1*, involved in NAD^+ biosynthesis, was highly expressed in yeasts subjected to RLS-extending interventions (p adjusted < 6.7×10^{-3}).

Finally, metabolites negatively associated with mouse lifespan included L-cystathionine (Figure 5G), an intermediate product of methionine degradation. Depletion of this molecule was accompanied by significant upregulation of genes responsible for its conversion into glutathione,[92] including *Cth*, *Gclc*, and *Gss* (median p < 0.007 for association with median and maximum mouse lifespan) (Figure 5J). This pathway also leads to the production of H_2S, which accumulates in mice subjected to CR[76] and by itself extends the lifespan of roundworms.[93] Our results support the role of this pathway in longevity regulation, as it is induced by lifespan-extending interventions both at metabolite and gene expression levels (Figure 5C). Surprisingly, genes involved in cystathionine degradation were downregulated in long-lived species (median p < 0.004 for liver ML signature) (Figure 5J), providing another example of distinct longevity-associated features within and across species.

Cellular processes mediating longevity and aging

Functional enrichment analysis of individual transcriptomic signatures (Figure 6A; Table S3) and significant co-regulated and distinct biomarkers across various models (Figure 6B; Table S5A) highlighted cellular processes that mediate longevity regulation and aging. Resembling results obtained on individual genes, age-associated functional changes were positively correlated with patterns of species longevity and negatively correlated with features of lifespan-extending interventions (Figure S6A).

Upregulation of ribosome protein genes was among the most consistently shared functional signatures of aging and both longevity models (Figures 6A and 6B). However, although genes encoding cytosolic ribosomal proteins demonstrated a positive association with all examined traits, mitochondrial ribosomal protein genes were upregulated in both longevity models but

Please cite this article in press as: Tyshkovskiy et al., Distinct longevity mechanisms across and within species and their association with aging, Cell (2023), https://doi.org/10.1016/j.cell.2023.05.002

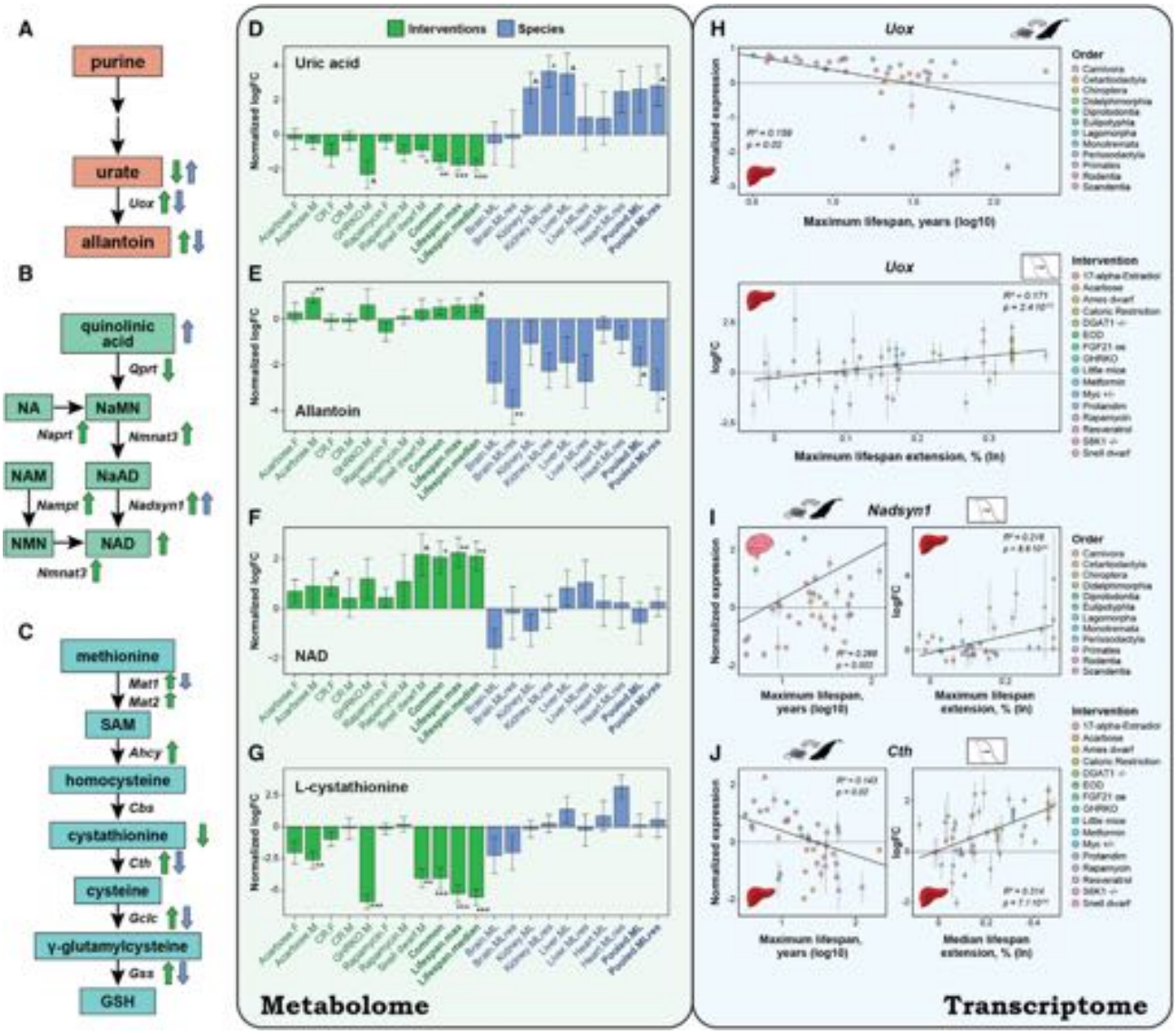

Figure 5. Molecular pathways associated with mammalian longevity

(A–C) Pathways associated with lifespan-extending interventions and species longevity. Metabolites and genes are shown in rectangles and Italic, respectively. Arrows represent significant positive (up) and negative (down) associations with longevity within (green) and across (blue) species.

(D–G)Association of uric acid (D), allantoin (E), NAD+ (F) and cystathionine (G) concentration with longevity within (green) and across (blue) species. The vertical axis reflects metabolite normalized logFC in murine liver in response to individual lifespan-extending interventions and aggregated across interventions (Common); slope of association with mouse median (Lifespan.median) and maximum lifespan (Lifespan.max); and slope of association with species maximum lifespan (ML) and maximum lifespan residual (MLres) in individual organs and aggregated across organs (Pooled). Error bars are ±SE.

(H–J) Association of *Uox* (H), *Nadsyn1* (I), and *Cth* (J) expressions with lifespan extension induced by interventions (survival curve icon) and across species (mouse/whale icon). Examined organs are reflected with liver and brain icons. The black line, slope p value and R^2 indicate the model fitted with phylogenetic (for species) or linear (for interventions) regression. Data are mean ± SE.

˙p adjusted < 0.1; *p adjusted < 0.05; **p adjusted < 0.01; ***p adjusted < 0.001.

CR, calorie restriction; EOD, every-other-day feeding; oe, overexpression; M, male; F, female; NA, nicotinic acid; NaMN, nicotinic acid mononucleotide; NaAD, nicotinic acid adenine dinucleotide; NAD, nicotinamide adenine dinucleotide; NMN, nicotinamide mononucleotide; NAM, nicotinamide; SAM, S-sdenosyl methionine; GSH, glutathione.

See also Figure S5.

downregulated with age (Figures 4D, 4E, and 6A). Mitochondrial translation was one of the most significant pathways enriched for gene expression signatures that separated longevity and aging (p adjusted = 5.7×10^{-6}) (Figure 6B), suggesting that mitochondrial function may be an essential conserved mechanism of lifespan regulation.

Energy metabolism, including the TCA cycle and oxidative phosphorylation, was significantly co-downregulated with age

Please cite this article in press as: Tyshkovskiy et al., Distinct longevity mechanisms across and within species and their association with aging, Cell (2023), https://doi.org/10.1016/j.cell.2023.05.002

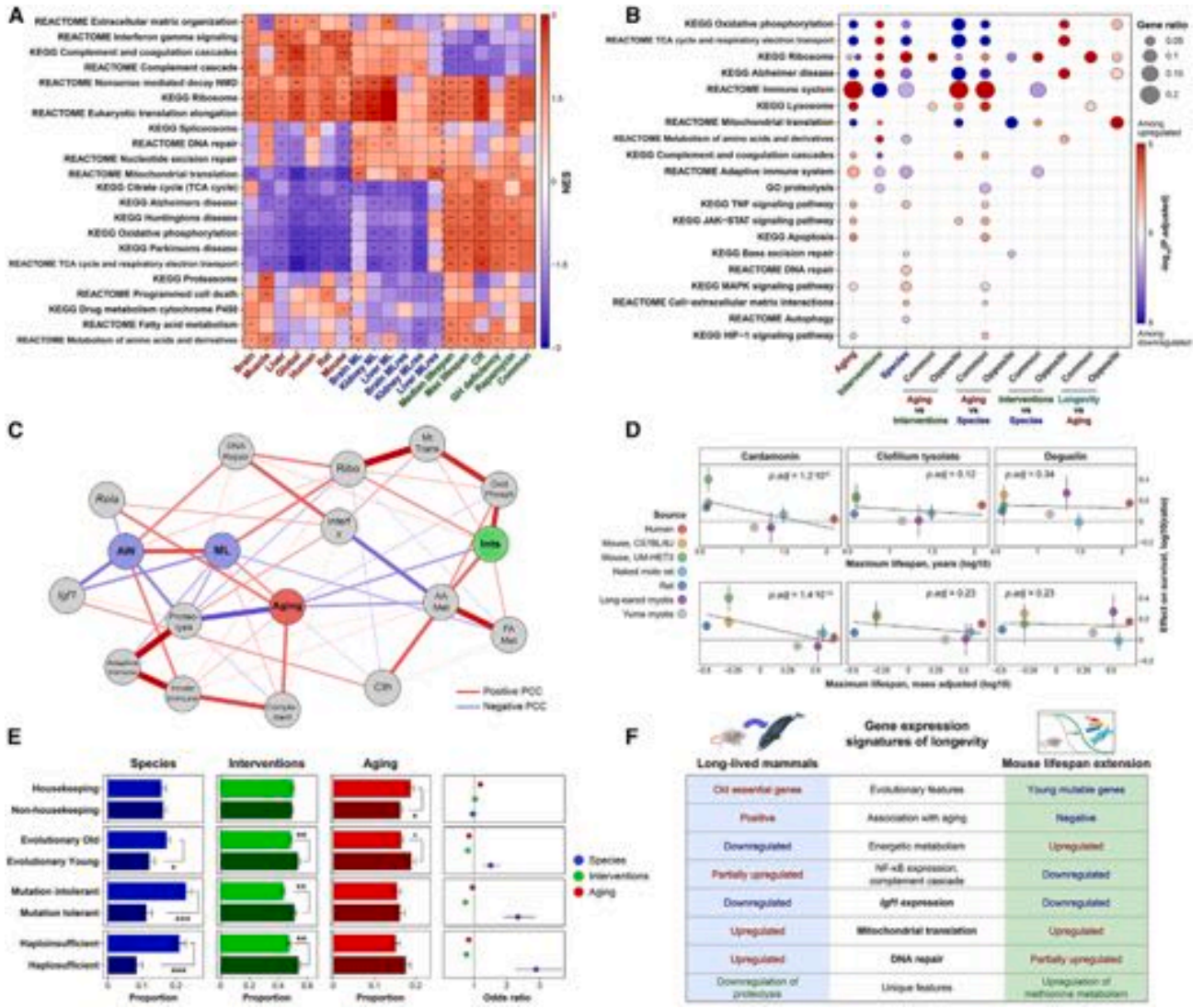

Figure 6. Common and distinct transcriptomic signatures of longevity

(A) Functional enrichment (GSEA) of longevity and aging-associated signatures. Only functions significantly enriched by at least one signature (p adjusted < 0.1) are presented. The whole list of enriched functions is in Table S3. NES, normalized enrichment score.

(B) Functional enrichment of aggregated, shared, and distinct signatures of longevity and aging. Proportion of pathway-associated genes and statistical significance estimated with Fisher exact test are reflected by bubble size and color, respectively. The whole list of functions is in Table S5A.

(C) Partial correlation network of gene expression signatures of longevity and aging. Sign of partial correlation coefficient (PCC) is indicated by color. AW, adult weight; Ints, signature of interventions effect on maximum lifespan; AA Met, metabolism of amino acids and derivatives; adaptive immune, adaptive immune system; complement, complement cascade; FA Met, fatty acid metabolism; innate immune, innate immune system; Interf γ, interferon gamma signaling; Mt trans, mitochondrial translation; Oxid Phosph, oxidative phosphorylation; Ribo, ribosome.

(D) Effect of cardamonin (left), clofilium tysolate (middle), and deguelin (right) on survival of fibroblasts from species with different lifespans following paraquat-induced oxidative stress. y axis displays log-ratio of the number of survived fibroblasts treated and untreated with the compound. x axis shows maximum lifespan unadjusted (top) and adjusted (bottom) for adult weight. Slope p value was assessed with mixed-effect linear model. Data are mean ± SE. n = 3–6 per treated and control group for every species/strain.

(E) Evolutionary features of longevity and aging-associated aggregated signature genes. Data are mean ± SE. Statistical significance of enrichment denoted with asterisks was assessed with Fisher's exact test.

(F) Common (bold), distinct, and unique transcriptomic signatures of longevity across and within species.

p adjusted < 0.1; *p adjusted < 0.05; **p adjusted < 0.01; ***p adjusted < 0.001.

ML, maximum lifespan; MLres, maximum lifespan residual.

See also Figure S6 and Tables S3 and S5.

Please cite this article in press as: Tyshkovskiy et al., Distinct longevity mechanisms across and within species and their association with aging, Cell (2023), https://doi.org/10.1016/j.cell.2023.05.002

and in long-lived species but upregulated by lifespan-extending interventions in mice (Figures 4D, 4E, 6A, and 6B). In contrast, genes associated with some branches of an innate immune response, including complement and coagulation cascades and tumor necrosis factor (TNF) signaling, were co-upregulated in aged animals and long-lived species, but not in response to lifespan-extending interventions (Figures 4D, 4E, 6A, and 6B). This association was also shared by *Rela*, a component of the NF-κB complex, a crucial regulator of inflammation and apoptosis.[94]

Inflammation and NF-κB activity facilitate the development of numerous age-related diseases,[94–97] and *Rela* targets are upregulated with age in several murine organs.[98] Based on our data, *Rela* expression is a universal biomarker of aging upregulated across different tissues, whereas its downregulation is associated with the extension of mouse lifespan (Figure 4D). Interestingly, *Rela* and other genes encoding NF-κB components were not downregulated in long-lived mammalian species, instead showing a trend toward positive association with species longevity (Figure 4D).

To examine the relationship between the identified mechanisms, we computed a sparse partial correlation network for features associated with longevity and aging (Figure 6C). Species AW was positively associated with the expression of genes involved in DNA repair and innate immune system response, pointing to the role of these pathways in cancer prevention, in agreement with Peto's paradox.[99] Even after the adjustment for AW and other features, species longevity was positively correlated with the expression of genes associated with complement cascade, DNA repair, translation, and aging and negatively correlated with *Igf1* expression and regulation of proteolysis and fatty acid metabolism. Complement cascade and proteolysis were strongly connected to aging, partially explaining its unexpected positive correlation with signatures of long-lived species. In contrast, intervention-induced mouse lifespan extension was associated with the upregulation of metabolic pathways (oxidative phosphorylation, fatty acid metabolism, and amino acid metabolism), translation and DNA repair, and downregulation of aging biomarkers, even after adjustment for all the examined features. Overall, longevity within and across species seems to be driven by multiple interconnected mechanisms, including age-related and independent regulators of lifespan.

We hypothesized that molecular signatures of lifespan-extending interventions in mice that are not shared by long-lived species, such as the inhibition of complement cascade and NF-κB pathway, may reflect marginally effective ways to promote longevity by regulating the response to the already accumulated damage. Since they have not been selected during the evolution of long-lived mammals, such approaches can be less effective in these organisms compared with short-lived species. In contrast, common signatures of longevity, including the upregulation of mitochondrial function and downregulation of *Igf1*, may represent core mechanisms that affect damage accumulation itself and can be effectively targeted in both short- and long-lived species.

To test this hypothesis, we subjected fibroblasts of mouse (inbred C57BL/6J and genetically heterogeneous UM-HET3 strains), rat, naked mole rat, western long-eared myotis, Yuma myotis, and human to oxidative stress using paraquat (dose close to LD50). Prior to stress induction, we treated cells with several compounds that promote mouse cell survival under these conditions[100]: cardamonin (CD), an inhibitor of NF-κB[101] and an activator of NRF2[100,102]; clofilium tysolate (CT), a K^+ channel blocker that facilitates mitochondrial DNA replication and restores mitochondrial mass in mutants with defective polymerase γ[103,104]; and deguelin (DG), a rotenoid that inhibits PI3K/Akt signaling[105] and upregulates mitochondrial translation genes.[106] We assessed if these compounds would also improve viability of cells obtained from long-lived species. As expected, all three compounds improved the average survival of mouse and rat fibroblasts subjected to oxidative stress (p adjusted < 0.011) (Figure 6D). However, the effect of CD was significantly reduced in fibroblasts of long-lived species, whereas CT and DG induced similar cell survival independent of species lifespan (Figure 6D, upper). The dependence of CD stress resistance effect on ML was even stronger after adjustment for animal AW (Figure 6D, bottom) and baseline level of cell survival under control conditions (Figure S6B), whereas the response to CT and DG did not depend on species ML after any of these adjustments. Therefore, the compound that targeted molecular mechanisms of mouse lifespan extension (NF-κB and NRF2 signaling) but not signatures of long-lived species was able to improve stress resistance of cells from short-lived species only. In contrast, compounds that targeted shared mechanisms of longevity (mitochondrial function and insulin signaling) had a comparable beneficial effect on cell survival independent of mammalian lifespan.

To make the identified transcriptomic signatures available to the research community, we developed an interactive database, mSALT (mammalian Signatures of Aging and Longevity Traits; http://gladyshevlab.org/mSALT/). For every gene, mSALT provides (1) a general association of its expression with various models of mammalian aging and longevity (Figure 4D); (2) the relationship between its expression and longevity across mammalian species (Figures 2A–2C); (3) the relationship between its expression and effect of various interventions on mouse lifespan (Figures 5H–5J); and (4) its age-related EC across various tissues and species (Figure 3F).

Evolutionary features of longevity-associated genes

To examine evolutionary features of longevity and aging biomarkers, we tested their enrichment for several characteristics, including involvement in the basic cellular maintenance, evolutionary age, mutation intolerance, and haploinsufficiency[44] (see STAR Methods). For every trait, we contrasted proportions of signature genes with opposite features (e.g., mutation tolerant/intolerant, evolutionary old/young, etc.), using randomly selected non-signature genes with a similar average expression level as a background (Figure S6C).

Significant overrepresentation of housekeeping genes was observed for aging biomarkers (odds ratio [OR] = 1.19, p adjusted = 0.038) (Figure 6E), indicating that aging is deeply connected with the reduction of core cellular homeostasis. Signatures of species longevity were enriched for evolutionary ancient genes, originated before the emergence of bony

vertebrates (OR = 1.5, p adjusted = 0.02), whereas transcriptomic biomarkers of lifespan-extending interventions were mostly evolutionary young genes originated in tetrapods (OR = 1.23, p adjusted = 0.003) (Figure 6E).

Gene essentiality was assessed by mutation intolerance, i.e., probability of being intolerant to gene loss-of-function mutation, and haploinsufficiency, i.e., sensitivity to a gene copy-number reduction. According to both metrics, signatures of long-lived species were enriched for essential genes (OR > 2, p adjusted < 10^{-4}) (Figure 6E). Biomarkers of lifespan-extending interventions showed the opposite pattern, being depleted for such genes (OR < 0.77, p adjusted < 0.004), underlying a significant difference in routes of lifespan regulation across and within species (Figure 6F). Essential evolutionarily old genes associated with species longevity were enriched for PI3K-Akt, cytokine, TNF and MAPK signaling, ubiquitin-mediated proteolysis, and cell cycle (Figure S6D; Table S5B), whereas evolutionarily young, mutation-tolerant signatures of lifespan-extending interventions were involved in metabolic pathways (fatty acid metabolism, respiratory electron transport, and peroxisome proliferator-activated receptor [PPAR] signaling), and complement and coagulation cascades (Figure S6E; Table S5C).

Longevity signatures reveal lifespan-regulating interventions

To discover genetic, environmental, and pharmacological interventions, whose effect on mammalian gene expression resembles transcriptomic signatures of aging and longevity, we utilized GeneQuery, a tool that searches for public datasets with similar ECs, and Connectivity Map (CMap), a resource containing transcriptomic profiles of human cells subjected to thousands of chemical compounds.[107,108]

Using GeneQuery, we identified 7 interventions in mice that induced ECs significantly associated with aggregated signatures of longevity and aging, including a hepatocyte-specific conditional knockout of *Keap1*,[109] chronic hypoxia,[110] high-fat diet,[111] deficiency of telomere-binding protein *Rap1*,[112] overexpression of p21 in skeletal muscle,[113] deficiency of *Dicer1* in hepatocytes,[114] and constitutive expression of NF-κB activator IKK2 in the liver[115] (Table S6A).

Utilizing a GSEA-based approach (see STAR Methods), we found that ECs generated by *Keap1* knockout and chronic hypoxia in mouse liver were positively associated with aggregated and multiple individual signatures of lifespan-extending interventions (CR, GH deficiency, etc.) (Figure 7A, upper). Accordingly, hypoxia response was protective against mitochondrial dysfunction associated with multiple aging-related diseases,[116,117] and chronic hypoxia extended healthspan and lifespan of mice with genetic mitochondrial disease produced by *Ndufs4* knockout.[116] KEAP1, an inhibitor of acute stress regulator NRF2, also significantly affects longevity. Its loss-of-function mutations extended the median lifespan of *Drosophila melanogaster* males,[118] whereas the overexpression of the NRF2 ortholog (SKN-1) increased the average lifespan of roundworms.[119] Based on our data, *Keap1* knockout and chronic hypoxia generate ECs associated with intraspecies longevity and do not significantly perturb aggregated biomarkers of aging or long-lived species, being good candidates for lifespan extension in healthy mice.

Other examined models induced ECs negatively associated with longevity interventions but positively associated with aging (Figure 7A, upper). Interestingly, some of them were also negatively correlated with aggregated signatures of long-lived species (e.g., *Dicer1* knockout), whereas others had no or even positive association (e.g., *Rap1* knockout and p21 overexpression). The identified models indeed exhibited age-related pathological phenotypes. Thus, high-fat diet produced hepatocellular damage, fibrosis, and reduced mitochondrial density in the liver and markedly affected lifespan of male C57BL/6J mice.[111] IKK2 activation in the liver generated severe chronic inflammation, also leading to organ fibrosis.[115] *Rap1* knockout induced glucose intolerance, liver steatosis, and excess fat accumulation associated with obesity.[112] Hepatocyte-specific deficiency of Dicer1, an enzyme involved in miRNA processing, produced progressive cellular damage, apoptosis, and inflammation in 2- to 4-month-old mice,[114,120] whereas its knockout in the skeletal muscle resulted in decreased muscle mass and abnormal myofiber morphology.[121] Finally, overexpression of tumor suppressor p21 induced cellular senescence in human cells[122,123] and contributed to the development of muscle atrophy.[113] Thus, aggregated signatures of lifespan-extending interventions and aging reasonably discriminate between potentially detrimental and beneficial interventions based on their effect on murine gene expression, whereas positive associations with biomarkers of long-lived species do not always result in the improvement of healthspan in short-lived mammals, as demonstrated by p21 overexpression and *Rap1* deficiency models.

Based on CMap predictions, we selected 3 chemical compounds that induced pro-longevity ECs according to signatures of lifespan-extending interventions and long-lived species, including PI3K inhibitor GDC-0941,[124] PKCβ and PI3K/Akt pathway inhibitor enzastaurin,[125] and MEK and TNF-α inhibitor AS-703026.[126,127] We applied these compounds orally to UM-HET3 male mice for 1 month and performed RNA-seq on their liver and kidney samples (Table S1C). Additionally, we expanded these data with transcriptomic profiles of mice subjected to 3 drugs identified in our previous study[33]: mTOR inhibitors KU0063794[128] and AZD8055,[129] and antioxidant ascorbyl-palmitate.[130]

By comparing expression profiles of treated mice with age-matched control samples, we identified compound-induced ECs in murine organs and examined their association with biomarkers of aging and longevity (Table S6B). Consistent with CMap predictions, all selected compounds generated changes positively associated with an aggregated signature of at least one longevity model (Figure 7A, lower). Moreover, pro-longevity effects of KU0063794, ascorbyl-palmitate, AZD8055, and GDC-0941 were supported simultaneously by aggregated biomarkers of lifespan-extending interventions (in the kidney and the liver; p adjusted < 0.004) and long-lived species (in kidney; p adjusted < 6×10^{-4}), along with multiple individual signatures (GH deficiency, CR, maximum and median lifespan, etc.).

To test if compounds that induce longevity-associated ECs extend murine lifespan and healthspan, we subjected 25-month-old C57BL/6 male mice to a diet containing a top hit from our analysis, KU0063794 (Figure 7B). KU0063794 at 10 ppm extended the remaining median and ML of old mice by

Please cite this article in press as: Tyshkovskiy et al., Distinct longevity mechanisms across and within species and their association with aging, Cell (2023), https://doi.org/10.1016/j.cell.2023.05.002

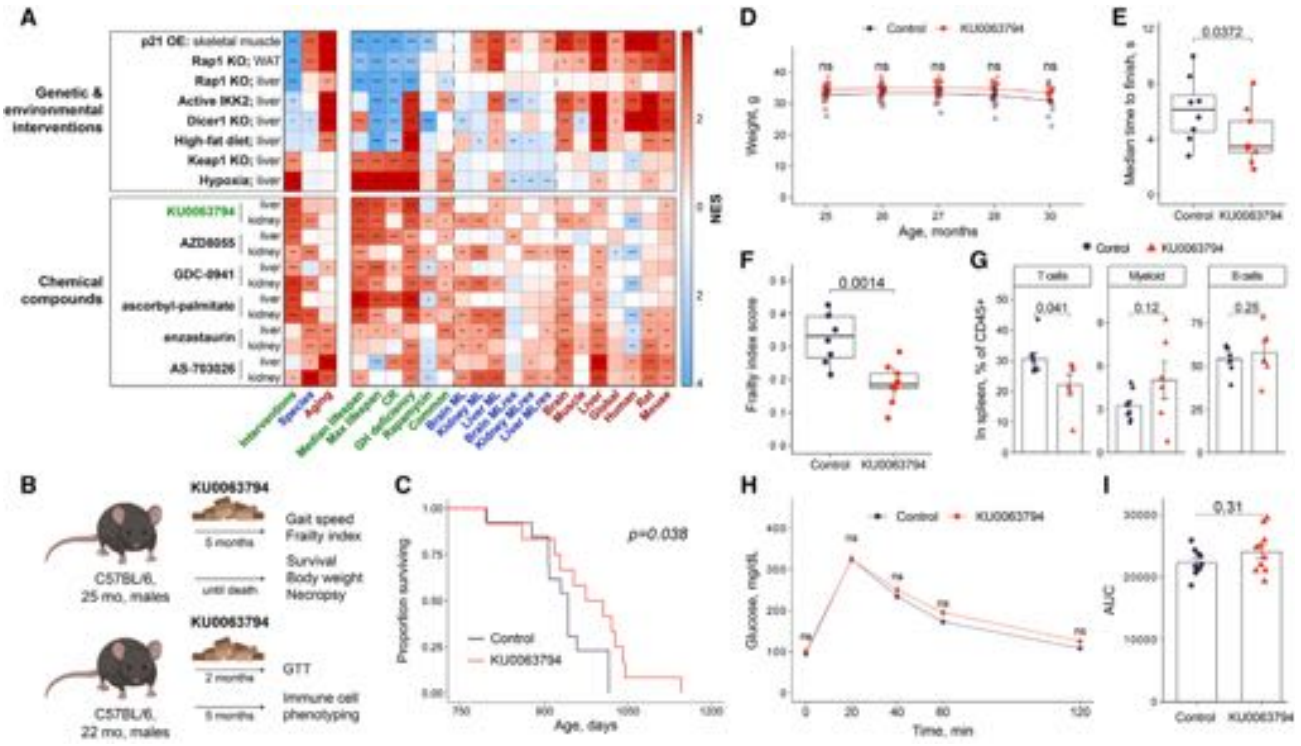

Figure 7. Transcriptomic longevity signatures reveal lifespan-regulating interventions

(A) Association of murine gene expression response to genetic, environmental (upper) and pharmacological (lower) interventions with signatures of aging (red), long-lived species (blue) and lifespan-extending interventions (green). Aggregated (left) and individual (right) signatures were utilized. Statistical significance denoted with asterisks was estimated with GSEA-based test. The output of the association analysis is in Table S6. ˙p adjusted < 0.1; *p adjusted < 0.05; **p adjusted < 0.01; ***p adjusted < 0.001.

(B) Design of the study testing the effect of KU0063794 on mouse survival and healthspan.

(C) Survival curves of male C57BL/6 mice subjected to KU0063794 (10 ppm) at 25 months old. p value was calculated with log-rank tests.

(D) Body weight of 30-month-old control and KU0063794-treated male C57BL/6 mice.

(E) Median time to finish measured in 30-month-old control and KU0063794-treated male C57BL/6 mice.

(F) Frailty index score of 30-month-old control and KU0063794-treated male C57BL/6 mice.

(G) Percentage of immune cell types in spleens of 27-month-old control and KU0063794-treated male C57BL/6 mice.

(H) Glucose tolerance in 24-month-old control and KU0063794-treated C57BL/6 mice. n = 10 for each group.

(I) Area under the curve (AUC) of glucose level shown in (H).

p values on (D)–(I) were calculated with one-tailed Wilcoxon rank-sum tests.

NES, normalized enrichment score; CR, calorie restriction; GH, growth hormone; ML, maximum lifespan; MLres, maximum lifespan residual; KO, knockout; OE, overexpression; WAT, white adipose tissue.

See also Figure S7 and Tables S1, S6, and S7.

32.6% and 10.9%, respectively (log-rank test p = 0.038) (Figure 7C), with no effect on animal body weight (Figure 7D). KU0063794 also improved mouse gait speed measured at 30 months (Figure 7E). The frailty index of mice before and 5 months after the treatment initiation showed no difference between the control and experimental groups prior to drug supplementation (Figure S7A); however, mice subjected to KU0063794 were significantly less frail following the treatment (Figure 7F). Detailed analyses also revealed a KU0063794-induced improvement of coat and eye-related features (Figure S7B).

Chronic treatment with another mTOR inhibitor, rapamycin, decreases the percentage of T cells in secondary lymphoid organs.[131] We tested if KU0063794 affected immune cell proportion in the spleen of 27-month-old mice after 5 months of treatment and observed a slightly reduced percentage of T cells relative to the total number of $CD45^+$ cells (Figure 7G). KU0063794 also affected the proportion of follicular B cells, but not other B cell populations (Figure S7C). Age-associated clonal B cells (ACBCs), which produce B cell lymphoma in aged mice,[132] were unaffected by KU0063794, suggesting that its lifespan-extending effect is not driven by the delay of B cell lymphoma.

Since chronic rapamycin treatment also leads to glucose intolerance in mice,[131] we performed a glucose tolerance test on a separate cohort of 24-month-old male mice subjected to KU0063794 for 2 months. KU0063794 did not affect glucose tolerance in old mice as there was no difference in glucose clearance dynamics between the control and treated groups (Figures 7H and 7I).

Please cite this article in press as: Tyshkovskiy et al., Distinct longevity mechanisms across and within species and their association with aging, Cell (2023), https://doi.org/10.1016/j.cell.2023.05.002

Necropsy analyses of mice from the lifespan cohort that died from natural causes or were euthanized due to the moribund state did not reveal significant differences in incidences of individual pathologies between control and treated groups (Table S7). Larger follow-up studies may provide more data on specific healthspan-promoting effects of KU0063794.

DISCUSSION

In this work, we characterized gene expression signatures of mammalian lifespan in 3 organs. Many patterns of species longevity were conserved across tissues, including up- and downregulation of genes associated with DNA repair and protein degradation, respectively. Interestingly, they were also observed in primary fibroblasts,[30] indicating that shared molecular mechanisms of longevity are presumably driven not only by the systemic effect of circulating signaling molecules (e.g., IGF-1) but also by genetically encoded features (e.g., mutations in regulatory regions). Activation, rather than suppression, of proteasome or autophagy extends the lifespan of model organisms, including roundworms,[133,134] fruit flies,[135] and mice.[136] Downregulation of proteolysis in long-lived species may be caused by higher accuracy of protein synthesis, lower level of damage, or better maintenance of the translation machinery.[137] Indeed, protein turnover rate is negatively correlated with species lifespan in mammals.[138]

The identified transcriptomic signatures were concordant with the metabolite data. Thus, urate concentration was positively correlated with species longevity, and the uricase gene expression was downregulated in long-lived mammals. Interestingly, the opposite effect was produced by lifespan-extending interventions in mice, demonstrating that different molecular mechanisms may be associated with longevity on short-term and evolutionary timescales. The double-edged sword effect of urate on healthspan is supported by its role both as an antioxidant and activator of the inflammasome, contributing to metabolic disorders.[139] Similarly, activation of genes involved in methionine metabolism was a specific feature of lifespan extension in mice, whereas the upregulation of NAD^+ biosynthesis induced by longevity interventions was only partially shared by long-lived mammals.

Mammalian age-related transcriptomic changes were also generally similar across different organs and species. Many of them were related to the established hallmarks of aging, including mitochondrial dysfunction, senescence, and inflammation.[64,65] Thus, detrimental molecular processes leading to the loss of physiological integrity appear to be partly modulated at the level of gene expression. Secretory signaling molecules associated with the accumulated damage, such as inflammatory cytokines, may be partially responsible for the induction of common aging-related changes across tissues, supported by the systemic effect of heterochronic parabiosis and plasma dilution on mouse organs.[140,141]

Comparison of the identified transcriptomic signatures of mammalian aging, species longevity, and lifespan-extending interventions in mice revealed a complex interplay between these traits. Overall, aging signatures were negatively correlated with features of mouse lifespan extension, suggesting that the beneficial effect of established longevity interventions may be associated with the deceleration of damage accumulation resulting in a younger biological age. At the same time, biomarkers of long-lived species were positively correlated with age-related changes. Genes responsible for this trend were involved in energy metabolism (e.g., oxidative phosphorylation) and certain branches of the innate immune response (e.g., complement cascade). This finding points to the existence of various strategies to achieve longevity (Figure 6F), some of which may be marginally efficient for short-lived species but do not provide a long-term benefit on an evolutionary timescale. In agreement with this hypothesis, CD, an inhibitor of the NF-κB complex, improved the survival of fibroblasts from short-lived species under oxidative stress but was significantly less effective in cells from long-lived mammals.

A positive association between biomarkers of aging and species longevity can also be driven by the multifaceted nature of age-related processes, incorporating both deleterious and adaptive effects, a pattern also observed for epigenetic changes in humans.[69] This hypothesis is further supported by the existence of signatures shared by aging and both longevity models, such as upregulation of ribosomal protein genes and downregulation of *Igf1*. The common adaptive effects can reflect the slowdown of damage accumulation achieved through the reduction of protein turnover rate and translation, which are associated with increased lifespan across species,[138] and occur during aging[142] and in response to lifespan-extending interventions.[143] On the other hand, shared biomarkers of longevity that display opposite association with aging, such as upregulated mitochondrial translation, may represent robust determinants of lifespan regulation through counteraction of harmful age-related changes driving the physiological deterioration. Accordingly, compounds that targeted these mechanisms provided similar improvement in cell survival to fibroblasts from short- and long-lived mammals.

Another notable difference between molecular signatures of longevity within and across species was the evolutionary age and essentiality of the corresponding genes. Biomarkers of long-lived species were enriched for evolutionarily ancient, mutation-intolerant genes, whereas lifespan-extending interventions mainly affected younger genes tolerant to mutations and copy-number variation. Overall, the data suggest that longevity on the evolutionary timescale is achieved by fine-tuning of fundamental machinery deep-rooted in natural history that affects primary damage emergence and rate of its accumulation (i.e., upregulation of DNA repair and innate immune response, and downregulation of the IGF-1 and PI3K-Akt pathway).[9] On the other hand, most established lifespan-extending interventions seem to operate through the modulation of less conserved components associated with metabolic remodeling (i.e., upregulation of oxidative phosphorylation and fatty acid and amino acid metabolisms) and deceleration of secondary detrimental processes induced in response to already accumulated damage (i.e., downregulation of NF-κB, and complement and coagulation cascades). These two mechanisms may represent complementary ways to deal with molecular damage and provide an instrument to search for efficient combinatorial therapies, targeting both longevity strategies simultaneously.

By employing the discovered signatures of longevity and aging, we identified several candidates for mouse healthspan and lifespan extension, including chronic hypoxia, hepatocyte-specific *Keap1* knockout, KU0063794, AZD8055, GDC-0941, and ascorbyl-palmitate. Interestingly, some of them were supported by both models of longevity, suggesting that they may be similarly effective in short- and long-lived mammalian species. In agreement with the prediction, one of the top candidates revealed by signature-based screening, KU0063794, significantly extended lifespan and healthspan of old C57BL/6 mice. Remarkably, its short-term effect on the transcriptomic profile was not negatively associated with aging, suggesting that it does not seem to be a necessary condition to achieve a longer lifespan. Future comprehensive studies may shed light on the differences in the mechanisms of longevity interventions operating via anti-aging or aging-independent routes. Thus, transcriptomic signatures of longevity may be used to identify lifespan- and healthspan-extending interventions based on their gene expression profiles, thereby facilitating the discovery of novel geroprotectors.

Limitations of the study

Some variation in biological age between examined species may be present due to the unknown precise age and exact health status of young adult animals collected in the wild. Future expansion of this dataset with samples of different ages for each species would be of high value for the identification of age-adjusted longevity signatures and analysis of differences in molecular mechanisms of aging across species. Besides, signatures of established lifespan-extending interventions identified for mouse models may not entirely translate to other mammals. The collection of similar data from other species would shed light on the universality and differences in mechanisms of CR, GH deficiency, and other interventions. Finally, the shared and distinct longevity signatures were analyzed based on transcriptomic and metabolomic data; however, multi-omics approaches may yield further insights into mechanisms of lifespan regulation.

STAR★METHODS

Detailed methods are provided in the online version of this paper and include the following:

ACKNOWLEDGMENTS

We thank Iaroslava Pavlova for valuable suggestions and assistance with data analysis and visualization. This study was supported by NIA grants to V.N.G., V.G., R.A.M., and N.J.S. A.T. and S.E.D. were members of Interdisciplinary Scientific and Educational School of Moscow University "Molecular Technologies of the Living Systems and Synthetic Biology."

AUTHOR CONTRIBUTIONS

A.T. and V.N.G. conceived and designed this research; A.T., S.M., A.V.S., S.T., S.-G.L., and J.P.C. performed research and data analysis; P.B., A.S., N.J.S., V.G., R.A.M., and V.N.G. contributed new reagents/sample/analytic tools; A.T., S.M., A.V.S., A.S., N.J.S., V.G., S.E.D., R.A.M., and V.N.G. interpreted the data; V.N.G. supervised the study; A.T. and V.N.G. wrote the manuscript with contributions from all other authors. All authors read the final version.

DECLARATION OF INTERESTS

A patent application (no. 17/625,425) is pending that includes some of the data described in this article.

INCLUSION AND DIVERSITY

We support inclusive, diverse, and equitable conduct of research.

Received: December 3, 2021
Revised: December 29, 2022
Accepted: May 2, 2023
Published: June 1, 2023

REFERENCES

1. Sacher, G.A. (1959). Relation of lifespan to brain weight and body weight in mammals. In Ciba Foundation Symposium - The Lifespan of Animals (Colloquia on Ageing), G.E.W. Wolstenholme and M. O'Conner, eds. (John Wiley Sons, Ltd), pp. 115–141. https://doi.org/10.1002/9780470715253.ch9.
2. de Magalhães, J.P., Costa, J., and Toussaint, O. (2005). HAGR: the human ageing genomic resources. Nucleic Acids Res. *33*, D537–D543. https://doi.org/10.1093/nar/gki017.

3. Buffenstein, R. (2008). Negligible senescence in the longest living rodent, the naked mole-rat: insights from a successfully aging species. J. Comp. Physiol. B *178*, 439–445. https://doi.org/10.1007/s00360-007-0237-5.

4. Seim, I., Fang, X., Xiong, Z., Lobanov, A.V., Huang, Z., Ma, S., Feng, Y., Turanov, A.A., Zhu, Y., Lenz, T.L., et al. (2013). Genome analysis reveals insights into physiology and longevity of the Brandt's bat Myotis brandtii. Nat. Commun. *4*, 2212. https://doi.org/10.1038/ncomms3212.

5. Ma, S., and Gladyshev, V.N. (2017). Molecular signatures of longevity: insights from cross-species comparative studies. Semin. Cell Dev. Biol. *70*, 190–203. https://doi.org/10.1016/j.semcdb.2017.08.007.

6. Zhao, Y., Tyshkovskiy, A., Muñoz-Espín, D., Tian, X., Serrano, M., de Magalhaes, J.P., Nevo, E., Gladyshev, V.N., Seluanov, A., and Gorbunova, V. (2018). Naked mole rats can undergo developmental, oncogene-induced and DNA damage-induced cellular senescence. Proc. Natl. Acad. Sci. USA *115*, 1801–1806. https://doi.org/10.1073/pnas.1721160115.

7. Harper, J.M., Salmon, A.B., Leiser, S.F., Galecki, A.T., and Miller, R.A. (2007). Skin-derived fibroblasts from long-lived species are resistant to some, but not all, lethal stresses and to the mitochondrial inhibitor rotenone. Aging Cell *6*, 1–13. https://doi.org/10.1111/j.1474-9726.2006.00255.x.

8. Whittemore, K., Vera, E., Martínez-Nevado, E., Sanpera, C., and Blasco, M.A. (2019). Telomere shortening rate predicts species life span. Proc. Natl. Acad. Sci. USA *116*, 15122–15127. https://doi.org/10.1073/pnas.1902452116.

9. Tian, X., Seluanov, A., and Gorbunova, V. (2017). Molecular mechanisms determining lifespan in short- and long-lived species. Trends Endocrinol. Metab. *28*, 722–734. https://doi.org/10.1016/j.tem.2017.07.004.

10. Cagan, A., Baez-Ortega, A., Brzozowska, N., Abascal, F., Coorens, T.H.H., Sanders, M.A., Lawson, A.R.J., Harvey, L.M.R., Bhosle, S., Jones, D., et al. (2022). Somatic mutation rates scale with lifespan across mammals. Nature *604*, 517–524. https://doi.org/10.1038/s41586-022-04618-z.

11. Zhou, Y., Xu, V., Maheshwari, H.G., He, L., Reed, M., Lozykowski, M., Okada, S., Cataldo, L., Coschigamo, K., Wagner, T.E., et al. (1997). A mammalian model for Laron syndrome produced by targeted disruption of the mouse growth hormone receptor/binding protein gene (the Laron mouse). Proc. Natl. Acad. Sci. USA *94*, 13215–13220. https://doi.org/10.1073/pnas.94.24.13215.

12. Harrison, D.E., Strong, R., Sharp, Z.D., Nelson, J.F., Astle, C.M., Flurkey, K., Nadon, N.L., Wilkinson, J.E., Frenkel, K., Carter, C.S., et al. (2009). Rapamycin fed late in life extends lifespan in genetically heterogeneous mice. Nature *460*, 392–395. https://doi.org/10.1038/nature08221.

13. Weindruch, R., Walford, R.L., Fligiel, S., and Guthrie, D. (1986). The retardation of aging in mice by dietary restriction: longevity, cancer, immunity and lifetime energy intake. J. Nutr. *116*, 641–654. https://doi.org/10.1093/jn/116.4.641.

14. David, J., Van Herrewege, J., and Fouillet, P. (1971). Quantitative underfeeding of drosophila: effects on adult longevity and fecundity. Exp. Gerontol. *6*, 249–257. https://doi.org/10.1016/0531-5565(71)90037-4.

15. Houthoofd, K., and Vanfleteren, J.R. (2006). The longevity effect of dietary restriction in *Caenorhabditis elegans*. Exp. Gerontol. *41*, 1026–1031. https://doi.org/10.1016/j.exger.2006.05.007.

16. Lin, S., Defossez, P., and Guarentet, L. (2000). Requirement of NAD and SIR2 for life-span extension by calorie restriction in Saccharomyces cerevisiae. Science *289*, 2126–2128. https://doi.org/10.1126/science.289.5487.2126.

17. Selman, C., Nussey, D.H., and Monaghan, P. (2013). Ageing: It's a dog's life. Curr. Biol. *23*, R451–R453. https://doi.org/10.1016/j.cub.2013.04.005.

18. Brown-Borg, H.M., Borg, K.E., Meliska, C.J., and Bartke, A. (1996). Dwarf mice and the ageing process. Nature *384*, 33. https://doi.org/10.1038/384033a0.

19. Flurkey, K., Papaconstantinou, J., Miller, R.A., and Harrison, D.E. (2001). Lifespan extension and delayed immune and collagen aging in mutant mice with defects in growth hormone production. Proc. Natl. Acad. Sci. USA *98*, 6736–6741. https://doi.org/10.1073/pnas.111158898.

20. Junnila, R.K., List, E.O., Berryman, D.E., Murrey, J.W., and Kopchick, J.J. (2013). The GH/IGF-1 axis in ageing and longevity. Nat. Rev. Endocrinol. *9*, 366–376. https://doi.org/10.1038/nrendo.2013.67.

21. Sziráki, A., Tyshkovskiy, A., and Gladyshev, V.N. (2018). Global remodeling of the mouse DNA methylome during aging and in response to calorie restriction. Aging Cell *17*, e12738. https://doi.org/10.1111/acel.12738.

22. Meer, M.V., Podolskiy, D.I., Tyshkovskiy, A., and Gladyshev, V.N. (2018). A whole lifespan mouse multi-tissue DNA methylation clock. eLife *7*, 1–16. https://doi.org/10.7554/eLife.40675.

23. Schaum, N., Lehallier, B., Hahn, O., Pálovics, R., Hosseinzadeh, S., Lee, S.E., Sit, R., Lee, D.P., Losada, P.M., Zardeneta, M.E., et al. (2020). Ageing hallmarks exhibit organ-specific temporal signatures. Nature *583*, 596–602. https://doi.org/10.1038/s41586-020-2499-y.

24. Almanzar, N., Antony, J., Baghel, A.S., Bakerman, I., Bansal, I., Barres, B.A., Beachy, P.A., Berdnik, D., Bilen, B., and Brownfield, D. (2020). A single-cell transcriptomic atlas characterizes ageing tissues in the mouse. Nature *583*, 590–595. https://doi.org/10.1038/s41586-020-2496-1.

25. Palmer, D., Fabris, F., Doherty, A., Freitas, A.A., and de Magalhães, J.P. (2021). Ageing transcriptome meta-analysis reveals similarities and differences between key mammalian tissues. Aging (Albany NY) *13*, 3313–3341. https://doi.org/10.18632/aging.202648.

26. de Magalhães, J.P., Curado, J., and Church, G.M. (2009). Meta-analysis of age-related gene expression profiles identifies common signatures of aging. Bioinformatics *25*, 875–881. https://doi.org/10.1093/bioinformatics/btp073.

27. Ma, S., Yim, S.H., Lee, S.G., Kim, E.B., Lee, S.R., Chang, K.T., Buffenstein, R., Lewis, K.N., Park, T.J., Miller, R.A., et al. (2015). Organization of the Mammalian Metabolome according to Organ Function, Lineage Specialization, and Longevity. Cell Metab. *22*, 332–343. https://doi.org/10.1016/j.cmet.2015.07.005.

28. Ma, S., Lee, S.G., Kim, E.B., Park, T.J., Seluanov, A., Gorbunova, V., Buffenstein, R., Seravalli, J., and Gladyshev, V.N. (2015). Organization of the mammalian ionome according to organ origin, lineage specialization, and longevity. Cell Rep. *13*, 1319–1326. https://doi.org/10.1016/j.celrep.2015.10.014.

29. Bozek, K., Khrameeva, E.E., Reznick, J., Omerbašić, D., Bennett, N.C., Lewin, G.R., Azpurua, J., Gorbunova, V., Seluanov, A., Regnard, P., et al. (2017). Lipidome determinants of maximal lifespan in mammals. Sci. Rep. *7*, 5. https://doi.org/10.1038/s41598-017-00037-7.

30. Ma, S., Upneja, A., Galecki, A., Tsai, Y.M., Burant, C.F., Raskind, S., Zhang, Q., Zhang, Z.D., Seluanov, A., Gorbunova, V., et al. (2016). Cell culture-based profiling across mammals reveals DNA repair and metabolism as determinants of species longevity. eLife *5*, 1–25. https://doi.org/10.7554/eLife.19130.

31. Fushan, A.A., Turanov, A.A., Lee, S.G., Kim, E.B., Lobanov, A.V., Yim, S.H., Buffenstein, R., Lee, S.R., Chang, K.T., Rhee, H., et al. (2015). Gene expression defines natural changes in mammalian lifespan. Aging Cell *14*, 352–365. https://doi.org/10.1111/acel.12283.

32. Lu, J.Y., Simon, M., Zhao, Y., Ablaeva, J., Corson, N., Choi, Y., Yamada, K.Y.H., Schork, N.J., Hood, W.R., Hill, G.E., et al. (2022). Comparative transcriptomics reveals circadian and pluripotency networks as two pillars of longevity regulation. Cell Metab. *34,* 836–856.e5. https://doi.org/10.1016/j.cmet.2022.04.011.

33. Tyshkovskiy, A., Bozaykut, P., Borodinova, A.A., Gerashchenko, M.V., Ables, G.P., Garratt, M., Khaitovich, P., Clish, C.B., Miller, R.A., and Gladyshev, V.N. (2019). Identification and application of gene expression signatures associated with lifespan extension. Cell Metab. *30,* 573–593.e8. https://doi.org/10.1016/j.cmet.2019.06.018.

34. Kim, E.B., Fang, X., Fushan, A.A., Huang, Z., Lobanov, A.V., Han, L., Marino, S.M., Sun, X., Turanov, A.A., Yang, P., et al. (2011). Genome sequencing reveals insights into physiology and longevity of the naked mole rat. Nature *479*, 223–227. https://doi.org/10.1038/nature10533.

35. Seim, I., Ma, S., Zhou, X., Gerashchenko, M.V., Lee, S.G., Suydam, R., George, J.C., Bickham, J.W., and Gladyshev, V.N. (2014). The transcriptome of the bowhead whale Balaena mysticetus reveals adaptations of the longest-lived mammal. Aging (Albany NY) *6*, 879–899. https://doi.org/10.18632/aging.100699.

36. Fang, X., Seim, I., Huang, Z., Gerashchenko, M.V., Xiong, Z., Turanov, A.A., Zhu, Y., Lobanov, A.V., Fan, D., Yim, S.H., et al. (2014). Adaptations to a subterranean environment and longevity revealed by the analysis of mole rat genomes. Cell Rep. *8*, 1354–1364. https://doi.org/10.1016/j.celrep.2014.07.030.

37. Brawand, D., Soumillon, M., Necsulea, A., Julien, P., Csárdi, G., Harrigan, P., Weier, M., Liechti, A., Aximu-Petri, A., Kircher, M., et al. (2011). The evolution of gene expression levels in mammalian organs. Nature *478*, 343–348. https://doi.org/10.1038/nature10532.

38. Merkin, J., Russell, C., Chen, P., and Burge, C.B. (2012). Evolutionary dynamics of gene and isoform regulation in mammalian tissues. Science *338*, 1593–1599. https://doi.org/10.1126/science.1228186.

39. Yim, H.S., Cho, Y.S., Guang, X., Kang, S.G., Jeong, J.Y., Cha, S.S., Oh, H.M., Lee, J.H., Yang, E.C., Kwon, K.K., et al. (2014). Minke whale genome and aquatic adaptation in cetaceans. Nat. Genet. *46*, 88–92. https://doi.org/10.1038/ng.2835.

40. Fan, Y., Huang, Z.Y., Cao, C.C., Chen, C.S., Chen, Y.X., Fan, D.D., He, J., Hou, H.L., Hu, L., Hu, X.T., et al. (2013). Genome of the Chinese tree shrew. Nat. Commun. *4*, 1426. https://doi.org/10.1038/ncomms2416.

41. Qiu, Q., Zhang, G., Ma, T., Qian, W., Wang, J., Ye, Z., Cao, C., Hu, Q., Kim, J., Larkin, D.M., et al. (2012). The yak genome and adaptation to life at high altitude. Nat. Genet. *44*, 946–949. https://doi.org/10.1038/ng.2343.

42. Kaessmann, H. (2010). Origins, evolution, and phenotypic impact of new genes. Genome Res. *20*, 1313–1326. https://doi.org/10.1101/gr.101386.109.

43. Khaitovich, P., Enard, W., Lachmann, M., and Pääbo, S. (2006). Evolution of primate gene expression. Nat. Rev. Genet. *7*, 693–702. https://doi.org/10.1038/nrg1940.

44. Wang, Z.Y., Leushkin, E., Liechti, A., Ovchinnikova, S., Mößinger, K., Brüning, T., Rummel, C., Grützner, F., Cardoso-Moreira, M., Janich, P., et al. (2020). Transcriptome and translatome co-evolution in mammals. Nature *588*, 642–647. https://doi.org/10.1038/s41586-020-2899-z.

45. Rops, A.L., Götte, M., Baselmans, M.H., Van Den Hoven, M.J., Steenbergen, E.J., Lensen, J.F., Wijnhoven, T.J., Cevikbas, F., Van Den Heuvel, L.P., Van Kuppevelt, T.H., et al. (2007). Syndecan-1 deficiency aggravates anti-glomerular basement membrane nephritis. Kidney Int. *72*, 1204–1215. https://doi.org/10.1038/sj.ki.5002514.

46. Vanhoutte, D., Schellings, M.W.M., Götte, M., Swinnen, M., Herias, V., Wild, M.K., Vestweber, D., Chorianopoulos, E., Cortés, V., Rigotti, A., et al. (2007). Increased expression of syndecan-1 protects against cardiac dilatation and dysfunction after myocardial infarction. Circulation *115*, 475–482. https://doi.org/10.1161/CIRCULATIONAHA.106.644609.

47. Luo, Y., He, Z., Liu, W., Zhou, F., Liu, T., and Wang, G. (2022). DTL Is a Prognostic biomarker and Promotes Bladder Cancer Progression through Regulating the AKT/mTOR axis. Oxid. Med. Cell. Longev. *2022*, 3369858. https://doi.org/10.1155/2022/3369858.

48. Wilson, D.J. (2019). The harmonic mean p-value for combining dependent tests. Proc. Natl. Acad. Sci. USA *116*, 1195–1200. https://doi.org/10.1073/pnas.1814092116.

49. Chu, T., Wang, Z., Pe'er, D., and Danko, C.G. (2022). Cell type and gene expression deconvolution with BayesPrism enables Bayesian integrative analysis across bulk and single-cell RNA sequencing in oncology. Nat. Cancer *3*, 505–517. https://doi.org/10.1038/s43018-022-00356-3.

50. Sinha, M., Jang, Y.C., Oh, J., Khong, D., Wu, E.Y., Manohar, R., Miller, C., Regalado, S.G., Loffredo, F.S., Pancoast, J.R., et al. (2014). Restoring systemic GDF11 levels reverses age-related dysfunction in mouse skeletal muscle. Science *344*, 649–652. https://doi.org/10.1126/science.1251152.

51. Moigneu, C., Abdellaoui, S., Ramos-Brossier, M., Pfaffenseller, B., Wollenhaupt-Aguiar, B., de Azevedo Cardoso, T., Chiche, A., Kuperwasser, N., Azevedo da Silva, R., Pedrotti Moreira, F., et al. (2023). Systemic GDF11 attenuates depression-like phenotype in aged mice via stimulation of neuronal autophagy. Nat. Aging *3*, 213–228. https://doi.org/10.1038/s43587-022-00352-3.

52. Mauer, J., Denson, J.L., and Brüning, J.C. (2015). Versatile functions for IL-6 in metabolism and cancer. Trends Immunol. *36*, 92–101. https://doi.org/10.1016/j.it.2014.12.008.

53. Mori, M.A., Ludwig, R.G., Garcia-Martin, R., Brandão, B.B., and Kahn, C.R. (2019). Extracellular miRNAs: from biomarkers to mediators of physiology and disease. Cell Metab. *30*, 656–673. https://doi.org/10.1016/j.cmet.2019.07.011.

54. Sobczak, A.I.S., Blindauer, C.A., and Stewart, A.J. (2019). Changes in plasma free fatty acids associated with type-2 diabetes. Nutrients *11*. https://doi.org/10.3390/nu11092022.

55. Yoshida, M., Satoh, A., Lin, J.B., Mills, K.F., Sasaki, Y., Rensing, N., Wong, M., Apte, R.S., and Imai, S.I. (2019). Extracellular vesicle-contained eNAMPT delays aging and extends lifespan in mice. Cell Metab. *30*, 329–342.e5. https://doi.org/10.1016/j.cmet.2019.05.015.

56. Hall, B.M., Gleiberman, A.S., Strom, E., Krasnov, P.A., Frescas, D., Vujcic, S., Leontieva, O.V., Antoch, M.P., Kogan, V., Koman, I.E., et al. (2020). Immune checkpoint protein VSIG4 as a biomarker of aging in murine adipose tissue. Aging Cell *19*, e13219. https://doi.org/10.1111/acel.13219.

57. Byun, J.M., Jeong, D.H., Choi, I.H., Lee, D.S., Kang, M.S., Jung, K.O., Jeon, Y.K., Kim, Y.N., Jung, E.J., Lee, K.B., et al. (2017). The significance of VSIG4 expression in ovarian cancer. Int. J. Gynecol. Cancer *27*, 872–878. https://doi.org/10.1097/IGC.0000000000000979.

58. Bianchi-Frias, D., Damodarasamy, M., Hernandez, S.A., Gil Da Costa, R.M., Vakar-Lopez, F., Coleman, I.M., Reed, M.J., and Nelson, P.S. (2019). The aged microenvironment influences the tumorigenic potential of malignant prostate epithelial cells. Mol. Cancer Res. *17*, 321–331. https://doi.org/10.1158/1541-7786.MCR-18-0522.

59. Xu, T., Jiang, Y., Yan, Y., Wang, H., Lu, C., Xu, H., Li, W., Fu, D., Lu, Y., and Chen, J. (2015). VSIG4 is highly expressed and correlated with poor prognosis of high-grade glioma patients. Am. J. Transl. Res. *7*, 1172–1180.

60. Lee, M.Y., Kim, W.J., Kang, Y.J., Jung, Y.M., Kang, Y.M., Suk, K., Park, J.E., Choi, E.M., Choi, B.K., Kwon, B.S., et al. (2006). Z39Ig is expressed on macrophages and may mediate inflammatory reactions in arthritis and atherosclerosis. J. Leukoc. Biol. *80*, 922–928. https://doi.org/10.1189/jlb.0306160.

61. Taylor, G.A., Rodriguiz, R.M., Greene, R.I., Daniell, X., Henry, S.C., Crooks, K.R., Kotloski, R., Tessarollo, L., Phillips, L.E., and Wetsel, W.C. (2008). Behavioral characterization of P311 knockout mice. Genes Brain Behav. *7*, 786–795. https://doi.org/10.1111/j.1601-183X.2008.00420.x.

62. Badri, K.R., Yue, M., Carretero, O.A., Aramgam, S.L., Cao, J., Sharkady, S., Kim, G.H., Taylor, G.A., Byron, K.L., and Schuger, V. (2013). Blood pressure homeostasis is maintained by a p311-TGF-β axis. J. Clin. Invest. *123*, 4502–4512. https://doi.org/10.1172/JCI69884.

63. Nunez, S.K., Young, C., Adebayo, O., Muppuru, K.M., and Badri, K.R. (2019). P311, a novel intrinsically disordered protein, regulates adipocyte development. Biochem. Biophys. Res. Commun. *515*, 234–240. https://doi.org/10.1016/j.bbrc.2019.05.105.

64. López-Otín, C., Blasco, M.A., Partridge, L., Serrano, M., and Kroemer, G. (2013). The hallmarks of aging. Cell *153*, 1194–1217. https://doi.org/10.1016/j.cell.2013.05.039.

65. López-Otín, C., Blasco, M.A., Partridge, L., Serrano, M., and Kroemer, G. (2023). Hallmarks of aging: An expanding universe. Cell *186*, 243–278. https://doi.org/10.1016/j.cell.2022.11.001.

66. Petkovich, D.A., Podolskiy, D.I., Lobanov, A.V., Lee, S.G., Miller, R.A., and Gladyshev, V.N. (2017). Using DNA methylation profiling to evaluate biological age and longevity interventions. Cell Metab. *25*, 954–960.e6. https://doi.org/10.1016/j.cmet.2017.03.016.

67. Wang, T., Tsui, B., Kreisberg, J.F., Robertson, N.A., Gross, A.M., Yu, M.K., Carter, H., Brown-Borg, H.M., Adams, P.D., and Ideker, T. (2017). Epigenetic aging signatures in mice livers are slowed by dwarfism, calorie restriction and rapamycin treatment. Genome Biol. *18*, 57. https://doi.org/10.1186/s13059-017-1186-2.

68. Cole, J.J., Robertson, N.A., Rather, M.I., Thomson, J.P., McBryan, T., Sproul, D., Wang, T., Brock, C., Clark, W., Ideker, T., et al. (2017). Diverse interventions that extend mouse lifespan suppress shared age-associated epigenetic changes at critical gene regulatory regions. Genome Biol. *18*, 58. https://doi.org/10.1186/s13059-017-1185-3.

69. Ying, K., Liu, H., Tarkhov, A.E., Lu, A.T., Horvath, S., Kutalik, Z., Shen, X., and Gladyshev, V.N. (2022). Causal epigenetic age uncouples damage and adaptation. Preprint at bioRxiv. https://doi.org/10.1101/2022.10.07.511382.

70. Kaya, A., Phua, C.Z.J., Lee, M., Wang, L., Tyshkovskiy, A., Ma, S., Barre, B., Liu, W., Harrison, B.R., Zhao, X., et al. (2021). Evolution of natural lifespan variation and molecular strategies of extended lifespan in yeast. eLife *10*, e64860. https://doi.org/10.7554/eLife.64860.

71. Kemmeren, P., Sameith, K., Van De Pasch, L.A.L., Benschop, J.J., Lenstra, T.L., Margaritis, T., O'Duibhir, E., Apweiler, E., Van Wageningen, S., Ko, C.W., et al. (2014). Large-scale genetic perturbations reveal regulatory networks and an abundance of gene-specific repressors. Cell *157*, 740–752. https://doi.org/10.1016/j.cell.2014.02.054.

72. McCormick, M.A., Delaney, J.R., Tsuchiya, M., Kaeberlein, M., and Kennedy, B.K. (2015). A comprehensive analysis of replicative lifespan in 4,698 single-gene deletion strains uncovers conserved mechanisms of aging. Cell Metab. *22*, 895–906. https://doi.org/10.1177/0333102415576222.ls.

73. Janssens, G.E., Meinema, A.C., González, J., Wolters, J.C., Schmidt, A., Guryev, V., Bischoff, R., Wit, E.C., Veenhoff, L.M., and Heinemann, M. (2015). Protein biogenesis machinery is a driver of replicative aging in yeast. eLife *4*, e08527. https://doi.org/10.7554/eLife.08527.

74. Fontana, L., Partridge, L., and Longo, V.D. (2010). Extending healthy life span—from yeast to humans. Science *328*, 321–326. https://doi.org/10.1126/science.1172539.

75. Coschigano, K.T., Clemmons, D., Bellush, L.L., and Kopchick, J.J. (2000). Assessment of growth parameters and lifespan of GHR/BP gene-disrupted mice. Endocrinology *141*, 2608–2613. https://doi.org/10.1210/endo.141.7.7586.

76. Mitchell, S.J., Madrigal-Matute, J., Scheibye-Knudsen, M., Fang, E., Aon, M., González-Reyes, J.A., Cortassa, S., Kaushik, S., Gonzalez-Freire, M., Patel, B., et al. (2016). Effects of sex, strain, and energy intake on hallmarks of aging in mice. Cell Metab. *23*, 1093–1112. https://doi.org/10.1016/j.cmet.2016.05.027.

77. Landin-Wilhelmsen, K., Lundberg, P.A., Lappas, G., and Wilhelmsen, L. (2004). Insulin-like growth factor I levels in healthy adults. Horm. Res. *62*, 8–16. https://doi.org/10.1159/000080753.

78. Thijssen, V.L.J.L., Postel, R., Brandwijk, R.J.M.G.E., Dings, R.P.M., Nesmelova, I., Satijn, S., Verhofstad, N., Nakabeppu, Y., Baum, L.G., Bakkers, J., et al. (2006). Galectin-1 is essential in tumor angiogenesis and is a target for antiangiogenesis therapy. Proc. Natl. Acad. Sci. USA *103*, 15975–15980. https://doi.org/10.1073/pnas.0603883103.

79. Sundblad, V., Morosi, L.G., Geffner, J.R., and Rabinovich, G.A. (2017). Galectin-1: A jack-of-all-trades in the resolution of acute and chronic inflammation. J. Immunol. *199*, 3721–3730. https://doi.org/10.4049/jimmunol.1701172.

80. Seropian, I.M., González, G.E., Maller, S.M., Berrocal, D.H., Abbate, A., and Rabinovich, G.A. (2018). Galectin-1 as an emerging mediator of cardiovascular inflammation: Mechanisms and therapeutic opportunities. Mediators Inflamm. *2018*, 8696543. https://doi.org/10.1155/2018/8696543.

81. Seropian, I.M., Cerliani, J.P., Toldo, S., Van Tassell, B.W., Ilarregui, J.M., González, G.E., Matoso, M., Salloum, F.N., Melchior, R., Gelpi, R.J., et al. (2013). Galectin-1 controls cardiac inflammation and ventricular remodeling during acute myocardial infarction. Am. J. Pathol. *182*, 29–40. https://doi.org/10.1016/j.ajpath.2012.09.022.

82. Marques, T.M., van Rumund, A., Bruinsma, I.B., Wessels, H.J.C.T., Gloerich, J., Esselink, R.A.J., Bloem, B.R., Kuiperij, H.B., and Verbeek, M.M. (2019). Cerebrospinal fluid galectin-1 levels discriminate patients with parkinsonism from controls. Mol. Neurobiol. *56*, 5067–5074. https://doi.org/10.1007/s12035-018-1426-9.

83. Yoon, S., Baik, B., Park, T., and Nam, D. (2021). Powerful p-value combination methods to detect incomplete association. Sci. Rep. *11*, 6980. https://doi.org/10.1038/s41598-021-86465-y.

84. Ngo, T.C., and Assimos, D.G. (2007). Uric acid nephrolithiasis: recent progress and future directions. Rev. Urol. *9*, 17–27.

85. Oda, M., Satta, Y., Takenaka, O., and Takahata, N. (2002). Loss of urate oxidase activity in hominoids and its evolutionary implications. Mol. Biol. Evol. *19*, 640–653. https://doi.org/10.1093/oxfordjournals.molbev.a004123.

86. Wu, X.W., Lee, C.C., Muzny, D.M., and Caskey, C.T. (1989). Urate oxidase: Primary structure and evolutionary implications. Proc. Natl. Acad. Sci. USA *86*, 9412–9416. https://doi.org/10.1073/pnas.86.23.9412.

87. Wu, X.W., Muzny, D.M., Lee, C.C., and Caskey, C.T. (1992). Two independent mutational events in the loss of urate oxidase during hominoid evolution. J. Mol. Evol. *34*, 78–84. https://doi.org/10.1007/BF00163854.

88. Gomes, A.P., Price, N.L., Ling, A.J.Y., Moslehi, J.J., Montgomery, M.K., Rajman, L., White, J.P., Teodoro, J.S., Wrann, C.D., Hubbard, B.P., et al. (2013). Declining NAD^+ induces a pseudohypoxic state disrupting nuclear-mitochondrial communication during aging. Cell *155*, 1624–1638. https://doi.org/10.1016/j.cell.2013.11.037.

89. Rajman, L., Chwalek, K., and Sinclair, D.A. (2018). Therapeutic potential of NAD-boosting molecules: the in vivo evidence. Cell Metab. *27*, 529–547. https://doi.org/10.1016/j.cmet.2018.02.011.

90. Yoshino, J., Baur, J.A., and Imai, S.I. (2018). NAD^+ intermediates: The biology and therapeutic potential of NMN and NR. Cell Metab. *27*, 513–528. https://doi.org/10.1016/j.cmet.2017.11.002.

91. Orlandi, I., Stamerra, G., and Vai, M. (2018). Altered expression of mitochondrial NAD^+ carriers influences yeast chronological lifespan by modulating cytosolic and mitochondrial metabolism. Front. Genet. *9*, 676. https://doi.org/10.3389/fgene.2018.00676.

92. Kabil, O., Vitvitsky, V., Xie, P., and Banerjee, R. (2011). The quantitative significance of the transsulfuration enzymes for H2S production in murine tissues. Antioxid. Redox Signal. *15*, 363–372. https://doi.org/10.1089/ars.2010.3781.

93. Miller, D.L., and Roth, M.B. (2007). Hydrogen sulfide increases thermotolerance and lifespan in Caenorhabditis elegans. Proc. Natl. Acad. Sci. USA *104*, 20618–20622. https://doi.org/10.1073/pnas.0710191104.

94. Tilstra, J.S., Clauson, C.L., Niedernhofer, L.J., and Robbins, P.D. (2011). NF-κB in aging and disease. Aging Dis. *2*, 449–465.

95. Leonardi, G.C., Accardi, G., Monastero, R., Nicoletti, F., and Libra, M. (2018). Ageing: From inflammation to cancer. Immun. Ageing *15*, 1. https://doi.org/10.1186/s12979-017-0112-5.

96. Lai, K.S.P., Liu, C.S., Rau, A., Lanctôt, K.L., Köhler, C.A., Pakosh, M., Carvalho, A.F., and Herrmann, N. (2017). Peripheral inflammatory markers in Alzheimer's disease: A systematic review and meta-analysis of 175 studies. J. Neurol. Neurosurg. Psychiatry *88*, 876–882. https://doi.org/10.1136/jnnp-2017-316201.

97. Amdur, R.L., Feldman, H.I., Gupta, J., Yang, W., Kanetsky, P., Shlipak, M., Rahman, M., Lash, J.P., Townsend, R.R., Ojo, A., et al. (2016).

Inflammation and progression of CKD: The CRIC study. Clin. J. Am. Soc. Nephrol. *11*, 1546–1556. https://doi.org/10.2215/CJN.13121215.

98. Anisimova, A.S., Meerson, M.B., Gerashchenko, M.V., Kulakovskiy, I.V., Dmitriev, S.E., and Gladyshev, V.N. (2020). Multifaceted deregulation of gene expression and protein synthesis with age. Proc. Natl. Acad. Sci. USA *117*, 15581–15590. https://doi.org/10.1073/pnas.2001788117.

99. Tollis, M., Boddy, A.M., and Maley, C.C. (2017). Peto's Paradox: How has evolution solved the problem of cancer prevention? BMC Biol. *15*, 60. https://doi.org/10.1186/s12915-017-0401-7.

100. Lombard, D.B., Kohler, W.J., Guo, A.H., Gendron, C., Han, M., Ding, W., Lyu, Y., Ching, T.T., Wang, F.Y., Chakraborty, T.S., et al. (2020). High-throughput small molecule screening reveals Nrf2-dependent and -independent pathways of cellular stress resistance. Sci. Adv. *6*, 1–14. https://doi.org/10.1126/sciadv.aaz7628.

101. Ren, G., Sun, A., Deng, C., Zhang, J., Wu, X., Wei, X., Mani, S., Dou, W., and Wang, Z. (2015). The anti-inflammatory effect and potential mechanism of cardamonin in DSS-induced colitis. Am. J. Physiol. Gastrointest. Liver Physiol. *309*, G517–G527. https://doi.org/10.1152/ajpgi.00133.2015.

102. Lewis, K.N., Wason, E., Edrey, Y.H., Kristan, D.M., Nevo, E., and Buffenstein, R. (2015). Regulation of Nrf2 signaling and longevity in naturally long-lived rodents. Proc. Natl. Acad. Sci. USA *112*, 3722–3727. https://doi.org/10.1073/pnas.1417566112.

103. Pitayu, L., Baruffini, E., Rodier, C., Rötig, A., Lodi, T., and Delahodde, A. (2016). Combined use of *Saccharomyces cerevisiae*, *Caenorhabditis elegans* and patient fibroblasts leads to the identification of clofilium tosylate as a potential therapeutic chemical against POLG-related diseases. Hum. Mol. Genet. *25*, 715–727. https://doi.org/10.1093/hmg/ddv509.

104. Facchinello, N., Laquatra, C., Locatello, L., Beffagna, G., Brañas Casas, R., Fornetto, C., Dinarello, A., Martorano, L., Vettori, A., Risato, G., et al. (2021). Efficient clofilium tosylate-mediated rescue of POLG-related disease phenotypes in zebrafish. Cell Death Dis. *12*, 100. https://doi.org/10.1038/s41419-020-03359-z.

105. Xu, H., Li, X., Ding, W., Zeng, X., Kong, H., Wang, H., and Xie, W. (2015). Deguelin induces the apoptosis of lung cancer cells through regulating a ROS driven Akt pathway. Cancer Cell Int. *15*, 25. https://doi.org/10.1186/s12935-015-0166-4.

106. Preston, S., Korhonen, P.K., Mouchiroud, L., Cornaglia, M., Mcgee, S.L., Young, N.D., Davis, R.A., Crawford, S., Nowell, C., Ansell, B.R.E., et al. (2017). Deguelin exerts potent nematocidal activity via the mitochondrial respiratory chain. FASEB J. *31*, 4515–4532. https://doi.org/10.1096/fj.201700288R.

107. Lamb, J., Crawford, E.D., Peck, D., Modell, J.W., Blat, I.C., Wrobel, M.J., Lerner, J., Brunet, J.P., Subramanian, A., Ross, K.N., et al. (2006). The connectivity map: using gene-expression signatures to connect small molecules, genes, and disease. Science *313*, 1929–1935. https://doi.org/10.1126/science.1132939.

108. Subramanian, A., Narayan, R., Corsello, S.M., Peck, D.D., Natoli, T.E., Lu, X., Gould, J., Davis, J.F., Tubelli, A.A., Asiedu, J.K., et al. (2017). A Next Generation Connectivity Map: L1000 platform and the first 1,000,000 profiles. Cell *171*, 1437–1452.e17. https://doi.org/10.1016/j.cell.2017.10.049.

109. Osburn, W.O., Yates, M.S., Dolan, P.D., Chen, S., Liby, K.T., Sporn, M.B., Taguchi, K., Yamamoto, M., and Kensler, T.W. (2008). Genetic or pharmacologic amplification of Nrf2 signaling inhibits acute inflammatory liver injury in mice. Toxicol. Sci. *104*, 218–227. https://doi.org/10.1093/toxsci/kfn079.

110. Baze, M.M., Schlauch, K., and Hayes, J.P. (2010). Gene expression of the liver in response to chronic hypoxia. Physiol. Genomics *41*, 275–288. https://doi.org/10.1152/physiolgenomics.00075.2009.

111. Zhou, B., Yang, L., Li, S., Huang, J., Chen, H., Hou, L., Wang, J., Green, C.D., Yan, Z., Huang, X., et al. (2012). Midlife gene expressions identify modulators of aging through dietary interventions. Proc. Natl. Acad. Sci. USA *109*, E1201–E1209. https://doi.org/10.1073/pnas.1119304109.

112. Yeung, F., Ramírez, C.M., Mateos-Gomez, P.A., Pinzaru, A., Ceccarini, G., Kabir, S., Fernández-Hernando, C., and Sfeir, A. (2013). Nontelomeric role for Rap1 in regulating metabolism and protecting against obesity. Cell Rep. *3*, 1847–1856. https://doi.org/10.1016/j.celrep.2013.05.032.

113. Bongers, K.S., Fox, D.K., Kunkel, S.D., Stebounova, L.V., Murry, D.J., Pufall, M.A., Ebert, S.M., Dyle, M.C., Bullard, S.A., Dierdorff, J.M., et al. (2015). Spermine oxidase maintains basal skeletal muscle gene expression and fiber size and is strongly repressed by conditions that cause skeletal muscle atrophy. Am. J. Physiol. Endocrinol. Metab. *308*, E144–E158. https://doi.org/10.1152/ajpendo.00472.2014.

114. Hand, N.J., Master, Z.R., Lay, J. Le, and Friedman, J.R. (2009). Hepatic function is preserved in the absence of mature microRNAs. Hepatology *49*, 618–626. https://doi.org/10.1002/hep.22656.

115. Sunami, Y., Leithäuser, F., Gul, S., Fiedler, K., Güldiken, N., Espenlaub, S., Holzmann, K.H., Hipp, N., Sindrilaru, A., Luedde, T., et al. (2012). Hepatic activation of IKK/NFκB signaling induces liver fibrosis via macrophage-mediated chronic inflammation. Hepatology *56*, 1117–1128. https://doi.org/10.1002/hep.25711.

116. Jain, I.H., Zazzeron, L., Goli, R., Alexa, K., Schatzman-Bone, S., Dhillon, H., Goldberger, O., Peng, J., Shalem, O., Sanjana, N.E., et al. (2016). Hypoxia as a therapy for mitochondrial disease. Science *352*, 54–61. https://doi.org/10.1126/science.aad9642.

117. Balaban, R.S., Nemoto, S., and Finkel, T. (2005). Mitochondria, oxidants, and aging. Cell *120*, 483–495. https://doi.org/10.1016/j.cell.2005.02.001.

118. Sykiotis, G.P., and Bohmann, D. (2008). Keap1/Nrf2 signaling regulates oxidative stress tolerance and lifespan in *Drosophila*. Dev. Cell *14*, 76–85. https://doi.org/10.1016/j.devcel.2007.12.002.

119. Tullet, J.M.A., Hertweck, M., An, J.H., Baker, J., Hwang, J.Y., Liu, S., Oliveira, R.P., Baumeister, R., and Blackwell, T.K. (2008). Direct inhibition of the longevity-promoting factor SKN-1 by insulin-like signaling in *C. elegans*. Cell *132*, 1025–1038. https://doi.org/10.1016/j.cell.2008.01.030.

120. Lu, X.F., Zhou, Y.J., Zhang, L., Ji, H.J., Li, L., Shi, Y.J., and Bu, H. (2015). Loss of Dicer1 impairs hepatocyte survival and leads to chronic inflammation and progenitor cell activation. World J. Gastroenterol. *21*, 6591–6603. https://doi.org/10.3748/wjg.v21.i21.6591.

121. O'Rourke, J.R., Georges, S.A., Seay, H.R., Tapscott, S.J., McManus, M.T., Goldhamer, D.J., Swanson, M.S., and Harfe, B.D. (2007). Essential role for Dicer during skeletal muscle development. Dev. Biol. *311*, 359–368. https://doi.org/10.1016/j.ydbio.2007.08.032.

122. McConnell, B.B., Starborg, M., Brookes, S., and Peters, G. (1998). Inhibitors of cyclin-dependent kinases induce features of replicative senescence in early passage human diploid fibroblasts. Curr. Biol. *8*, 351–354. https://doi.org/10.1016/s0960-9822(98)70137-x.

123. Fang, L., Igarashi, M., Leung, J., Sugrue, M.M., Lee, S.W., and Aaronson, S.A. (1999). p21Waf1/Cip1/Sdi1 induces permanent growth arrest with markers of replicative senescence in human tumor cells lacking functional p53. Oncogene *18*, 2789–2797. https://doi.org/10.1038/sj.onc.1202615.

124. Folkes, A.J., Ahmadi, K., Alderton, W.K., Alix, S., Baker, S.J., Box, G., Chuckowree, I.S., Clarke, P.A., Depledge, P., Eccles, S.A., et al. (2008). The identification of 2-(1H-Indazol-4-yl)-6-(4-methanesulfonyl-piperazin-1-ylmethyl)-4-morpholin-4-yl-thieno[3,2-d]pyrimidine (GDC0941) as a potent, selective, orally bioavailable inhibitor of class I PI3 kinase for the treatment of cancer. J. Med. Chem. *51*, 5522–5532. https://doi.org/10.1021/jm800295d.

125. Graff, J.R., McNulty, A.M., Hanna, K.R., Konicek, B.W., Lynch, R.L., Bailey, S.N., Banks, C., Capen, A., Goode, R., Lewis, J.E., et al. (2005). The protein kinase Cβ-selective inhibitor, enzastaurin. Cancer Res. *65*, 7462–7469. https://doi.org/10.1158/0008-5472.CAN-05-0071.

126. Li, P., Wu, Y., Li, M., Qiu, X., Bai, X., and Zhao, X. (2015). AS-703026 inhibits LPS-induced TNFα production through MEK/ERK dependent and ndependent mechanisms. PLoS One *10*, e0137107. https://doi.org/10.1371/journal.pone.0137107.

127. Park, S.J., Hong, S.W., Moon, J.H., Jin, D.H., Kim, J.S., Lee, C.K., Kim, K.P., Hong, Y.S., Choi, E.K., Lee, J.S., et al. (2013). The MEK1/2 inhibitor AS703026 circumvents resistance to the BRAF inhibitor PLX4032 in human malignant melanoma cells. Am. J. Med. Sci. *346*, 494–498. https://doi.org/10.1097/MAJ.0b013e318298a185.

128. García-Martínez, J.M., Moran, J., Clarke, R.G., Gray, A., Cosulich, S.C., Chresta, C.M., and Alessi, D.R. (2009). Ku-0063794 is a specific inhibitor of the mammalian target of rapamycin (mTOR). Biochem. J. *421*, 29–42. https://doi.org/10.1042/BJ20090489.

129. Chresta, C.M., Davies, B.R., Hickson, I., Harding, T., Cosulich, S., Critchlow, S.E., Vincent, J.P., Ellston, R., Jones, D., Sini, P., et al. (2010). AZD8055 is a potent, selective, and orally bioavailable ATP-competitive mammalian target of rapamycin kinase inhibitor with in vitro and in vivo antitumor activity. Cancer Res. *70*, 288–298. https://doi.org/10.1158/0008-5472.CAN-09-1751.

130. Cort, W.M. (1974). Antioxidant activity of tocopherols, ascorbyl palmitate, and ascorbic acid and their mode of action. J. Am. Oil Chem. Soc. *51*, 321–325. https://doi.org/10.1007/BF02633006.

131. Arriola Apelo, S.I., Neuman, J.C., Baar, E.L., Syed, F.A., Cummings, N.E., Brar, H.K., Pumper, C.P., Kimple, M.E., and Lamming, D.W. (2016). Alternative rapamycin treatment regimens mitigate the impact of rapamycin on glucose homeostasis and the immune system. Aging Cell *15*, 28–38. https://doi.org/10.1111/acel.12405.

132. Shindyapina, A.V., Castro, J.P., Barbieri, A., Strelkova, O.S., Paulo, J.A., Kerepesi, C., Petrashen, A.P., Marriotti, M., Meer, M., Hu, Y., et al. (2021). Integrative analysis reveals aged clonal B cells, microenvironment and c-Myc activation in the origin of age-related lymphoma. Preprint at bioRxiv. https://doi.org/10.1101/2021.02.23.432500.

133. Chondrogianni, N., Georgila, K., Kourtis, N., Tavernarakis, N., and Gonos, E.S. (2015). 20S proteasome activation promotes life span extension and resistance to proteotoxicity in Caenorhabditis elegans. FASEB J. *29*, 611–622. https://doi.org/10.1096/fj.14-252189.

134. Ghazi, A., Henis-Korenblit, S., and Kenyon, C. (2007). Regulation of Caenorhabditis elegans lifespan by a proteasomal E3 ligase complex. Proc. Natl. Acad. Sci. USA *104*, 5947–5952. https://doi.org/10.1073/pnas.0700638104.

135. Simonsen, A., Cumming, R.C., Brech, A., Isakson, P., Schubert, D.R., and Finley, K.D. (2008). Promoting basal levels of autophagy in the nervous system enhances longevity and oxidant resistance in adult Drosophila. Autophagy *4*, 176–184. https://doi.org/10.4161/auto.5269.

136. Pyo, J.O., Yoo, S.M., Ahn, H.H., Nah, J., Hong, S.H., Kam, T.I., Jung, S., and Jung, Y.K. (2013). Overexpression of Atg5 in mice activates autophagy and extends lifespan. Nat. Commun. *4*, 2300. https://doi.org/10.1038/ncomms3300.

137. Anisimova, A.S., Alexandrov, A.I., Makarova, N.E., Gladyshev, V.N., and Dmitriev, S.E. (2018). Protein synthesis and quality control in aging. Aging (Albany NY) *10*, 4269–4288. https://doi.org/10.18632/aging.101721.

138. Swovick, K., Firsanov, D., Welle, K.A., Hryhorenko, J.R., Wise, J.P.,J.P., George, C., Sformo, T.L., Seluanov, A., Gorbunova, V., and Ghaemmaghami, S. (2021). Interspecies differences in proteome turnover kinetics are correlated with life spans and energetic demands. Mol. Cell. Proteomics *20*, 100041. https://doi.org/10.1074/mcp.RA120.002301.

139. Kushiyama, A., Nakatsu, Y., Matsunaga, Y., Yamamotoya, T., Mori, K., Ueda, K., Inoue, Y., Sakoda, H., Fujishiro, M., Ono, H., et al. (2016). Role of uric acid metabolism-related inflammation in the pathogenesis of metabolic syndrome components such as atherosclerosis and nonalcoholic steatohepatitis. Mediators Inflamm. *2016*, 8603164. https://doi.org/10.1155/2016/8603164.

140. Zhang, B., Lee, D.E., Trapp, A., Tyshkovskiy, A., Lu, A.T., Bareja, A., Kerepesi, C., Katz, L.H., Shindyapina, A.V., Dmitriev, S.E., et al. (2021). Multi-omic rejuvenation and lifespan extension upon exposure to youthful circulation. Preprint at bioRxiv. https://doi.org/10.1101/2021.11.11.468258.

141. Mehdipour, M., Mehdipour, T., Skinner, C.M., Wong, N., Liu, C., Chen, C.C., Jeon, O.H., Zuo, Y., Conboy, M.J., and Conboy, I.M. (2021). Plasma dilution improves cognition and attenuates neuroinflammation in old mice. GeroScience *43*, 1–18. https://doi.org/10.1007/s11357-020-00297-8.

142. Gerashchenko, M.V., Peterfi, Z., Yim, S.H., and Gladyshev, V.N. (2021). Translation elongation rate varies among organs and decreases with age. Nucleic Acids Res. *49*, e9. https://doi.org/10.1093/nar/gkaa1103.

143. Tavernarakis, N. (2008). Ageing and the regulation of protein synthesis: a balancing act? Trends Cell Biol. *18*, 228–235. https://doi.org/10.1016/j.tcb.2008.02.004.

144. Tacutu, R., Craig, T., Budovsky, A., Wuttke, D., Lehmann, G., Taranukha, D., Costa, J., Fraifeld, V.E., and De Magalhães, J.P. (2013). Human Ageing Genomic Resources: Integrated databases and tools for the biology and genetics of ageing. Nucleic Acids Res. *41*, D1027–D1033. https://doi.org/10.1093/nar/gks1155.

145. Lee, S.G., Mikhalchenko, A.E., Yim, S.H., Lobanov, A.V., Park, J.K., Choi, K.H., Bronson, R.T., Lee, C.K., Park, T.J., and Gladyshev, V.N. (2017). Naked mole rat induced pluripotent stem cells and their contribution to interspecific chimera. Stem Cell Rep. *9*, 1706–1720. https://doi.org/10.1016/j.stemcr.2017.09.013.

146. Bolger, A.M., Lohse, M., and Usadel, B. (2014). Trimmomatic: A flexible trimmer for Illumina sequence data. Bioinformatics *30*, 2114–2120. https://doi.org/10.1093/bioinformatics/btu170.

147. Subramanian, A., Tamayo, P., Mootha, V.K., Mukherjee, S., Ebert, B.L., Gillette, M.A., Paulovich, A., Pomeroy, S.L., Golub, T.R., Lander, E.S., et al. (2005). Gene set enrichment analysis: a knowledge-based approach for interpreting genome-wide expression profiles. Proc. Natl. Acad. Sci. USA *102*, 15545–15550. https://doi.org/10.1073/pnas.0506580102.

148. Kolberg, L., Raudvere, U., Kuzmin, I., Vilo, J., and Peterson, H. (2020). gprofiler2 – an R package for gene list functional enrichment analysis and namespace conversion toolset g:Profiler. F1000Res *9*, 709. https://doi.org/10.12688/f1000research.24956.2.

149. Raudvere, U., Kolberg, L., Kuzmin, I., Arak, T., Adler, P., Peterson, H., and Vilo, J. (2019). G:Profiler: a web server for functional enrichment analysis and conversions of gene lists (2019 update). Nucleic Acids Res. *47*, W191–W198. https://doi.org/10.1093/nar/gkz369.

150. Chang, W., Cheng, J., Allaire, J., Xie, Y., and McPherson, J. (2016). shiny: web application framework for R. R package version 0.14.2. https://CRAN.R-project.org/package=shiny.

151. Robinson, M.D., and Oshlack, A. (2010). A scaling normalization method for differential expression analysis of RNA-seq data. Genome Biol. *11*, R25. https://doi.org/10.1186/gb-2010-11-3-r25.

152. Ritchie, M.E., Phipson, B., Wu, D., Hu, Y., Law, C.W., Shi, W., and Smyth, G.K. (2015). Limma powers differential expression analyses for RNA-sequencing and microarray studies. Nucleic Acids Res. *43*, e47. https://doi.org/10.1093/nar/gkv007.

153. Viechtbauer, W. (2010). Conducting Meta-Analyses in R with the metafor Package. J. Stat. Softw. *36*, 1–48.

154. Anders, S., and Huber, W. (2010). Differential expression analysis for sequence count data. Genome Biol. *11*, R106. https://doi.org/10.1186/gb-2010-11-10-r106.

155. Dobin, A., Davis, C.A., Schlesinger, F., Drenkow, J., Zaleski, C., Jha, S., Batut, P., Chaisson, M., and Gingeras, T.R. (2013). STAR: Ultrafast universal RNA-seq aligner. Bioinformatics *29*, 15–21. https://doi.org/10.1093/bioinformatics/bts635.

156. Liao, Y., Smyth, G.K., and Shi, W. (2014). FeatureCounts: An efficient general purpose program for assigning sequence reads to genomic features. Bioinformatics *30*, 923–930. https://doi.org/10.1093/bioinformatics/btt656.

157. Friedman, J., Hastie, T., and Tibshirani, R. (2008). Sparse inverse covariance estimation with the graphical lasso. Biostatistics *9*, 432–441. https://doi.org/10.1093/biostatistics/kxm045.

158. Schliep, K.P. (2011). phangorn: Phylogenetic analysis in R. Bioinformatics *27*, 592–593. https://doi.org/10.1093/bioinformatics/btq706.

159. Seluanov, A., Hine, C., Bozzella, M., Hall, A., Sasahara, T.H.C., Ribeiro, A.A.C.M., Catania, K.C., Presgraves, D.C., and Gorbunova, V. (2008). Distinct tumor suppressor mechanisms evolve in rodent species that differ in size and lifespan. Aging Cell *7*, 813–823. https://doi.org/10.1111/j.1474-9726.2008.00431.x.

160. Pickering, A.M., Lehr, M., Kohler, W.J., Han, M.L., and Miller, R.A. (2015). Fibroblasts from longer-lived species of primates, rodents, bats, carnivores, and birds resist protein damage. J. Gerontol. A Biol. Sci. Med. Sci. *70*, 791–799. https://doi.org/10.1093/gerona/glu115.

161. Salphati, L., Wong, H., Belvin, M., Bradford, D., Edgar, K.A., Prior, W.W., Sampath, D., and Wallin, J.J. (2010). Pharmacokinetic-pharmacodynamic modeling of tumor growth inhibition and biomarker modulation by the novel phosphatidylinositol 3-kinase inhibitor GDC-0941. Drug Metab. Dispos. *38*, 1436–1442. https://doi.org/10.1124/dmd.110.032912.

162. Raynaud, F.I., Eccles, S.A., Patel, S., Alix, S., Box, G., Chuckowree, I., Folkes, A., Gowan, S., De Haven Brandon, A., Di Stefano, F., et al. (2009). Biological properties of potent inhibitors of class I phosphatidylinositide 3-kinases: From PI-103 through PI-540, PI-620 to the oral agent GDC-0941. Mol. Cancer Ther. *8*, 1725–1738. https://doi.org/10.1158/1535-7163.MCT-08-1200.

163. Gelardi, T., Caputo, R., Damiano, V., Daniele, G., Pepe, S., Ciardiello, F., Lahn, M., Bianco, R., and Tortora, G. (2008). Enzastaurin inhibits tumours sensitive and resistant to anti-EGFR drugs. Br. J. Cancer *99*, 473–480. https://doi.org/10.1038/sj.bjc.6604493.

164. Kim, K., Kong, S.Y., Fulciniti, M., Li, X., Song, W., Nahar, S., Burger, P., Rumizen, M.J., Podar, K., Chauhan, D., et al. (2010). Blockade of the MEK/ERK signaling cascade by AS703026, a novel selective MEK1/2 inhibitor, induces pleiotropic anti-myeloma activity in vitro and in vivo. Br. J. Haematol. *149*, 537–549. https://doi.org/10.1111/j.1365-2141.2010.08127.x.

165. Yongxi, T., Haijun, H., Jiaping, Z., Guoliang, S., and Hongying, P. (2015). Autophagy inhibition sensitizes KU-0063794-mediated anti-HepG2 hepatocellular carcinoma cell activity in vitro and in vivo. Biochem. Biophys. Res. Commun. *465*, 494–500. https://doi.org/10.1016/j.bbrc.2015.08.045.

166. García-Martínez, J.M., Wullschleger, S., Preston, G., Guichard, S., Fleming, S., Alessi, D.R., and Duce, S.L. (2011). Effect of PI3K- and mTOR-specific inhibitors on spontaneous B-cell follicular lymphomas in PTEN/LKB1-deficient mice. Br. J. Cancer *104*, 1116–1125. https://doi.org/10.1038/bjc.2011.83.

167. Veurink, G., Liu, D., Taddei, K., Perry, G., Smith, M.A., Robertson, T.A., Hone, E., Groth, D.M., Atwood, C.S., and Martins, R.N. (2003). Reduction of inclusion body pathology in ApoE-deficient mice fed a combination of antioxidants. Free Radic. Biol. Med. *34*, 1070–1077. https://doi.org/10.1016/S0891-5849(03)00042-X.

168. Edgar, R., Domrachev, M., and Lash, A.E. (2002). Gene Expression Omnibus: NCBI gene expression and hybridization array data repository. Nucleic Acids Res. *30*, 207–210. https://doi.org/10.1093/nar/30.1.207.

169. Hashimshony, T., Senderovich, N., Avital, G., Klochendler, A., de Leeuw, Y., Anavy, L., Gennert, D., Li, S., Livak, K.J., Rozenblatt-Rosen, O., et al. (2016). CEL-Seq2: sensitive highly-multiplexed single-cell RNA-Seq. Genome Biol. *17*, 77. https://doi.org/10.1186/s13059-016-0938-8.

170. Schultz, M.B., Kane, A.E., Mitchell, S.J., MacArthur, M.R., Warner, E., Vogel, D.S., Mitchell, J.R., Howlett, S.E., Bonkowski, M.S., and Sinclair, D.A. (2020). Age and life expectancy clocks based on machine learning analysis of mouse frailty. Nat. Commun. *11*, 4618. https://doi.org/10.1038/s41467-020-18446-0.

171. Shindyapina, A.V., Cho, Y., Kaya, A., Tyshkovskiy, A., Castro, J.P., Deik, A., Gordevicius, J., Poganik, J.R., Clish, C.B., Horvath, S., et al. (2022). Rapamycin treatment during development extends life span and health span of male mice and *Daphnia magna*. Sci. Adv. *8*, eabo5482. https://doi.org/10.1126/sciadv.abo5482.

172. Felsenstein, J. (1985). Phylogenies and the comparative method. Am. Nat. *125*, 1–15. https://doi.org/10.1086/284325.

173. Revell, L.J. (2012). phytools: An R package for phylogenetic comparative biology (and other things). Methods Ecol. Evol. *3*, 217–223. https://doi.org/10.1111/j.2041-210X.2011.00169.x.

174. Benjamini, Y., and Hochberg, Y. (1995). Controlling the false discovery rate: A practical and powerful approach to multiple testing. J. R. Stat. Soc. B *57*, 289–300.

175. Kolesnikov, N., Hastings, E., Keays, M., Melnichuk, O., Tang, Y.A., Williams, E., Dylag, M., Kurbatova, N., Brandizi, M., Burdett, T., et al. (2015). ArrayExpress update–simplifying data submissions. Nucleic Acids Res. *43*, D1113–D1116. https://doi.org/10.1093/nar/gku1057.

176. Linnet, K. (1993). Evaluation of regression procedures for methods comparison studies. Clin. Chem. *39*, 424–432. https://doi.org/10.1093/clinchem/39.3.424.

177. Lek, M., Karczewski, K.J., Minikel, E.V., Samocha, K.E., Banks, E., Fennell, T., O'Donnell-Luria, A.H., Ware, J.S., Hill, A.J., Cummings, B.B., et al. (2016). Analysis of protein-coding genetic variation in 60,706 humans. Nature *536*, 285–291. https://doi.org/10.1038/nature19057.

178. Shihab, H.A., Rogers, M.F., Campbell, C., and Gaunt, T.R. (2017). HIPred: An integrative approach to predicting haploinsufficient genes. Bioinformatics *33*, 1751–1757. https://doi.org/10.1093/bioinformatics/btx028.

179. Shao, Y., Chen, C., Shen, H., He, B.Z., Yu, D., Jiang, S., Zhao, S., Gao, Z., Zhu, Z., Chen, X., et al. (2019). GenTree, an integrated resource for analyzing the evolution and function of primate-specific coding genes. Genome Res. *29*, 682–696. https://doi.org/10.1101/gr.238733.118.

Please cite this article in press as: Tyshkovskiy et al., Distinct longevity mechanisms across and within species and their association with aging, Cell (2023), https://doi.org/10.1016/j.cell.2023.05.002

STAR★METHODS

KEY RESOURCES TABLE

REAGENT or RESOURCE	SOURCE	IDENTIFIER
Antibodies		
Anti-mouse CD19	BioLegend	Cat#115503; RRID: AB_313638
Anti-mouse/human CD11b	BioLegend	Cat#101203; RRID: AB_312786
Anti-mouse CD3	BioLegend	Cat#100243; RRID: AB_2563946
Anti-mouse CD45	BioLegend	Cat#103103; RRID: AB_312968
Chemicals, peptides, and recombinant proteins		
DMEM, high glucose, GlutaMAX™	Gibco	Cat#10566016
Fetal Bovine Serum	R&D Systems	Cat#S11150
Bovine Serum Albumin	Sigma	Cat#A9418
Antibiotic-Antimycotic (100X)	Gibco	Cat#15240096
DMSO (Dimethyl sulfoxide)	Sigma	Cat#D2650
Paraquat dichloride hydrate	Sigma	Cat#36541
Cardamonin	Selleck Chemicals	Cat#S3942
Clofilium tosylate	Targetmol	Cat#T14982
Deguelin	Selleck Chemicals	Cat#S8132
KU-0063794	MedChemExpress	Cat#HY-50710
AZD8055	MedChemExpress	Cat#HY-10422
Ascorbyl-palmitate	MedChemExpress	Cat#HY-B0987
GDC-0941	MedChemExpress	Cat#HY-50094
Enzastaurin	MedChemExpress	Cat#HY-10342
AS-703026	MedChemExpress	Cat#HY-12042
Critical commercial assays		
PureLink RNA Mini Kit	Thermo Fisher Scientific	Cat#12183020
CellTiter-Glo® Luminescent Cell Viability Assay	Promega	Cat#G7570
Deposited data		
Raw data files and processed data files for RNA-seq	This paper	GEO: GSE227360
mSALT database	This paper	http://gladyshevlab.org/mSALT/
Metabolite profiling data	Ma et al.[27]; Tyshkovskiy et al.[33]	N/A
Public gene expression data from tissues and fibroblasts of mammalian species	Fushan et al.[31]; Brawand et al.[37]; Kim et al.[34]; Merkin et al.[38]; Qiu et al.[41]; Seim et al.[4]; Fan et al.[40]; Seim et al.[35]; Yim et al.[39]; Fang et al.[36]	GEO: GSE43013, GSE30352, GSE30337, GSE41637, GSE33300, GSE42297, GSE39150, GSE50726; SRA: PRJNA263931, PRJNA72723
Public gene expression data on mammalian aging	See Table S1B for a list of sources	N/A
Gene expression signatures of lifespan-extending interventions	Tyshkovskiy et al.[33]	N/A
Yeast gene expression signatures of longevity	Kaya et al.[70]	N/A
Public gene expression data of yeast replicative aging	Janssens et al.[73]	N/A
Public gene expression profiles of mouse tissues subjected to interventions	Osburn et al.[109]; Baze et al.[110]; Zhou et al.[111]; Yeung et al.[112]; Bongers et al.[113]; Hand et al.[114]; Sunami et al.[115]	GEO: GSE15891, GSE11287, GSE11899, GSE46209, GSE63007, GSE28085, GSE36838

(*Continued on next page*)

Continued

REAGENT or RESOURCE	SOURCE	IDENTIFIER
Animal Ageing and Longevity (AnAge) Database	Tacutu et al.[144]	https://genomics.senescence.info/species/index.html
Gene sets of housekeeping, essential and evolutionary old genes	Wang et al.[44]	N/A
Tabula Muris single-cell atlas	Almanzar et al.[24]	GEO: GSE109774
Experimental models: Cell lines		
C57Bl/6J mouse fibroblasts (*Mus musculus*)	Lee et al.[145]	N/A
UM-HET3 mouse fibroblasts (*Mus musculus*)	University of Michigan	N/A
Rat fibroblasts (*Rattus norvegicus*)	University of Rochester	N/A
Naked mole rat fibroblasts (*Heterocephalus glaber*)	Lee et al.[145]	N/A
Western long-eared myotis fibroblasts (*Myotis evotis*)	University of Michigan	N/A
Yuma myotis fibroblasts (*Myotis yumanensis*)	University of Michigan	N/A
Human fibroblasts (*Homo sapiens*)	Lee et al.[145]	N/A
Experimental models: Organisms/strains		
Baboon (*Papio anubis*)	Southwest National Primate Research Center (SNPRC)	N/A
Canadian beaver (*Castor canadensis*)	Southwest National Primate Research Center (SNPRC)	N/A
Long-tailed macaque (*Macaca fascicularis*)	Southwest National Primate Research Center (SNPRC)	N/A
Siberian chipmunk (*Tamias sibiricus*)	Fushan et al.[31]	N/A
American black bear (*Ursus americanus*)	Fushan et al.[31]	N/A
Sugar glider (*Petaurus breviceps*)	Fushan et al.[31]	N/A
Greater tube-nosed bat (*Murina leucogaster*)	Fushan et al.[31]	N/A
White-footed mouse (*Peromyscus leucopus*)	Fushan et al.[31]	N/A
Mouse: C57BL/6J	National Institute on Aging Aged Rodent Colony	N/A
Mouse: UM-HET3	University of Michigan Medical School	N/A
Software and algorithms		
Flow cytometry analysis: FlowJo™	BD Biosciences	N/A
Adaptor removing: Trimmomatic (version 0.32)	Bolger et al.[146]	http://www.usadellab.org/cms/index.php?page=trimmomatic
Functional enrichment: GSEA	Subramanian et al.[147]	http://software.broadinstitute.org/gsea/index.jsp
Functional enrichment: gprofiler2	Kolberg et al.[148]; Raudvere et al.[149]	https://cran.r-project.org/web/packages/gprofiler2/index.html
App development: shiny	Chang et al.[150]	https://shiny.rstudio.com/
Programming environment: RStudio	https://www.rstudio.com/	N/A
Differential gene expression analysis of RNAseq: edgeR	Robinson et al.[151]	https://bioconductor.org/packages/release/ bioc/html/edgeR.html
Differential gene expression analysis of microarrays: limma	Ritchie et al.[152]	https://bioconductor.org/packages/release/ bioc/html/limma.html
Mixed-effect model: metafor	Viechtbauer et al.[153]	http://CRAN.R-project.org/package=metafor

(*Continued on next page*)

Continued

REAGENT or RESOURCE	SOURCE	IDENTIFIER
RNAseq normalization: RLE	Anders and Huber[154]	https://bioconductor.org/packages/release/ bioc/html/edgeR.html
Prediction of compounds with similar gene expression response: CMap	Lamb et al.[107]; Subramanian et al.[147]	https://clue.io
Identification of similar gene expression profiles: GeneQuery	https://artyomovlab.wustl.edu/genequery/	N/A
Mapping: STAR (version 2.5.2b)	Dobin et al.[155]	https://github.com/alexdobin/STAR
Counting: featureCoutns (version 1.5)	Liao et al.[156]	https://subread.sourceforge.net/
Harmonic mean p value: harmonicmeanp	Wilson et al.[48]	https://cran.r-project.org/web/packages/harmonicmeanp/index.html
Cell type deconvolution: bayesPrism	Chu et al.[49]	https://github.com/Danko-Lab/BayesPrism
Sparse partial correlation matrix: glasso	Friedman et al.[157]	https://cran.r-project.org/web/packages/glasso/index.html
Phylogenetic analysis: phangorn	Schliep et al.[158]	https://cran.r-project.org/web/packages/phangorn/index.html

RESOURCE AVAILABILITY

Lead contact

Further information and requests for resources and reagents should be directed to and will be fulfilled by the Lead Contact, Vadim N. Gladyshev (vgladyshev@rics.bwh.harvard.edu).

Materials availability

This study did not generate new unique reagents.

Data and code availability

- RNA-seq data reported in this work are available at NCBI GEO data repository under accession number GEO: GSE227360 (SubSeries GSE227358 and GSE227359). Accession numbers for publicly available datasets analyzed in this study are listed in the key resources table.
- mSALT database can be accessed through the following link: http://gladyshevlab.org/mSALT/. Data analysis code is available from the authors upon request.
- Any additional information required to reanalyze the data reported in this paper is available from the lead contact upon request.

EXPERIMENTAL MODEL AND STUDY PARTICIPANT DETAILS

Mammalian species sample collection

The 39 organ samples for young adults of baboon (*Papio anubis*), beaver (*Castor canadensis*), and long-tailed macaque (*Macaca fascicularis*) were collected from the Southwest National Primate Research Center (SNPRC). The 9 organ samples for young adults of chipmunk (*Tamias sibiricus*), American black bear (*Ursus americanus*), sugar glider (*Petaurus breviceps*), tube-nosed bat (*Murina leucogaster*), and white-footed mouse (*Peromyscus leucopus*) were collected as previously described.[31]

Cell lines and culture

Fibroblasts from 6 species were cultured, including *Mus musculus* (C57BL/6J and UM-HET3 strains), *Rattus norvegicus*, *Heterocephalus glaber*, *Myotis evotis*, *Myotis yumanensis* and *Homo sapiens*. Mouse (C57BL/6J strain) and naked mole rat (NMR) fibroblast cell lines were established as previously described from 3 individual animals per species/strain.[145] Primary human fibroblasts were derived from skin biopsy. The rat fibroblast line was obtained from the University of Rochester collection.[159] Primary fibroblast lines from UM-HET3 mice and two bats (western long-eared myotis and Yuma myotis) were from the University of Michigan collection.[160] All fibroblasts were maintained in Dulbecco's modified Eagle's medium (DMEM) with Glutamax and supplemented with 10% fetal bovine serum and 1X antibiotic/antimycotic. All cells were cultured at 37°C and 5% CO_2, while NMR cells were cultured at 32°C, 3% O_2 and 5% CO_2.

Animals and predicted compounds

Three-month old UM-HET3 mice were subjected to diets containing compounds predicted with the longevity gene expression signatures via Connectivity map (CMap)[107,108]: GDC-0941 (pictilisib) (50 ppm, as in Salphati et al.[161] and Raynaud et al.[162]), enzastaurin (75 ppm, as in Graff et al.[125] and Gelardi et al.[163]), AS-703026 (30 ppm, as in Kim et al.[164]), KU0063794 (10 ppm, as in Yongxi et al.[165]), AZD8055 (20 ppm, as in García-Martínez et al.[166]) and ascorbyl-palmitate (6.3 ppm, as in Veurink et al.[167]) for 1 month. Liver and kidney samples were taken from treated mice along with their untreated sex- and age-matched littermates, which were fed *ad libitum*. In all cases, interventions continued until the animals were sacrificed. All animal protocols were approved by the Brigham and Women's Hospital and University of Michigan Institutional Animal Care and Use Committees.

All organisms received the same diet (Purina 5LG6) made in the same commercial diet kitchen (TestDiet, Richmond, IN, USA). Genetically heterogeneous UM-HET3 strain, in which each mouse had unique genetic background but was derived from inbred grandparents of the same background (C57BL/6J, BALB/cByJ, C3H/HeJ, and DBA/2J), was used in this setting. This cross produces a set of genetically diverse animals, which minimizes the possibility that the identified signatures represent gene expression patterns specific to inbred lines. Moreover, this strain was used by ITP to test the lifespan extension potential of the compounds analyzed in this study. In all cases, interventions continued until the animals were sacrificed.

All mice were kept at a density of 3 males per ventilated cage, in a specific-pathogen free vivarium, with 12:12 light:dark cycle. Animals were moved to fresh cages every 14 days. Maintenance of specific-pathogen free status was documented quarterly, using sentinel mice exposed to spent bedding sampled from each experimental cage, and evaluated by a mixture of fecal RT-PCR tests and serology for anti-viral antibodies. Health was evaluated daily for each mouse.

Animals and KU0063794 treatment

Old C57BL/6J male mice were obtained from the National Institute on Aging Aged Rodent Colony. 22 months old and 25 months old mice were subjected either to control 5053 diet or to 10 ppm KU0063794 incorporated into 5053 diet and were fed *ad libitum*. All diets were irradiated and heat-sealed and stored at 4°C for 6 months or less. During lifespan analysis mice were checked every weekday. Mice died from natural causes or were euthanized due to the moribund state (characterized by body condition score of 1.5 or less, tumor size over 2 cm, reluctance to move, or labor breathing). Animals from cross-sectional cohort were euthanized with CO_2 following by cervical dislocation. All experiments using mice were performed in accordance with institutional guidelines for the use of laboratory animals and were approved by the Brigham and Women's Hospital and Harvard Medical School Institutional Animal Care and Use Committees.

METHOD DETAILS

RNA-seq profiling of mammalian tissues

For RNA-seq analysis of mammalian species, 48 samples were collected from different tissues of young males corresponding to 8 species: baboon, beaver, long-tailed macaque, American black bear, chipmunk, sugar glider, tube-nosed bat, and white-footed mouse (Table S1A). RNA-seq libraries were prepared as previously described.[31] Paired-end sequencing with 200bp (for baboon, beaver, long-tailed macaque) or 100 bp (for bear, chipmunk, sugar glider, tube-nosed bat, white-footed mouse) read length was performed on Illumina HiSeq2000 platform. Additional RNA-seq libraries were obtained from the following NCBI Gene Expression Omnibus (GEO)[168] and Sequence Read Archive (SRA) datasets: GSE43013,[31] GSE30352,[37] GSE30337,[34] GSE41637,[38] GSE33300,[41] GSE42297,[4] GSE39150,[40] PRJNA263931,[35] PRJNA72723[39] and GSE50726[36] (Table S1A). Total mammalian dataset included 371 biological samples from brain (36 species), kidney (36 species), liver (41 species), cerebellum (10 species), heart (13 species), and testis (10 species). As an out-group, we also included 12 chicken (*Gallus gallus*) samples obtained from the same organs. All analyzed samples were obtained from males, except for vervet and horse where females were used.

For RNA-seq analysis corresponding to drugs predicted with longevity signatures, we used 4 and 8 biological replicates per experimental group for treated and control mice, respectively (Table S1C). RNA was extracted from tissues with PureLink RNA Mini Kit as described in the protocol and passed to sequencing. RNA-seq libraries were prepared as described in Hashimshony et al.[169] and sequenced with 100 bp read length option on the Illumina HiSeq 2500.

Stress resistance assay

Stress resistance assay was performed as described previously.[100] Briefly, on day 1, fibroblasts were suspended at a concentration of 5,000 cells/100 μl (0.5×10^5 cells/ml) in DMEM plus 0.5% BSA. Cells were then aliquoted into 96-well plates and incubated overnight at 37°C or 32°C (in the case of NMR cells) in a 5% humidified CO_2 or 5% humidified CO_2, 3% O_2 (for NMR) incubator. On day 2, 0.1 μl of Cardamonin, Clofilium tosylate, Deguelin or DMSO (control) were added, for an initial compound concentration of 8 μM (Cardamonin), 4 μM (Clofilium tosylate), 2 μM (Deguelin) and the initial DMSO concentration of 0.1%. Plates were then incubated overnight. On day 3, 5 μl of medium alone (control) or medium plus paraquat were added to the plates. Paraquat concentration was optimized for each species so that, on average, approximately 50% of fibroblasts survived following this treatment. On day 4, 100 μl of CellTiter-Glo detection reagent was added to each well, and luminescence (RLU) was measured on a SynergyTM HT Multi-Mode Microplate Reader (BioTek® Instruments, Inc). The experiment was reproduced 3-6 times for each compound and control group for every species and mouse strain.

Please cite this article in press as: Tyshkovskiy et al., Distinct longevity mechanisms across and within species and their association with aging, Cell (2023), https://doi.org/10.1016/j.cell.2023.05.002

Frailty index and gait speed

Frailty index was measured as described in Schultz et al.[170] prior to the start of the treatment (in 25-month-old mice) and after 5 months of treatment for control mice and mice subjected to KU0063794 (30-month-old mice). Frailty index score was calculated per the original protocol. Gait speed was measured as in Shindyapina et al.[171] for same groups of mice. In brief, mice were positioned in the standard mouse cage that had free space on the one end and a food container on the other end. The time of finish was determined as the time when the mouse nose crossed the finish line. Each mouse was let run four times and the median value was recorded. An attempt was considered successful if the mouse crossed the finish line without standing or turning 90 degrees or more during the run. Ten seconds were recorded if a mouse failed to finish the run in 10 seconds.

Glucose tolerance test

24-month-old mice subjected KU0063794 for 2 months and age-matched control mice were placed into food-free cages for 16 hours (usually from 7 pm until 11 am the next day). The next day, mice were weighted, marked, bled from the tail and the fasting blood glucose level was measured with a glucometer Accu-Chek Perform Nano (Accu-check inform II strips). Filtered 30% glucose in sterile saline solution (Sigma) was injected i.p. at a final dose of 1 g/kg of body weight. Injections were done at 30-second intervals between the mice. Glucose level was measured again at 20, 40, 60 and 120 minutes after the injection with a 30-second interval between the mice.

Flow cytometry

Myeloid cells were gated as $CD45^+CD3^-CD11b^+CD19^-$, B cells as $CD45^+CD11b^-CD3^-CD19^+$, T cells as $CD45^+CD3^+CD11b^-CD19^-$. mAbs used for staining included: anti-CD19 [6D5], anti-CD11b [M1/70], anti-CD3 [17A2], and anti-CD45 [30-F11] (all from Biolegend). Dead cells were excluded by DAPI staining. Data was collected on a Cytek DXP11 and analyzed by FlowJo software (BD). Spleens were gently pressed between microscopy slides to get single-cell suspensions. One ml of cell suspensions were 1) incubated with 14 ml of red blood lysis buffer for 10 min on ice, 2) centrifuged at 4°C, 250 g for 10 min, 3) washed once with 1 ml of FACS buffer (1% FBS in PBS), 4) stained in 100 ul of AB solution (2 ng/ul of each AB) at 4°C for 20 min protected from light, 5) washed again, 6) filtered into tubes with cell strainer snap cap (Corning), and 7) analyzed with flow cytometry.

Necropsy analysis

Mice were euthanized with CO_2 followed by cervical dislocation. The chest and abdomen were opened, and the body was immersed into formalin solution and stored at 4°C until further analysis. For necropsy, all organs, including small endocrine organs, were dissected, trimmed at 5 mm thickness and embedded in paraffin blocks. Paraffin blocks were sectioned at 5 μm and stained with hematoxylin and eosin. The slides were examined blindly by a pathologist.

QUANTIFICATION AND STATISTICAL ANALYSIS

RNA-seq data processing

For tissue samples from mammalian species, we utilized the pipeline from Ma et al.[30] to generate reference sequences and identify species-specific ortholog gene sets (using the published annotated genomes in Ensembl or NCBI if available; otherwise generating *de novo* transcriptome assembly with Trinity). Genome annotation for 29 out of 42 species was available in NCBI or Ensembl, whereas the other 13 species required *de novo* assembly of the transcriptomes. The RNA-seq reads were then mapped to the species-specific ortholog sets using STAR[155] and read counting was performed by featureCounts.[156] Those ortholog sets with too high counts (i.e. read counts contributing to >5% of the total counts) or too low counts (i.e. less than 10 counts in >30% of the samples) were discarded. The library sizes were scaled by trimmed mean of M-values (TMM) method, $\log_{10}$-transformed, and quantile-normalized.[151] The final expression set consisted of 13,784 gene orthologs across 42 species, including 41 mammalian species and chicken (*Gallus gallus*) used as an out-group. Phylogenetic tree on Figure 1A was constructed based on nucleotide sequences of 13,784 gene orthologs using neighbor joining method.

For samples corresponding to predicted compounds, quality filtering and adapter removal were performed using Trimmomatic (version 0.32).[146] Processed/cleaned reads were then mapped with STAR (version 2.5.2b)[155] and counted via featureCounts (version 1.5).[156] To filter out genes with low number of reads, we left only genes with at least 6 reads in at least 66.6% of samples, which resulted in 9,011 detected genes according to Entrez annotation. Filtered data was then passed to RLE normalization.[154]

Ortholog quality of mammalian species samples

Before proceeding with data analysis of mammalian species RNA-seq samples, we assessed the quality of the orthologs in terms of the following areas (Figure S1). The coding sequences were checked for completeness of open-reading frame (including start codon, stop codon, and correct coding frame). Sequence fragments or partially missing sequences (e.g. those species with no published genomes and had to rely on *de novo* transcriptome assembly) were filled up using the consensus of related species. In the mammalian transcriptome dataset, 80% of the orthologs did not require filling up or were filled up <10% of sequence length, and there was no significant bias against those filled up using consensus in terms of standardized expression values (Figure S1B). To assess the quality of our *de novo* assembly strategies, we also generated *de novo* transcriptomes for those species with published genomes (18

species with genomes available in Ensembl and 11 species with genomes available in NCBI; Table S2). Read alignment rates to the ortholog sets were consistent across the samples with and without complete genomes (Figure S1A, upper), and the Spearman correlation coefficients between the read counts based on *de novo* assembled ortholog set alignment and those based on genome alignment were >0.95 for most of these species (Figure S1A, lower), suggesting that the *de novo* assembled ortholog sets accurately reflected the gene expression counts. Lastly, for each of the 18 species with annotated genomes in Ensembl, we compared our ortholog definition with the Ensembl ortholog definition. Ortholog data for ~10,000 to ~15,000 of our orthologs (per species) could be found in Ensembl, and 90-99% of them matched our definition (Table S2), suggesting that the results of our pipeline were consistent with other databases.

Life history data of the species

The adult weight (AW), maximum lifespan (ML) and female time to maturity (FTM) data of the species (or if not available, for a closely related species) were obtained from the Animal Ageing and Longevity (AnAge) Database.[144] In addition, since both ML and FTM increase with AW, we calculated the body mass adjusted residuals (i.e. MLres and FTMres), to represent the ratio between the observed longevity and the expected longevity based on body mass.[27,30] Two allometric equations were used to calculate the residuals. The MLres equation, $MLres = ML/(4.88 \times AW^{0.153})$, was based directly on the documentation of the AnAge database (http://genomics.senescence.info/help.html#anage). The FTMres equation, $FTMres = FTM/(78.1 \times AW^{0.217})$, was based on linear regression using the FTM and body mass records of 1330 mammalian species in the AnAge database.

Mammalian RNA-seq data analysis

Principal component analysis (PCA) was performed on the standardized expression values and the first three Principal Components (PCs) were extracted. 6,050 genes significantly enriched or depleted in one organ relative to the others (p value <0.01) were identified with Wilcoxon rank-sum test. Heatmap showing organ-specific expression patterns was constructed based on standardized expression values of these genes. Complete linkage hierarchical clustering was performed based on Spearman correlation distance.

ANOVA was used to assess the percentage of variation in the expression of individual genes explained by species and tissues across all available samples. Within tissues, 82-94% of variance was explained by species (Figure S1D). To account for a potential batch effect introduced by different data sources aggregated during analysis, we also performed a similar analysis within datasets, running it on samples from the same data source. Datasets with at least 4 different species and 8 biological replicates available for a given organ were considered. For each of them, we applied ANOVA for every gene to estimate the percentage of variation in the expression explained by species. The calculated estimates were pooled together and visualized on boxplots. This analysis resulted in similar estimates (78-95% of variance explained by species), suggesting that batch effect introduced by various sources of data is relatively small compared to species-specific differences (Figure S1D).

Spearman correlation between average expression profiles of different species for each tissue was calculated in a pairwise manner (Figure 1C). To adjust for differences in the number of species and biological replicates available for each organ, a similar analysis was performed for nine species that were available for all presented organs (bonobo, chicken, chimpanzee, gorilla, human, macaque, mouse, opossum, and platypus). Besides, the same number of biological replicates for each species was selected across all tissues. The difference between the median correlation coefficient in the testis and other organs was assessed using Wilcoxon rank-sum test (Figure S1E).

To identify genes with significant correlation to the longevity traits (ML, MLres, FTM or FTMres), regression was performed using the generalized least square approach, by incorporating the phylogenetic relationship in the variance-covariance matrix.[27,30,172,173] As previously described,[27,30] four different trait evolution models ('null', 'Brownian motion', 'Pagel's lambda', and 'Ornstein-Uhlenbeck') were tested and the best fit model was selected based on maximum likelihood. A two-step procedure was applied to verify the robustness of the results. In the first step, the species whose exclusion would lead to most improvement in the slope p value (i.e. a potential outlier), was identified and removed. The regression p value of this step was reported as 'sensitive p value'. In the second step, maximum p value after exclusion of each individual species was identified, reported as 'robust p value'. The False Discovery Rate (FDR) correction based on Benjamini-Hochberg (BH) approach was performed to adjust for multiple hypothesis testing.[174] To qualify as a top hit, we required a gene to have adjusted p value < 0.05. To test if genes associated with longevity retained their association after adjustment for body mass, we performed the same procedure for identified top hits (adjusted p value < 0.05) using MLres or FTMres as outcome variables. We qualified gene as significant if corresponding p value < 0.05 after this adjustment.

To account for a potential bias introduced by differences in gene length and sequence variation across species, for every gene in the ortholog set we calculated its length in all examined species based on the *de novo* assembled transcriptomes together with the nucleotide sequence distance from the corresponding *Mus musculus* sequence. Pairwise sequence distance was estimated based on Jukes-Cantor model with 'dist.ml' function from R package *phangorn*.[158] We then introduced estimated values of gene length and sequence distance as additional covariates in the regression model, which was used to identify significant gene expression signatures of ML and FTM across mammalian species. For every tissue, we then calculated the proportion of signature genes that retained a statistically significant association with the longevity traits following this adjustment (p value < 0.05). Adjustment for variation in gene length and nucleotide sequence across species did not affect the statistically significant association with ML and FTM for more than 96.5% and 93.5% of identified signatures, respectively.

To build an unbiased model of ML prediction based on tissue gene expression, we applied an Elastic Net linear regression algorithm from scikit-learn library (linear_model.ElasticNet function). We divided species in training and test sets using leave-one-out (LOO) procedure. Each individual species was consequently used as a test sample, while other species were used for training and cross-validation (CV). Hyperparameters of the model were trained using 10-fold cross-validation. Trained hyperparameters included Pearson's correlation coefficient threshold for feature selection (between 0.15 and 0.75), alpha (between 10^{-4} and 10^{2}) and l1 ratio (between 0.2 and 1). Hyperparameters associated with the lowest mean absolute error (MAE) on CV set were chosen during each LOO iteration. The trained model was then applied to the test sample, and predicted value of $\log_{10}$(Maximum Lifespan) was calculated. Afterwards, predictions for each test sample were pooled together, and the accuracy of the model was assessed using mean absolute error (MAE), R^2 and Pearson's correlation coefficient. When applied to test set, final model resulted in $R^2 = 0.78$ and MAE = 0.13, corresponding to ~35% difference in ML (Figure 2D). The same approach was used to estimate the accuracy of prediction based on tissue gene expression and adult AW as well as AW alone. AW was included in the model in both linear and logarithmic scales. Model based only on AW resulted in $R^2 = 0.39$ and MAE = 0.24 (Figure S2D).

Top gene expression predictors of mammalian ML were assessed based on model coefficient distributions across Elastic Net models trained on different subsets. For every gene, mean model coefficient was calculated together with its standard error. Statistical significance of gene coefficient difference from zero was estimated using t test. p values were adjusted for multiple comparisons using BH approach. To quality as a robust predictor of maximum lifespan, we required a gene to have adjusted p value < 0.05.

Signatures of maximum lifespan in cultured primary skin fibroblasts collected from 16 mammalian species were obtained from Ma et al.[30] Spearman correlation between gene expression signatures associated with mammalian longevity in different organs and fibroblasts was calculated in a pairwise manner. The union of top 500 longevity-associated genes (with the lowest p values) was used for each pair of signatures. Hierarchical clustering of signatures was performed based on complete linkage and Euclidean distance. To determine the statistical significance of overlap between signatures associated with ML or MLres in different tissues, we performed Fisher exact test separately for up- and downregulated genes, considering 13,784 genes as a background.

Aggregation of aging data for meta-analysis

To identify signatures associated with mammalian aging, we aggregated gene expression data from the following GEO, ArrayExpress[175] and SRA datasets: GSE9103, GSE123981, GSE3150, GSE6591, GSE74463, GSE53960, GSE66715, GSE11291, GSE34378, GSE27625, GSE12480, GSE36192, GSE1572, GSE28422, GSE25941, GSE53890, GSE38718, GSE674, GSE17612, GSE21935, GSE362, GSE132040, E-MTAB-3374, PRJNA281127, PRJNA516151. The datasets included RNA-seq and microarray samples obtained from different tissues of *Mus musculus*, *Rattus norvegicus* and *Homo sapiens*. In total, our meta-analysis covered aging-associated changes in 17 different tissues based on 92 datasets from 25 different sources (Figures 3A and S3A; Table S1B).

Prior to aggregating the data into signatures, the following preprocessing protocol was executed for individual datasets. For RNA-seq data, low-covered genes were filtered out using a soft threshold. Then gene Ensembl IDs were mapped to Entrez IDs. The read was filtered out if there were zero or multiple Entrez IDs corresponding to the Ensembl ID. In case of multiple Ensembl IDs corresponding to one Entrez ID, the gene coverage was calculated as the sum of the corresponding read coverages. Afterwards, the expression data was normalized using RLE method,[154] log-transformed and scaled.

For microarray data, gene expression was log-transformed to conform to normal distribution if needed. Then samples within every study were normalized by scaling and quantile normalization. Afterwards, platform IDs were mapped to Entrez ID gene format. If multiple IDs corresponded to the same Entrez IDs, average log-expression was calculated.

For both types of data, self-consistency was evaluated using PCA, and outlier samples were discarded. Finally, mean and standard error of aging-associated gene EC for every gene was calculated together with p value using limma.[152] Pairwise comparison model was utilized for datasets with 2 age groups, whereas linear model was used for datasets with multiple ages, resulting in log fold change (logFC) or slope coefficient as a metric of EC, respectively. Since both these metrics estimate gene expression change with age – in old animals compared to young ones or per unit of time, respectively – we considered them equally in the subsequent pipeline (differences in time units were adjusted via normalization later, see "aging gene expression signatures"). Obtained p values were adjusted for multiple hypothesis testing using BH approach. Therefore, for every dataset we estimated mean EC, standard error of EC, p value and adjusted p value for each expressed gene. Importantly, one study may include multiple datasets if several species or tissues have been analyzed there. This may be a source of batch effect, which we removed during subsequent steps of the analysis.

Dependence of pairwise correlation between the gene expression age-related ECs from individual datasets on meta-features (belonging to the same study, species and tissue) (Figure 3G) was examined using the following model:

$$\rho = b_0 + b_1 \times study + b_2 \times tissue + b_3 \times species,$$

where ρ is a pairwise Spearman correlation coefficient, and study, tissue and species are binary factor variables, equal to 1 if source ID, tissue and species, respectively, are the same for both datasets in the certain pair, and 0 otherwise. Belonging to the same tissue had the highest effect on the similarity between aging-associated gene ECs (adding, on average, 0.23 to Spearman ρ), followed by dataset- and species-specific effects (each adding, on average, 0.06 to the Spearman ρ).

Please cite this article in press as: Tyshkovskiy et al., Distinct longevity mechanisms across and within species and their association with aging, Cell (2023), https://doi.org/10.1016/j.cell.2023.05.002

To assess independent effects of tissue and species on similarity across datasets, we tested if they are maintained regardless of whether the other factor matches. Specifically, we calculated Spearman correlation coefficients for the datasets corresponding to (i) different tissues and species, (ii) different tissues and the same species, (iii) the same tissue and different species, (iv) the same tissue and species (Figure S3B). To account for a potential batch effect associated with the source of data, for this analysis we utilized only the pairs of datasets from independent studies. Differences between the groups were assessed with Wilcoxon rank sum test. Interestingly, increased similarity between age-related ECs within the same species or tissue was maintained both when the other factor matched and when it differed, pointing to the existence of independent tissue- and species-specific aging transcriptomic biomarkers. Statistical significance of positive average correlation between the datasets corresponding to different species, tissues and studies (group (i)) was assessed with Wilcoxon signed-rank test.

Aging gene expression signatures

Prior to signatures identification, normalization of ECs from individual datasets was performed based on the following algorithm. First, denoised Pearson correlation of age-related ECs was calculated for each pair of datasets (Figure S3A). For that, we used the union of top statistically significant aging-associated genes (with the lowest p values) in each dataset within certain pair. The threshold for the number of genes was chosen so that it maximizes the number of significant pairwise correlations (adjusted p value < 0.05 & absolute $\rho > 0.1$). We identified the threshold of 250 genes to be optimal for noise removal. Second, to bring ECs to the same scale across individual datasets, we calculated normalization coefficients using multiple Deming regression model. Contrary to the simple linear regression, Deming regression fits data by minimizing errors on both x and y axes, treating both variables equally. Therefore, it is well suited for calibration of similar measurements performed in different studies.[176] We optimized this method by applying it to all pairs of aging datasets simultaneously, producing the set of normalization coefficients that would minimize sum of pairwise differences in ECs across all the data. During this step, we applied multiple Deming regression to the pairs of datasets with significant correlations (adjusted p value < 0.05 & absolute $\rho > 0.1$), considering top 250 significant genes in each case. The cumulative squared loss across considered pairs of datasets was minimized with R function optim using L-BFGS-B method. Normalization coefficients were allowed to vary between 0.01 and 100. To establish global minimum of error function, the multiple Deming regression was carried out 10 times with random initial sets of normalization coefficients, and final coefficients were chosen from the run with the smallest cumulative regression error. Among these 10 runs, the error minimum was the same for the majority of runs indicating that the global minimum was achieved for each signature (Figure S4).

Finally, normalized ECs from individual datasets were used to identify robust aging signatures. To account for standard error of gene ECs and to remove batch effect related to the belonging of several datasets to the same study, we applied linear mixed-effect model using R package *metafor*.[33,153] As an input, we used both mean and standard error of EC. To mitigate source batch effect and adjust for non-equal representation of various tissues and species in our data, random terms corresponding to the dataset ID (GEO/ArrayExpress/SRA ID), tissue and species were introduced in the model. Such approach allowed us to account for the size of the effect and variance of the estimated EC within each individual dataset, which provides a more sensitive and accurate analysis compared to previous studies focused on the comparison of lists of differentially expressed genes.

Using this procedure, we obtained aggregated normalized age-related EC and corresponding p value for every gene. We declared genes to be statistically significant signatures of aging if adjusted p value was less than 0.05. The described algorithm was utilized separately for 3 species-specific (human, mouse and rat), 3 tissue-specific (liver, brain and muscle) and 1 global (based on all presented tissues and species) aging signatures (Figure S3C).

To validate that described approach produces aging signatures that can be generalized to the independent data, we performed 4-fold cross-validation. Specifically, we divided the list of datasets into 4 similar subsets so that each independent source of data is contained only in one subset. Iteratively, we used 3 folds to identify signatures applying the method described above, while the 4^{th} fold was used as a test set. We estimated pairwise Spearman correlations between gene expression changes from different datasets in the test fold, using (i) all genes or (ii) significant signature genes (adjusted p value < 0.05) obtained on the training set. To assess the efficiency of normalization based on multiple Deming regression, we also calculated correlation coefficients using (iii) significant signature genes identified without the Deming regression step (with simple scaling normalization). Pairwise Spearman correlation coefficients from test folds were then pooled together and visualized on boxplot (Figure S3D). Differences in average correlation coefficients estimated using the described sets of genes were assessed with Wilcoxon signed-rank test and adjusted for multiple comparisons using BH approach. On average, correlation between test datasets estimated based on signature genes was significantly higher compared to those calculated based on the whole transcriptome, and it was further increased with multiple Deming regression normalization, supporting validity of the utilized approach.

The significance of overlap between different aging signatures was estimated by Fisher exact test separately for up- and down-regulated genes, considering all genes tested for age association as a background. BH procedure was used to adjust p values for multiple comparisons. Normalized ECs for visualization of gene expression changes across individual aging datasets and aggregated signatures (Figures 3F and 3H) were calculated as $\frac{EC_i}{sd(EC)}$, where i denotes a certain gene and $sd(EC)$ is a standard deviation of ECs across all genes in the given dataset or signature.

Please cite this article in press as: Tyshkovskiy et al., Distinct longevity mechanisms across and within species and their association with aging, Cell (2023), https://doi.org/10.1016/j.cell.2023.05.002

Aggregated biomarkers of aging and longevity

To identify genes robustly associated with certain trait (aging, lifespan-extending interventions and longevity across species), we calculated harmonic mean p value (HMP) for every gene across individual signatures corresponding to the trait using R package *harmonicmeanp*.[48] To account for EC direction, harmonic mean p values were estimated for both positive and negative association as described in Yoon et al.[83] Briefly, individual p values obtained from two-tailed tests were halved and synchronized according to the effect direction. In other words, every p_i was converted to pi/2 if the directions of true effects and tested association coincide or to $1 - p_i$ otherwise. Then harmonic mean p values were calculated for both cases, and the smaller of the two combined p values was selected. This p value was multiplied by two for the two-tailed meta-analysis p value and adjusted for multiple comparisons using Benjamini-Hochberg method. We considered a gene as significant in the aggregated signature of the trait if its adjusted HMP was <0.05 and the rate of signatures where it was changed in the same direction was higher than 80%. Overlap of significant trait signatures was assessed using Pearson's chi-squared test separately for each pair of traits.

Expression of signatures across cell types

Cell type deconvolution of mammalian organ samples was performed with R package *BayesPrism*.[49] Tabula Muris single-cell atlas (both 10x and FACS data) corresponding to liver, kidney, brain (myeloid and non-myeloid), limb muscle and heart, was downloaded from GEO database (GSE109774) and used as a reference for cell type annotation.[24] For visualization, different types of epithelial and endothelial cells were pooled together. B cells, T cells, microglial cells, Kupffer cells, macrophages, natural killer cells and other leukocytes were considered as immune cells. The average proportion of each cell type and standard error was calculated for every organ (Figure S2F). To adjust for subtle variation in blood cell abundance across species, we introduced the proportion of immune cells estimated for individual samples as a separate covariate into the regression model. For every tissue, we then estimated the percentage of previously identified signature genes that retained a statistically significant association with mammalian maximum lifespan (p value < 0.05) after this adjustment.

A gene was considered to be expressed in a certain cell type if at least 3 counts were detected in at least 5% of cells corresponding to this type. For every gene, we calculated a proportion of individual cell types where it was expressed. To estimate it, we considered 99 cell types present in the Tabula Muris single-cell atlas across all available tissues. For individual and aggregated signatures of mammalian lifespan and aging, we visualized the distributions of calculated proportions for the corresponding significant genes (adjusted p value < 0.05) using boxplots (Figure S2E).

We defined genes as blood cell specific biomarkers, if they were expressed in a higher proportion of blood cell types than non-blood cell types, and less than in 10% of non-blood cell types, according to the Tabula Muris atlas. This threshold resulted in 830 blood cell specific genes. Blood cell specific biomarkers accounted for fewer than 1.5% of genes significantly associated with maximum lifespan of mammalian species, and their removal did not affect significant positive correlation between signatures of individual tissues (Spearman $\rho > 0.21$ for all pairwise comparisons).

Comparison of longevity signatures and traits

To compare mean ECs corresponding to individual gene expression signatures associated with mammalian aging and longevity at inter- and intra-species level, we utilized denoised Spearman correlation method as described previously. p values were adjusted for multiple comparisons using BH method. Normalized ECs for barplot visualization were calculated by dividing aggregated gene expression changes on standard deviation of ECs across all genes within the signature as described previously (Figure 4D). Genes were selected for visualization if they (i) were significantly associated (adjusted p value < 0.05) with multiple longevity or aging traits and (ii) were established to be associated with longevity based on other studies or were annotated as a member of gene set demonstrating significant association with the analyzed traits.

To identify a comprehensive list of shared and distinct molecular biomarkers across examined traits, we utilized Fisher's combined probability test from R package *metap*, an effective and sensitive technique to integrate p values from various tests. Contrary to the HMP method, this approach requires aggregated tests to be independent, but provides high statistical power for detection of incomplete associations.[83] To detect common biomarkers for a group of traits, Fisher's combined probability test was applied to every gene, using HMP corresponding to each model and adjusting for the direction of EC (similar to the HMP algorithm). To detect distinct biomarkers, the same algorithm was applied, but sign of EC was inverted for one of the models. In each case, Fisher's combined probability test was applied separately for both positive and negative associations, and the minimum of the two resulted p values was chosen, similar to the HMP algorithm described previously. BH method was used to adjust resulted p values for multiple hypothesis testing. We considered a gene as a significant common or distinct biomarker of the traits if its adjusted Fisher's combined probability p value was <0.05 and the rate of signatures where it was changed in the same direction was higher than 80% within each of the traits included in the analysis. The described algorithm was performed separately for identification of common and distinct biomarkers within each pair of traits (''Aging & Interventions'', ''Aging & Species'', ''Interventions & Species'') as well as between aging traits and both longevity traits at once (''Longevity & Aging''). As a result, we found 300-1,200 significant shared and opposite signatures across various pairs of traits (Figure 4F). Difference between the number of significant common and distinct biomarkers for each of the analyzed trait sets was evaluated using two-sample proportion test.

Yeast signatures of longevity and aging

Gene expression signatures of budding yeast longevity across natural strains and deletion mutants were identified in our previous study.[70] Briefly, 40 natural strains of *S. cerevisiae* were used to evaluate biomarkers of replicative lifespan (RLS) across strains, while signatures of long-lived deletion strains were calculated based on RLS and gene expression data of 1,376 knockout strains from McCormick et al.[72] and Kemmeren et al.,[71] respectively.

To obtain gene signatures of yeast replicative aging, we utilized deconvolved transcriptome data from Janssens et al.[73] Genes, which expression was associated with time in linear and logarithmic scale, were identified using limma.[152] Resulted p values were adjusted for multiple hypothesis testing using BH method. Genes with adjusted p value < 0.05 were considered significant.

Mean slope coefficients corresponding to ECs associated with yeast aging and longevity across natural and deletion strains were compared using Spearman correlation. p values were adjusted for multiple comparisons using BH method. Normalized ECs for barplot visualization were calculated by dividing gene expression changes on standard deviation as described previously.

Functional enrichment analysis of signatures

For identification of functions enriched by individual aging and longevity signatures, we performed gene set enrichment analysis (GSEA)[147] on a pre-ranked list of genes based on $\log_{10}$(p value) corrected by the sign of regulation, calculated as:

$$-log_{10}(pv) \times sgn(ec),$$

where *pv* and *ec* are p value and aggregated expression change for certain gene, respectively, estimated with mixed-effect model, and *sgn* is signum function (is equal to 1, -1 and 0 if value is positive, negative and equal to 0, respectively). REACTOME, KEGG and GO BP from Molecular Signature Database (MSigDB) have been used as gene sets for GSEA.[147] Adjusted p value cutoff of 0.1 was used to select statistically significant functions.

To identify functions enriched by aggregated biomarkers of traits as well as common and distinct signatures of various models, we performed Fisher exact test using R package *gprofiler2*,[148,149] considering all genes tested for association with the corresponding trait as a background. KEGG, REACTOME and GO BP ontologies were used. We declared functions to be enriched if their BH adjusted Fisher exact test p value was smaller than 0.1. Gene ratio was estimated for enriched functions as proportion of genes in the given signature, which are associated with the given pathway. Significance score was calculated as $\log_{10}$(adjusted p value) corrected by the sign of direction.

Hierarchical clustering of enriched functions for a heatmap was performed based on normalized enrichment scores (NES) and significance score for GSEA and Fisher exact test, respectively, using complete linkage and Spearman correlation distance. Enriched functions that (i) were significantly enriched (adjusted p value < 0.1) by multiple signatures and (ii) represented different aspects of cellular biology, as assessed manually and based on the overlap of corresponding gene sets, were selected for visualization. The whole lists of statistically significant enriched functions are available in Tables S3 and S5.

Metabolomics analysis

Metabolite profiling data corresponding to 26 mammalian species and the effect of 5 lifespan-extending interventions on mouse liver in males and females were based on data from Ma et al.[27] and Tyshkovskiy et al.[33] Each species in the mammalian dataset was represented by 1-4 biological replicates per tissue (2.6 samples on average), while each treatment in the longevity intervention dataset was represented by 5-6 biological replicates per sex. To filter out metabolites with low coverage, only metabolites detected in at least 66.6% of the samples were kept. Afterwards, filtered data were $\log_{10}$-transformed and scaled.

The effect of individual interventions on metabolite concentration was assessed separately for males and females using limma. Besides, a single model combining the effect of all interventions was built to identify common signatures of lifespan extension. Finally, to find metabolites associated with the quantitative effect of interventions, a linear model incorporating the effect of certain intervention on median and maximum lifespan (taken from Tyshkovskiy et al.[33]) was created. In each case, sex and batch were introduced in the model as separate covariates to account for the possible bias. Metabolites were declared significant if their p values, adjusted by BH method, were <0.1.

To investigate associations of metabolite levels with ML, MLres, FTM and FTMres across species, phylogenetic regression model was built separately for each tissue (brain, liver, kidney, and heart), as described previously for gene expression data. To identify signatures of mammalian longevity across tissues, we aggregated mean slopes of metabolite concentration from all the organs together with their standard errors in a fixed-effect model using R package *metafor*. Metabolites were declared significant if their p values, adjusted by BH method, were less than 0.1.

Partial correlation network

To assess interdependence between various molecular mechanisms of longevity and aging, we utilized the mammalian tissue gene expression dataset and computed a partial correlation network for species maximum lifespan, adult weight, transcriptomic signatures of aging and lifespan-extending interventions as well as the expression of key individual genes (*Igf1*, *Rela*, *C*th) and functional gene sets significantly associated with different models of longevity and aging (Figure 6C). For every available tissue and species, each of these features was calculated. For functional gene sets, the score was estimated as mean normalized expression of all genes

Please cite this article in press as: Tyshkovskiy et al., Distinct longevity mechanisms across and within species and their association with aging, Cell (2023), https://doi.org/10.1016/j.cell.2023.05.002

associated with this function according to KEGG or REACTOME ontology. For the signatures of aging and interventions, the difference of mean normalized expression between genes positively and negatively associated with this trait was calculated. Biomarkers of mouse maximum lifespan and the aggregated signature across species and tissues were used as gene sets associated with longevity interventions and aging, respectively. Sparse partial correlation network of estimated features was computed with R package *glasso*, using graphical lasso regularization and model selection based on Extended Bayesian information criterion (EBIC).[157] The resulted Gaussian graphical model was visualized with R package *qgraph*.

Effect of compounds on fibroblast survival

Percentage of viable cells in each sample was subjected to log transformation. The effect of every compound on cell survival under oxidative stress conditions was calculated as a difference between mean log percentage of viable cells in experimental group (treated with certain compound) and mean log percentage of viable cells in control group (treated by DMSO). Standard error was calculated using t test. To estimate the average effect of the compound on the survival of cells from short-lived species (mice and rats), we aggregated the corresponding estimates of an average compound effect and SE across these species in a single random-effect model using R package *metafor*. An association between the effect of a compound and species longevity was assessed with fixed effect model where ML or MLres was included as an independent variable. Percentage of viable cells in the control group was not significantly correlated with species lifespan (Spearman $\rho = 0.16$, p value = 0.24). To adjust for a potential effect of this factor on the compound effect, we included mean log percentage of viable cells in control group to the regression model as a covariate. This adjustment did not affect statistical significance of investigated associations.

Enrichment of trait biomarkers by gene sets

To identify enrichment of trait biomarkers by housekeeping, essential and evolutionary old genes, we utilized gene sets from Wang et al.[44] Gene essentiality was defined based on two metrics: mutation intolerance (the probability of being intolerant to loss-of-function mutation)[177] obtained from ExAC release 0.3.1 (http://exac.broadinstitute.org/), and haploinsufficiency (sensitivity to a gene copy number reduction) estimated in Shihab et al.[178] Phylogenetic age of the genes was obtained from the GenTree database.[179] Evolutionary old and young genes were defined as 1:1 therian orthologs that originated before the emergence of bony vertebrates and after the emergence of tetrapods, respectively.

To assess if significant trait biomarkers as well as common and opposite signatures of various traits are enriched for a certain feature described above, we utilized Fisher exact test. For each pair of gene sets (housekeeping / non-housekeeping, haplosufficient / haploinsufficient, mutation tolerant / intolerant, evolutionary old / young), we estimated overrepresentation of one gene set over the other in a subset of signature genes. As a background for each trait, we used genes that were tested for an association with the corresponding trait in the signature analysis but did not reach statistical significance. Besides, to account for the fact that some of the gene sets may be enriched for genes with a higher expression, and highly expressed genes have also a larger chance of being identified as a signature of a certain trait due to a higher statistical power, we controlled for this potential confounder by randomly selecting background genes in such a way that the genes associated and not associated with the trait have a similar distribution of average expression in mammals (Figure S6C). Specifically, for every trait, we divided the range of average log(expression) of genes across mammals in 100 uniform windows, and for every window we randomly picked up the same proportion of genes showing and not showing a significant association with the trait. The resulting subset of non-significant genes was used as a background for Fisher exact test. Enrichment for certain feature within each pair of gene sets was considered significant if BH adjusted p value was smaller than 0.1. Odds ratios (OR) were calculated as:

$$\frac{\left(\frac{sign_{set1}}{nonsign_{set1}}\right)}{\left(\frac{sign_{set2}}{nonsign_{set2}}\right)},$$

where *set*1 and *set*2 correspond to the opposite sets of genes (etc. housekeeping and non-housekeeping genes), while *sign* and *nonsign* correspond to the number of genes associated and not associated with the trait, respectively.

Pathway enrichment analysis for evolutionary old, haploinsufficient and mutation-intolerant signatures of longevity across species and evolutionary young, haplosufficient and mutation-tolerant signatures of lifespan-extending interventions was performed using Fisher exact test in a similar way. REACTOME and KEGG ontologies were utilized.

Prediction of longevity interventions

To identify interventions associated with longevity at gene expression level, we employed GSEA-based algorithm developed in our previous study.[33] First, for every individual signature and global trait we specified 1000 genes with the lowest p values and divided them into up- and downregulated genes. These lists were considered as gene sets. Then we ranked genes related to interventions of interest based on their p values, as described in functional enrichment section.

To find interventions associated with longevity traits from publicly available sources, we utilized GeneQuery tool (https://artyomovlab.wustl.edu/genequery/). Datasets of interest were then downloaded from GEO under the following accession numbers:

GSE15891,[110] GSE11287,[109] GSE11899,[114] GSE46209,[112] GSE63007,[113] GSE28085[115] and GSE36838.[111] We preprocessed each dataset, performed quantile normalization and Entrez ID transformation and applied limma model for calculation of p values, which were converted to $\log_{10}$(p value) corrected by the sign of regulation, as described earlier.

For compounds predicted via CMap, we calculated p values of gene expression logFC in livers of treated mice compared to control independently for every drug using edgeR. We then converted them to $\log_{10}$(p value) corrected by the sign of regulation as described earlier and proceeded to GSEA-based analysis.

We calculated GSEA scores separately for up- and downregulated lists of gene set as described in Lamb et al.[107] and defined final GSEA score as a mean of the two. To calculate statistical significance of obtained GSEA score, we performed permutation test where we randomly assigned genes to the lists of gene set maintaining their size. To get p value of association between certain intervention and longevity signature, we calculated the frequency of observed final GSEA score being bigger by absolute value than random final GSEA scores obtained from 5,000 random permutations. Permutation test p values were further adjusted for multiple hypothesis testing using BH method. Associations were considered significant if adjusted p value was smaller than 0.1.

ADDITIONAL RESOURCES

Interactive database mSALT based on *shiny* framework[150]: http://gladyshevlab.org/mSALT/.

Supplemental figures

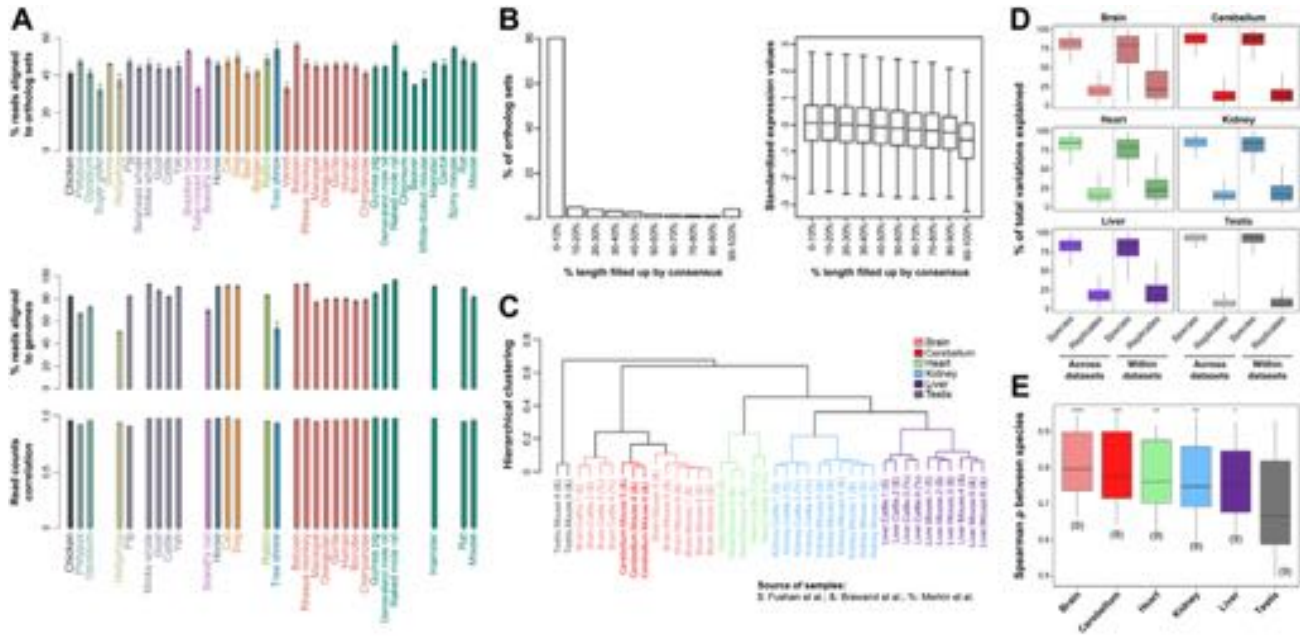

Figure S1. Mammalian RNA-seq data quality assessment, related to Figure 1

(A) Comparison of read alignment to ortholog sets and to genome. Percentage of reads for each species aligned to the ortholog sets are shown (top). For species with complete genomes, the reads were also aligned to the respective genomes (middle), and the average Spearman correlation coefficient between the read counts of ortholog set alignment and the read counts of genome alignment was calculated (bottom). Data are mean ± SE. See Table S2 for more details.

(B) The effect of filling up with consensus. The ortholog sets were categorized by their lengths that required filling up (left), and corresponding relative expression values are shown (right).

(C) Clustering of the samples from different sources. The symbols in the parenthesis indicate the source of sample. Hierarchical clustering was performed using complete linkage on a Pearson correlation distance matrix.

(D) Percentage of gene expression variation explained by species and replicates in various tissues. Boxplots reflect the percentage of explained variance in gene expression estimated using ANOVA across datasets (left) and within individual datasets (right).

(E) Gene expression patterns are least conserved in testes. Pairwise Spearman correlation coefficients were calculated for each tissue based on 9 species with all organs being present. Same number of biological replicates were used across tissues. Median values of correlation coefficients between testis and other tissues were compared using Wilcoxon rank-sum test.

*p adjusted < 0.05; **p adjusted < 0.01; ***p adjusted < 0.001.

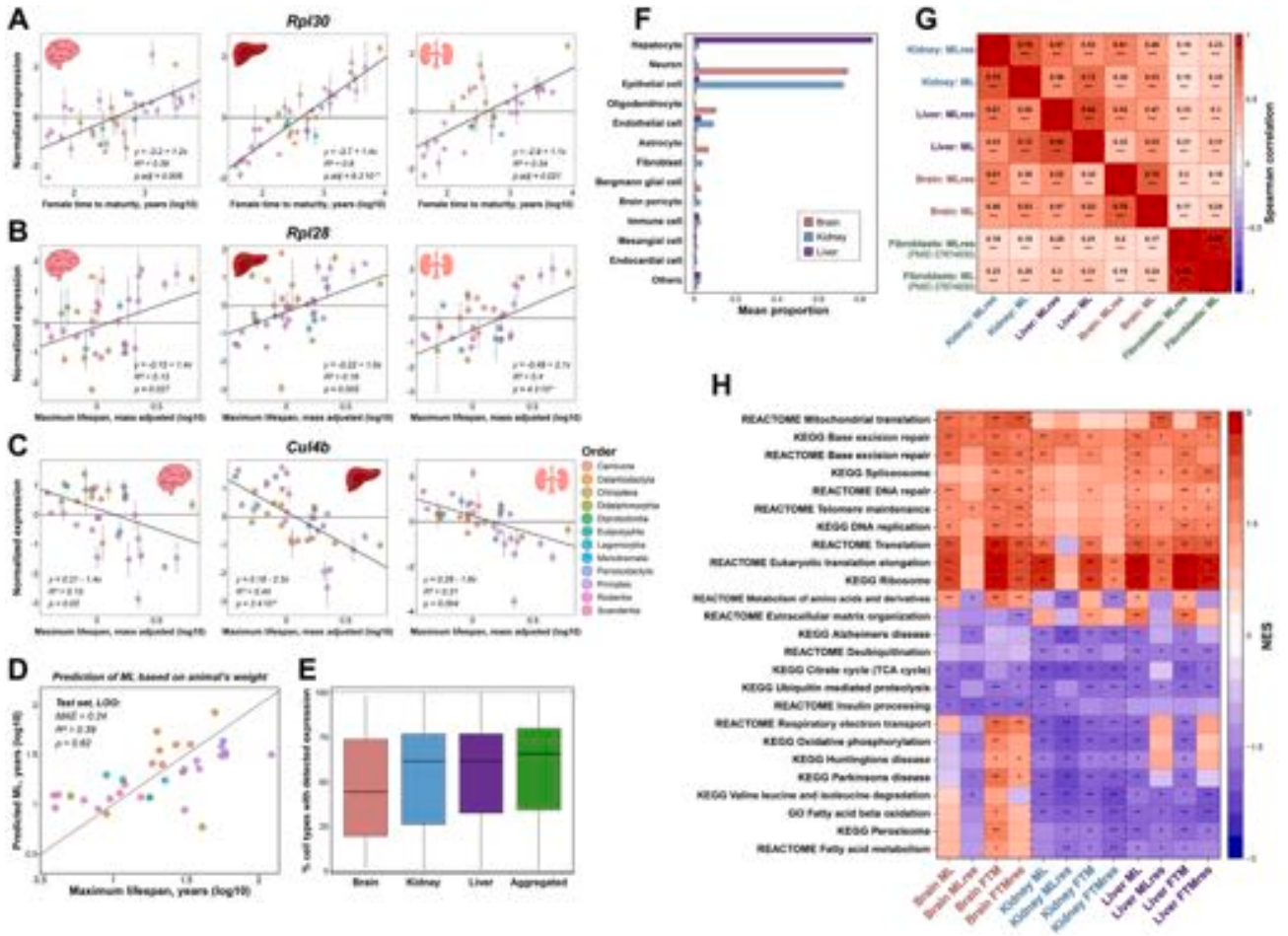

Figure S2. Additional features of gene expression signatures of longevity across mammalian species, related to Figure 2

(A–C) Association of selected genes with female time to maturity (A) and maximum lifespan adjusted for body mass (B and C). Selected genes include *Rpl30* (A), *Rpl28* (B), and *Cul4b* (C). Association between log10(female time to maturity) (A) or log10(maximum lifespan adjusted for body mass) (B and C) and average normalized log10(expression) is shown for brain (left), liver (middle), and kidney (right). The black line, equation, slope p value, and R^2 correspond to the model fitted with phylogenetic regression. Data are mean ± SE.

(D) Accuracy of Elastic Net species maximum lifespan prediction based on adult animal weight evaluated on a test set. Adult weight was introduced in linear and logarithmic scale. Each dot represents a single species and is colored by taxonomic group, as in (A)–(C). Mean absolute error (MAE), R^2 and Pearson's correlation coefficient are shown in text.

(E) Expression of genes associated with mammalian maximum lifespan across cell types. Percentages of cell types with detected expression of significant individual (brain, liver, and kidney) and aggregated longevity-associated genes (adjusted p value < 0.05) are shown.

(F) Proportion of various cell types in brain, liver, and kidney samples. Immune cells, including Kupffer cells, microglial cells, macrophages, B cells, T cells, natural killer cells, and other leukocytes, were pooled together. Data are mean proportions across species ± SE.

(G) Spearman correlation between transcriptomic signatures of longevity across species in organs and primary fibroblasts. Spearman correlation coefficients and adjusted p values are reflected by numbers and asterisks, respectively.

(H) Functional enrichment of mammalian longevity signatures. Only functions significantly enriched by at least one signature are shown (adjusted p value < 0.1). Statistical significance is reflected with asterisks. The whole list of enriched functions is in Table S3A.

˙p adjusted < 0.1; *p adjusted < 0.05; **p adjusted < 0.01; ***p adjusted < 0.001.

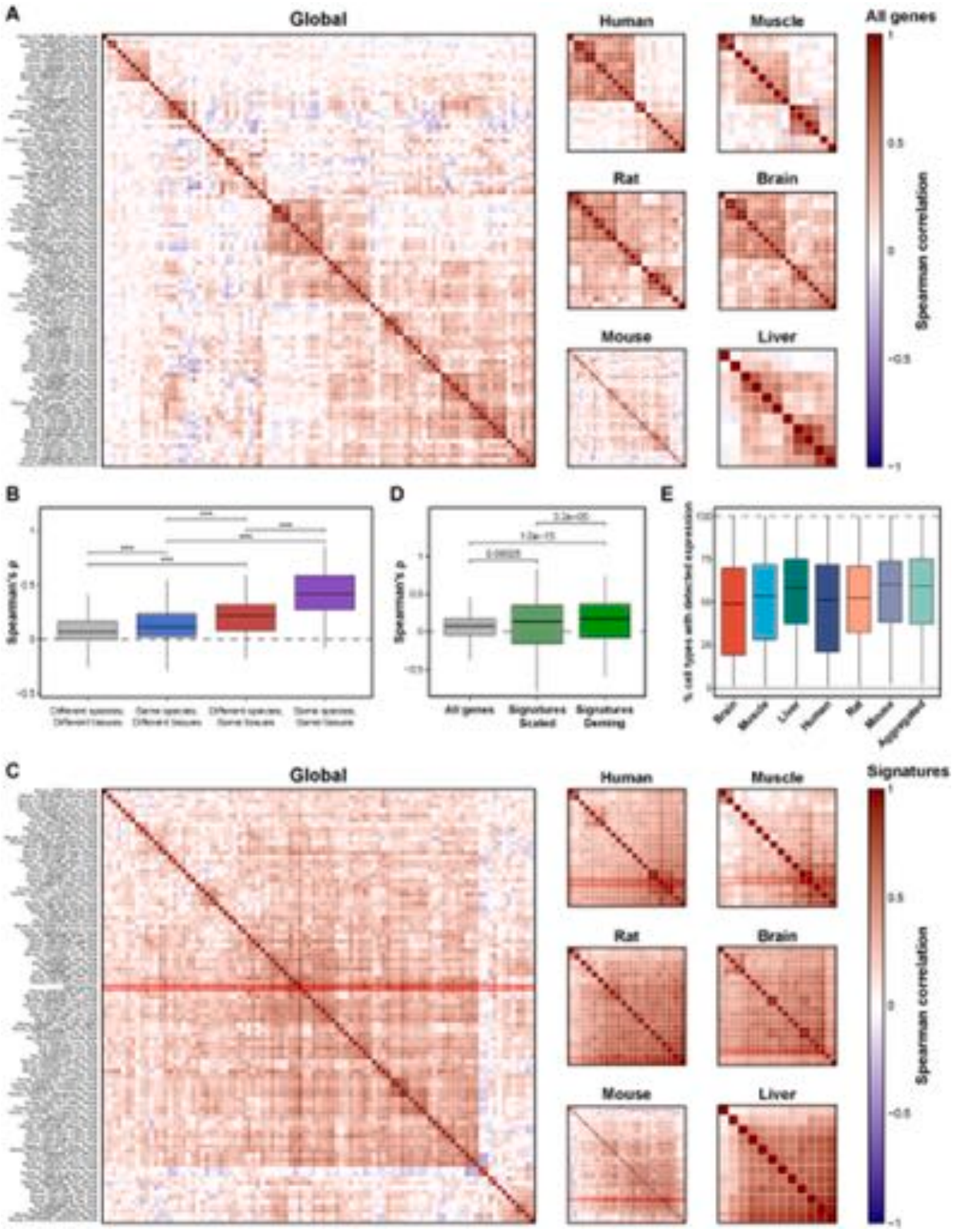

(legend on next page)

Figure S3. Identification of gene expression signatures of aging, related to Figure 3

(A) Denoised Spearman correlation between aging-associated gene expression changes across individual datasets. Correlations are shown separately for all the datasets (global), species-specific signatures (human, rat, and mouse), and tissue-specific signatures (brain, skeletal muscle, and liver).

(B) Similarity of aging-related gene expression changes across datasets corresponding to the same or different tissues and species. Denoised Spearman correlation coefficients were calculated for every pair of datasets from independent sources. Statistical difference between 4 subsets of dataset pairs was assessed with Wilcoxon rank-sum test. *p adjusted < 0.05; **p adjusted < 0.01; ***p adjusted < 0.001.

(C) Spearman correlation of age-associated changes across datasets calculated based on the signatures of aging. Correlations were calculated separately for the global signature, species-specific signatures (human, rat, and mouse), and tissue-specific signatures (brain, skeletal muscle, and liver).

(D) Spearman correlation of age-associated changes across datasets in test set calculated based on all genes or significant signature genes identified from the training test. Signatures were calculated without (middle) or with (right) normalization based on multiple Deming regression. BH-adjusted p values calculated with Wilcoxon signed-rank test are shown in the text.

(E) Expression of aging-associated genes across cell types. Percentages of cell types with detected expression of tissue-specific (brain, liver, and skeletal muscle), species-specific (human, rat, and mouse), and aggregated signatures of aging (adjusted p value < 0.05) are shown.

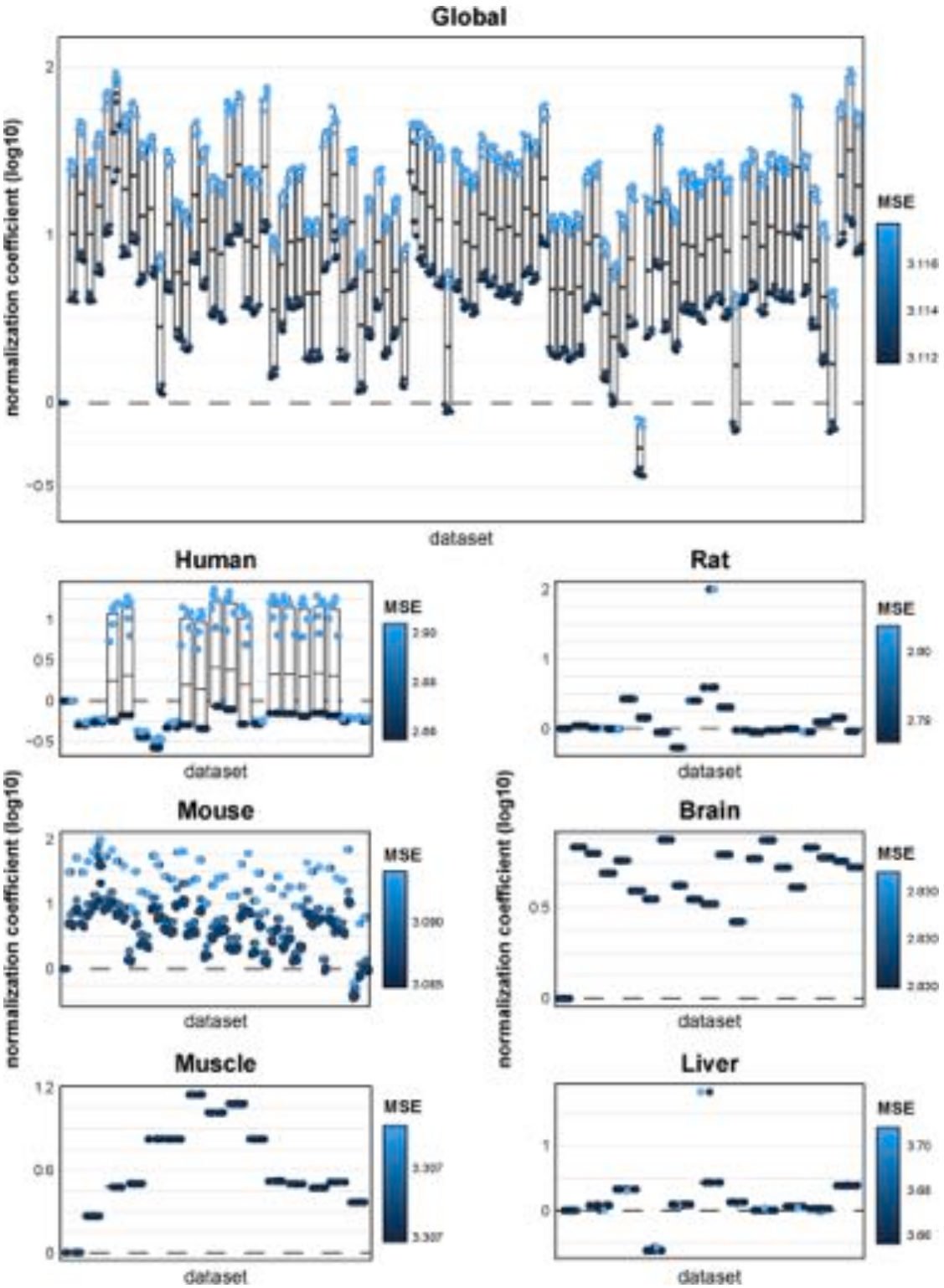

Figure S4. Normalization of aging datasets based on multiple Deming regression, related to Figure 3

Each dot represents a single run from a different set of initial parameters. Boxplots represent the distribution of final normalization coefficients for a given dataset, whereas color of the dots reflects the associated mean squared error (MSE).

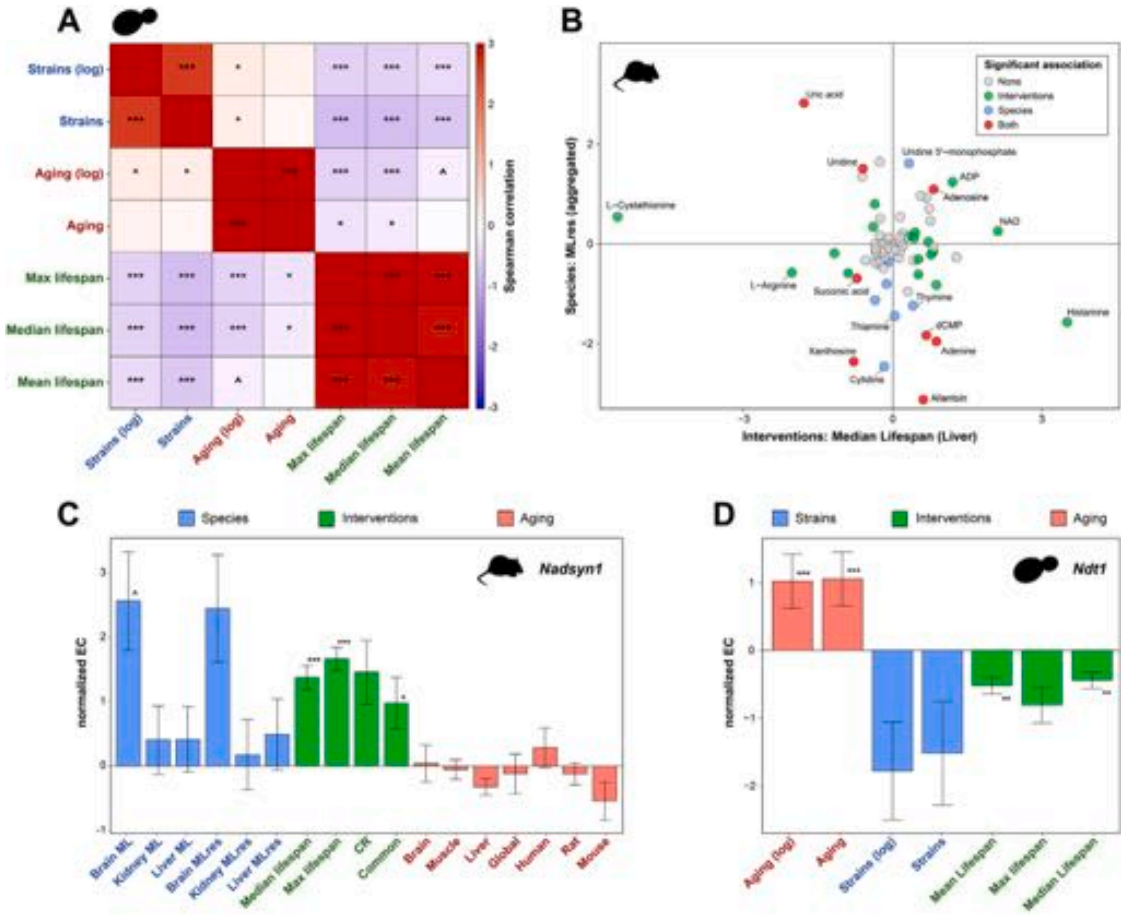

Figure S5. Metabolite changes associated with longevity across and within species, related to Figures 4 and 5

(A) Denoised Spearman correlation of *S. cerevisiae* aging and longevity signatures. Signatures of replicative aging, lifespan-extending deletions, and inter-strain longevity are shown in red, green, and blue, respectively. Statistical significance of each pairwise correlation is shown with asterisks.

(B) Metabolites associated with the effect of lifespan-extending interventions in mice and longevity across mammalian species. Normalized slopes of association between metabolite concentration and mouse median lifespan (y axis) or mammalian maximum lifespan adjusted for body mass (y axis) are shown. Metabolites, whose concentration is significantly associated with longevity according to interventions, species, or both models, are shown in green, blue, and red, respectively.

(C) Association of murine *Nadsyn1* expression change with longevity signatures. Statistical significance of each association denoted with asterisks was estimated with phylogenetic regression (for species longevity signatures) and mixed-effect model (for other signatures). Data are mean normalized ECs ± SE.

(D) Association of yeast *Ndt1* (*YIA6*) expression change with longevity signatures. Statistical significance of each association denoted with asterisks was estimated with linear regression. Data are mean normalized ECs ± SE.

˙p adjusted < 0.1; *p adjusted < 0.05; **p adjusted < 0.01; ***p adjusted < 0.001. EC, expression change; CR, calorie restriction; GH, growth hormone; ML, maximum lifespan; MLres, maximum lifespan residual.

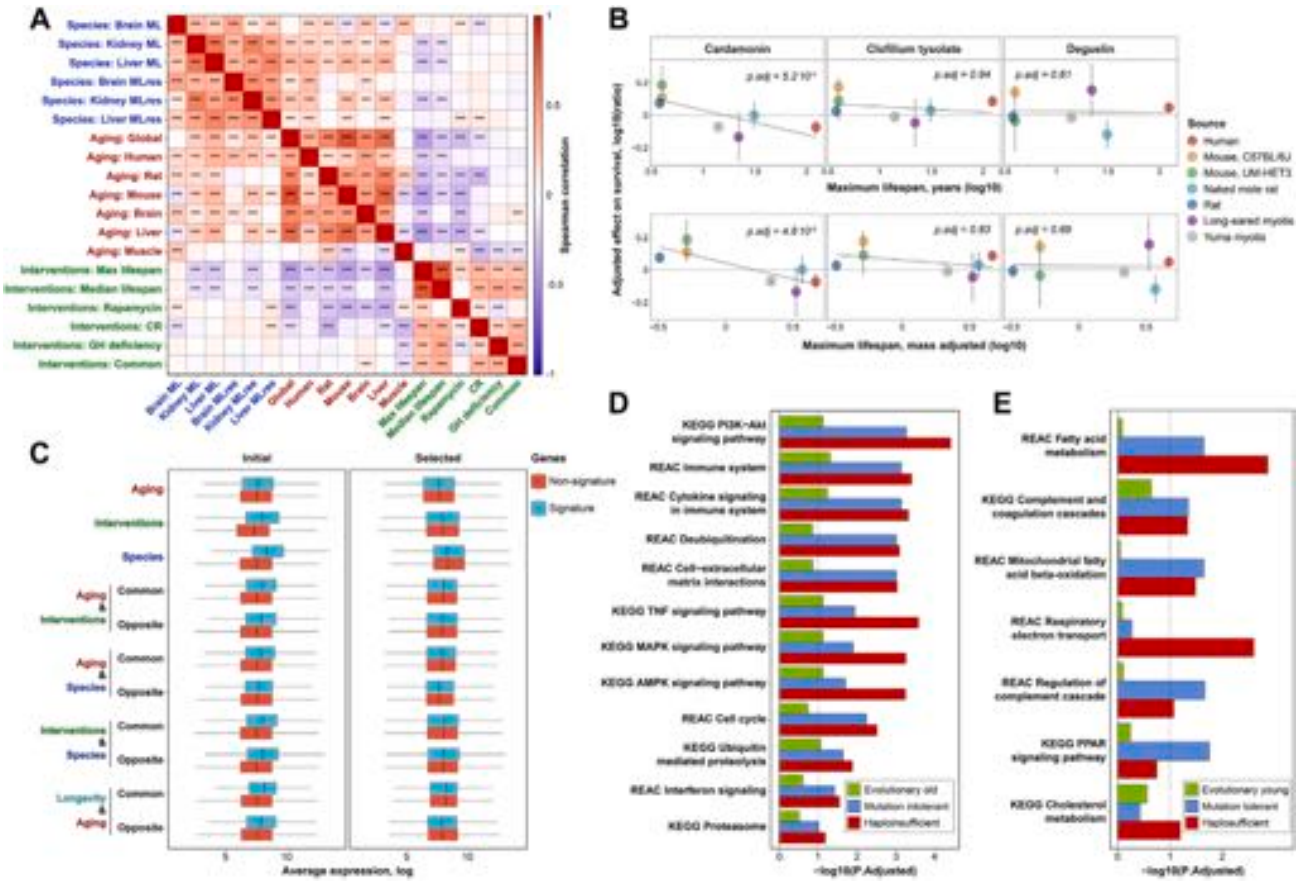

Figure S6. Common and distinct molecular signatures of longevity across and within species, related to Figure 6

(A) Spearman correlation of gene expression signatures based on functional enrichment (GSEA) scores. Only functions enriched by at least one signature (adjusted p value < 0.1) were used for the calculation.

(B) Adjusted effect of cardamonin (left), clofilium tysolate (middle), and deguelin (right) on the survival of fibroblasts from species with different lifespans following paraquat-induced oxidative stress. The effect of compound was calculated as a log ratio of the number of survived fibroblasts with and without treatment. Here, the effect on survival was adjusted for the baseline survival rate (estimated for fibroblasts treated with DMSO) by incorporating the latter term into the regression model. Dependence with maximum lifespan unadjusted (top) and adjusted (bottom) for adult weight was examined. Slope adjusted p value is shown in text. Data are mean ± SE. n = 3–6 per compound and control group for every species and mouse strain.

(C) Average expression of genes associated and not associated with longevity and aging traits before (left) and after (right) filtering. 100 uniform windows were used to randomly select subsets of signature and non-signature genes with similar distribution of log expression for every trait.

(D) Pathways enriched by evolutionary old, mutation-intolerant, and haploinsufficient genes associated with longevity across mammalian species. Adjusted p value threshold of 0.1 is shown as a dotted line. The whole list of enriched functions is in Table S5A.

(E) Pathways enriched for evolutionary young, mutation-tolerant, and haplosufficient genes associated with lifespan-extending interventions in mouse. Adjusted p value threshold of 0.1 is shown as a dotted line. The whole list of enriched functions is in Table S5B.

CR, calorie restriction; GH, growth hormone; ML, maximum lifespan; MLres, maximum lifespan residual; REAC, REACTOME.

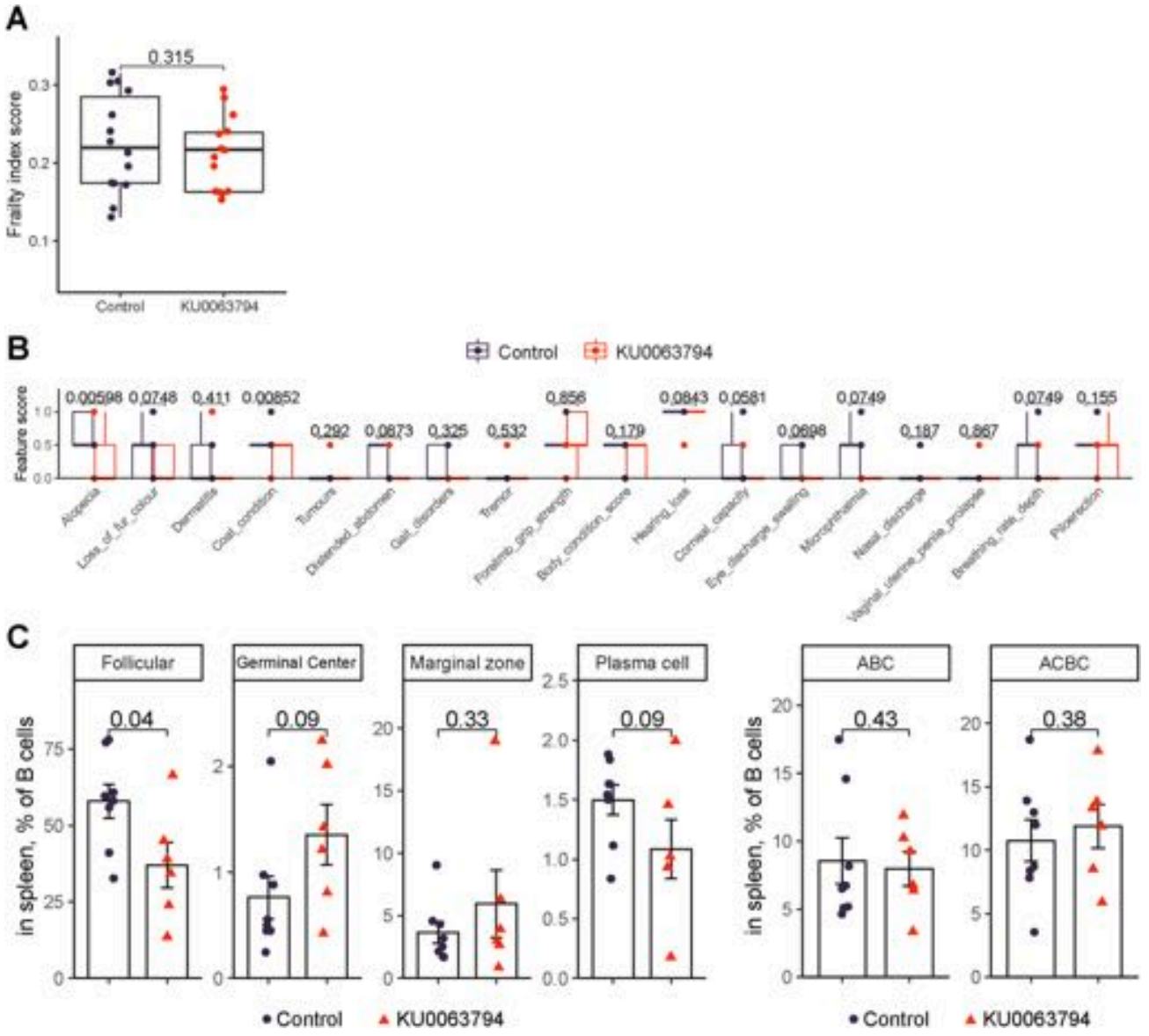

Figure S7. KU0063794 effect on frailty features and B cell population in old mice, related to Figure 7

(A) Frailty index score in 25-month-old male C57BL/6 mice that were later assigned to treated and control groups.

(B) Frailty index score features in 30-month-old male C57BL/6 mice from treated and control groups.

(C) Percentage of B cell subpopulations in spleens of 27-month-old male C57BL/6 mice treated for 5 months or age-matched control groups measured by flow cytometry. ABC, age-associated B cells; ACBCs, age-associated clonal B cells.

p values were calculated with one-tailed Wilcoxon rank-sum tests.